YANKEE ATOMIC ELECTRIC COMPANY

YAEC-1600

VERMONT YANKEE
CYCLE 13
CORE PERFORMANCE ANALYSIS

May 1987

Major Contributors:

V. Chandola
B. Y. Hubbard
M. P. LeFrancois
J. Pappas
R. C. Potter
J. D. Robichaud
K. E. St.John
T. A. Schmidt
R. A. Woehlke

Prepared by: _____ 6/5/87
M. A. Sironen (Date)
Nuclear Engineering Coordinator

Approved by: B C Slifer for RJC 6/5/87
R. J. Cacciapouti, Manager (Date)
Reactor Physics Group

Approved by: B C Slifer for PAB 6/5/87
P. A. Bergeron, Manager (Date)
Transient Analysis Group

Approved by: _____ 6/5/87
S. P. Schultz, Manager (Date)
LOCA Analysis Group

Approved by: B C Slifer 6/5/87
B. C. Slifer, Director (Date)
Nuclear Engineering Department

2810R

DISCLAIMER OF RESPONSIBILITY

This document was prepared by Yankee Atomic Electric Company for its own use and on behalf of Vermont Yankee Nuclear Power Corporation. This document is believed to be completely true and accurate to the best of our knowledge and information. It is authorized for use specifically by Yankee Atomic Electric Company, Vermont Yankee Nuclear Power Corporation and/or the appropriate subdivisions within the Nuclear Regulatory Commission only.

With regard to any unauthorized use whatsoever, Yankee Atomic Electric Company, Vermont Yankee Nuclear Power Corporation and their officers, directors, agents and employees assume no liability nor make any warranty or representation with respect to the contents of this document or to its accuracy or completeness.

ABSTRACT

This report presents design information, calculational results, and operating limits pertinent to the operation of Cycle 13 of the Vermont Yankee Nuclear Power Station. These include the fuel design and core loading pattern descriptions; calculated reactor power distributions, exposure distributions, shutdown capability, and reactivity functions; and the results of safety analyses performed to justify plant operation throughout the cycle.

TABLE OF CONTENTS

TABLE OF CONTENTS
(Continued)

LIST OF FIGURES

LIST OF FIGURES
(Continued)

LIST OF TABLES

ACKNOWLEDGEMENTS

The authors and principal contributors would like to acknowledge the contributions to this work by the YAEC Word Processing Center. Their assistance in preparing text for this document is recognized and greatly appreciated.

1.0 INTRODUCTION

This report provides information to support the operation of the Vermont Yankee Nuclear Power Station through the forthcoming Cycle 13. In this report, Cycle 13 will frequently be referred to as the Reload Cycle. The preceding Cycle 12 will frequently be referred to as the Current Cycle. The refueling between the two will involve the discharge of 136 irradiated fuel bundles and the insertion of 136 new fuel bundles. The resultant core will consist of 136 new fuel bundles and 232 irradiated fuel bundles. Some of the irradiated fuel was present in the reactor in Cycles 10 and 11, as well as the Current Cycle. These cycles will frequently be referred to as Past Cycles.

The new fuel bundles differ from the irradiated bundles in the following ways: 1) the average bundle enrichment has been raised from 2.89 to 2.99, 2) the cladding now has a barrier; and 3) the pellet diameter has been increased. The use of this new bundle type will provide a transition to longer cycles.

This report contains descriptions and analyses results pertaining to the mechanical, thermal-hydraulic, physics, and safety aspects of the Reload Cycle.

The Cycle 13 MCPR operating limits and the MAPLHGR operating limits for the new fuel bundles are given in Appendix A.

2.0 RECENT REACTOR OPERATING HISTORY

2.1 Operating History of the Current Cycle

The currently operating cycle is Cycle 12. To date, the Current Cycle has been operated smoothly at, or near, full power with the exception of normal maintenance, sequence exchanges, and a schedule coastdown. The operating history highlights and control rod sequence exchange schedule of the Current Cycle are found in Table 2.1.1.

2.2 Operating History of Past Applicable Cycles

The irradiated fuel in the Reload Cycle includes some fuel bundles initially inserted in Cycles 10 and 11. These Past Cycles operated smoothly at, or near, full power with the exception of normal maintenance, sequence exchanges, and coastdown to the end of cycle. The highlights of the Past Cycles are found in Tables 2.2.1 and 2.2.2. The Past Cycles are described in detail in References 1 and 2.

TABLE 2.1.1

VY CYCLE 12 OPERATING HIGHLIGHTS

Beginning of Cycle Date	June 30, 1986
End of Cycle Date	August 8, 1987*
Weight of Uranium As-Loaded (Short Tons)	74.44
Beginning of Cycle Core Average Exposure (MWD/ST)	9820
End of Full Power Core Average Exposure (MWD/ST)	16370
End of Cycle Core Average Exposure (MWD/ST)	17720*
Number of Fresh Assemblies	120
Number of Irradiated Assemblies	248

Control Rod Sequence Exchange Schedule:

	Sequence	
Date	From	To
September 6, 1986	A2-1	B1-1
November 1, 1986	B1-1	A1-1
December 20, 1986	A1-1	B2-1
February 7, 1987	B2-1	A2-2
April 4, 1987	A2-2	B1-2

* Projected Dates and Exposures.

TABLE 2.2.1

VY CYCLE 11 OPERATING HIGHLIGHTS

Beginning of Cycle Date	August 6, 1984
End of Cycle Date	September 21, 1985
Weight of Uranium As-Loaded (Short Tons)	74.25
Beginning of Cycle Core Average Exposure (MWD/ST)	10,418
End of Full Power Core Average Exposure (MWD/ST)	16,733
End of Cycle Core Average Exposure (MWD/ST)	18,283
Capacity Factor While Operating (%)	89.2
Number of Fresh Assemblies	104
Number of Irradiated Assemblies	264

Control Rod Sequence Exchange Schedule:

	Sequence	
Date	From	To
October 24, 1984	A1-1	B2-1
December 15, 1984	B2-1	A2-1
February 2, 1985	A2-1	B1-1
March 23, 1985	B1-1	A1-2
May 18, 1985	A1-2	B2-2

TABLE 2.2.2

VY CYCLE 10 OPERATING HIGHLIGHTS

Beginning of Cycle Date	June 17, 1983
End of Cycle Date	June 15, 1984
Weight of Uranium As-Loaded (Short Tons)	74.13
Beginning of Cycle Core Average Exposure (MWD/ST)	10,463
End of Full Power Core Average Exposure (MWD/ST)	17,185
End of Cycle Core Average Exposure (MWD/ST)	17,806
Capacity Factor While Operating (%)	93.6
Number of Fresh Assemblies	108
Number of Irradiated Assemblies	260

Control Rod Sequence Exchange Schedule:

	Sequence	
Date	From	To
August 12, 1983	A1-1	B2-1
October 1, 1983	B2-1	A2-1
November 5, 1983	A2-1	B1-1
December 17, 1983	B1-1	A1-2
January 23, 1984	A1-2	B2-2
March 3, 1984	B2-2	A2-2
April 16, 1984	A2-2	B1-2

3.0 RELOAD CORE DESIGN DESCRIPTION

3.1 Core Fuel Loading

The Reload Cycle core will consist of both new and irradiated assemblies. All the assemblies have bypass flow holes drilled in the lower tie plate. Table 3.1.1 characterizes the core by fuel type, batch size, and first cycle loaded. A description of the fuel is found in Reference 3.

3.2 Design Reference Core Loading Pattern

The Reload Cycle assembly locations are indicated on the map in Figure 3.2.1. For the sake of legibility only the upper right quadrant is shown. The other quadrants are mirror images with bundles of the same type having nearly identical exposures. The bundles are identified by the reload number in which they were first introduced into the core. If any changes are made to the loading pattern at the time of refueling, they will be evaluated under 10CFR50.59. The final loading pattern with specific bundle serial numbers will be supplied in the Startup Test Report.

3.3 Assembly Exposure Distribution

The assumed nominal exposure on the fuel bundles in the Reload Cycle design reference loading pattern is given in Figure 3.2.1. To obtain this exposure distribution, Past Cycles were depleted with the SIMULATE model [4,5] using actual plant operating history. For the Current Cycle, plant operating history was used through January 6, 1987. Beyond this date, the exposure was accumulated using a best-estimate rodded depletion analysis to End of Full Power Life (EOFPL) followed by a projected coastdown to End of Cycle (EOC).

Table 3.3.1 gives the assumed nominal exposure on the Current Cycle and the Beginning of Cycle (BOC) core average exposure that results from the shuffle into the Reload Cycle loading pattern. The Reload Cycle EOFPL core average exposure and cycle capability are provided.

TABLE 3.1.1

VY CYCLE 13 FUEL BUNDLE TYPES AND NUMBERS

	Fuel Designation	Reload Designation	Cycle Loaded	Number	Possible Bundle IDs
Irradiated	P8DPB289	R9	10	8	LY4XXX
	P8DPB289	R10	11	104	LY6XXX, LY7XXX
	P8DPB289	R11	12	120	LY7XXX, LYCXXX
New	BP8DRB299	R12	13	136	LYJXXX

NOTE: XXX stands for the last three digits of the bundle serial number.

TABLE 3.3.1

DESIGN BASIS VY CYCLE 12 AND CYCLE 13 EXPOSURES

Assumed Current Cycle Core Average Exposure End of Cycle 12	17.72 GWD/ST
Assumed Reload Cycle Core Average Exposure Beginning of Cycle 13	8.43 GWD/ST
Haling Calculated Core Average Exposure at End of Full Power Life, Cycle 13	16.80 GWD/ST
Cycle 13 Exposure Capability	8.37 GWD/ST

2810R

VERMONT YANKEE
CYCLE 13
BOC BUNDLE AVERAGE EXPOSURES

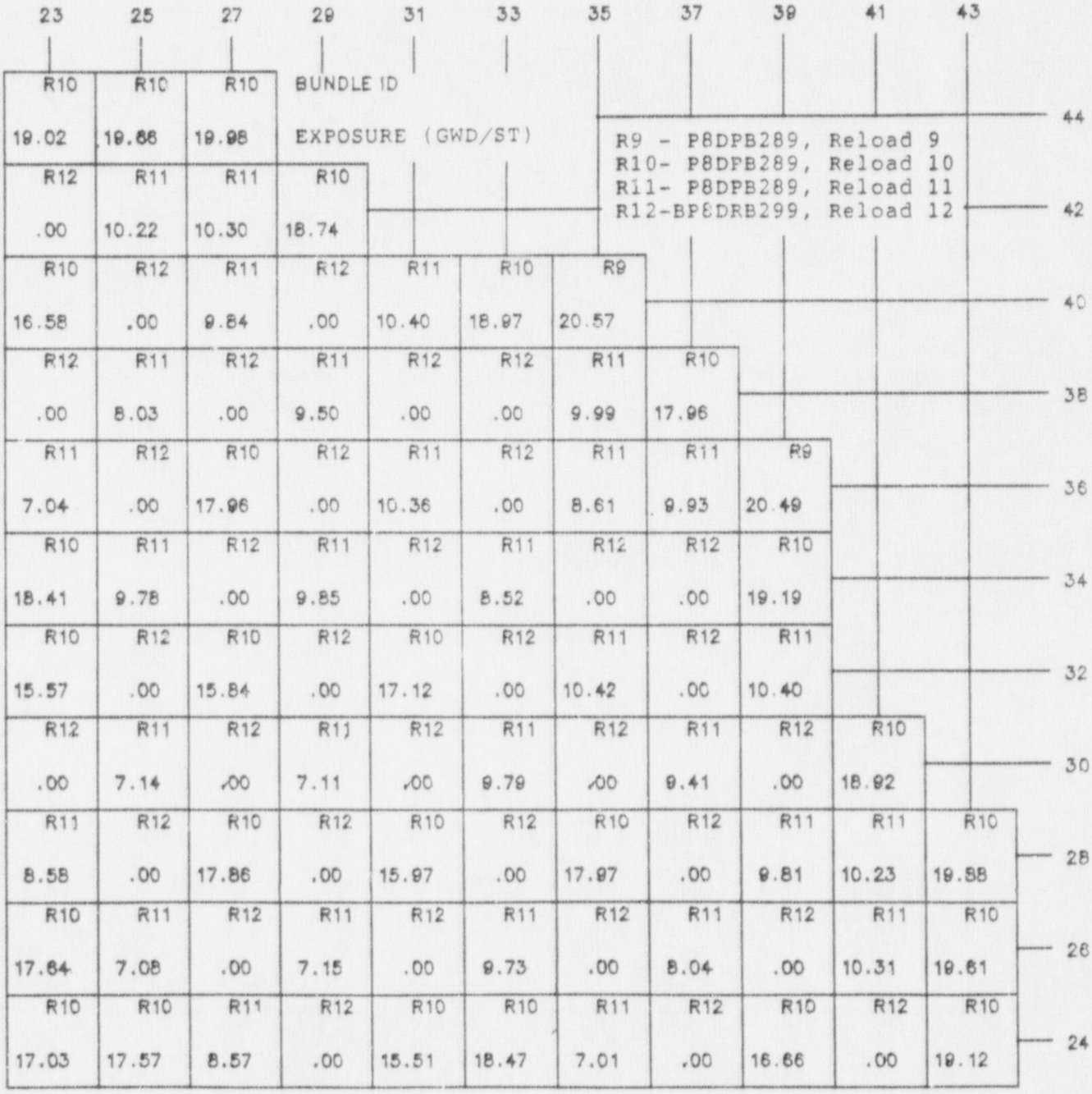

FIGURE 3.2.1

VY CYCLE 13 DESIGN REFERENCE LOADING PATTERN, UPPER RIGHT QUADRANT

4.0 FUEL MECHANICAL AND THERMAL DESIGN

4.1 Mechanical Design

All fuel to be inserted into the Reload Cycle was fabricated by the General Electric Company (GE). The major mechanical design parameters are given in Table 4.1.1 and Reference 3. Fuel rod design changes have been incorporated in the Reload Cycle fuel design. The new fuel pellet diameter is increased and is fabricated to a higher nominal fuel pellet density with less in-reactor densification. In addition, the new fuel cladding incorporates a barrier on the internal surface designed to reduce the effects of pellet-cladding interaction. Detailed descriptions of the fuel rod mechanical design and mechanical design analyses are provided in Reference 3. These design analyses remain valid with respect to the Reload Cycle operation. Mechanical and chemical compatibility of the fuel assemblies with the in-service reactor environment is also addressed in Reference 3.

4.2 Thermal Design

The fuel thermal effects calculations were performed using the FROSSTEY computer code [6,7]. The FROSSTEY code calculates pellet-to-cladding gap conductance and fuel temperatures from a combination of theoretical and empirical models which include fuel and cladding thermal expansion, fission gas release, pellet swelling, pellet densification, pellet cracking, and fuel and cladding thermal conductivity.

The thermal effects analysis included the calculation of fuel temperatures and fuel cladding gap conductance under nominal core steady state and peak linear heat generation rate conditions. Figure 4.2.1 provides the core average response of gap conductance. These calculations integrate the responses of individual fuel batch average operating histories over the core average exposure range of the Reload Cycle. The gap conductance values are weighted axially by power distributions and radially by volume. The core-wide gap conductance values for the RETRAN system simulations, described in Sections 7.1 through 7.3, are from this data set at the corresponding exposure statepoints.

The gap conductance values input to the hot channel calculations (Section 7.1) were evaluated for the given fuel bundle type as a function of the assembly exposure. The calculation assumed a 1.4 chopped cosine axial power shape with the peak power node running at the maximum average planar linear heat generation rate (MAPLHGR) limit defined in Reference 8 and Table A.2. Figure 4.2.2 provides the hot channel response of gap conductance. In Figure 4.2.2, "planar exposure" refers to the exposure of the node operating at the MAPLHGR limit. Gap conductance values for the hot channel analysis were extracted from Figure 4.2.2 using the limiting bundle exposure of any minimum critical power ratio (MCPR) limiting bundle within the exposure interval of interest. The SIMULATE rodded depletion (Section 5.1.2) provides predictions of both limiting MCPR and the associated bundle exposure for the entire cycle.

Table 4.2.1 provides the core average and hot channel gap conductance values used in the transient analyses (Section 7.1). The values for gap conductance are higher than those calculated in previous cycles for the following reasons: 1) the diametral gap of the fresh fuel has been reduced as a result of an increase in pellet diameter, 2) the as-fabricated pellet density has been increased which results in a decrease in the in-reactor fuel pellet densification, thereby causing a smaller reduction in the irradiated pellet-cladding gap, and 3) the specification for surface roughness for the fuel pellet and the fuel cladding has been revised. These changes improve the heat transfer capability of the fuel which result in reduced fuel pellet temperatures, fission gas releases, and fuel rod internal pressures.

Fuel rod local linear heat generation rates (LHGR) at fuel centerline incipient melt and 1% cladding plastic strain as a function of local axial segment exposure for the peak gadolinia concentrations used in Vermont Yankee fuel bundles were calculated. These values are displayed in Table 4.2.2. Initial conditions assumed that fuel rods operated at the local segment power level of the maximum allowable LHGR prior to the power increase.

4.3 Operating Experience

All irradiated fuel bundles scheduled to be reinserted in the Reload Cycle have operated as expected in Past Cycles of Vermont Yankee. Off-gas measurements in the Current Cycle indicate that a small number of fuel rod failures may have occurred. Vermont Yankee is planning to identify the failed rods during the outage.

TABLE 4.1.1

NOMINAL FUEL MECHANICAL DESIGN PARAMETERS

	Fuel Types	
	Irradiated	New
Fuel Bundle*		
Bundle Type	P8X8R	BP8X8R
Vendor Designation (Table 3.1.1)	P8DPB289	BP8DRB299
Initial Enrichment, w/o U-235	2.89	2.99
Rod Array	8X8	8X8
Fuel Rods per Bundle	62	62
Fuel Channel		
Material	Zr-4	Zr-4
Wall Thickness, Inches	0.080	0.080

*Complete bundle, pellet, and rod descriptions are found in Reference 3.

TABLE 4.2.1

GAP CONDUCTANCE VALUES USED IN VY CYCLE 13 TRANSIENT ANALYSES

Cycle Exposure Statepoint (MWD/ST)	Core Average Gap Conductance (BTU/Hr-Ft^2- ^{o}F)	Hot Channel Bundle Exposure (MWD/ST)	Hot Channel Gap Conductance (1) (BTU/Hr-Ft^2 - ^{o}F)
BOC13	1910	9447 (2)	4850
EOFPL13-2000 MWD/ST	3130	8096	4450
EOFPL13-1000 MWD/ST	3290	9363	4820
EOFPL13	3475	9447	4850

NOTE
(1) Hot channel gap conductance values are all derived for the BP8DRB299 fuel type.

(2) Between BOC13 and EOFPL13-2000 MWD/ST, the highest exposure limiting hot channel bundle is once-burned.

TABLE 4.2.2

PEAK LINEAR HEAT GENERATION RATES CORRESPONDING TO INCIPIENT FUEL CENTERLINE MELTING AND 1% CLADDING PLASTIC STRAIN (1)

		0.0 w/o Gd_2O_3		3.0 w/o Gd_2O_3	
	Exposure (MWD/MT)	Melt (kW/ft)	1% ε_p (kW/ft)	Melt (kW/ft)	1% ε_p (kW/ft)
Fuel Type P8x8R					
P8DPB289	0	24.0	24.0	22.5	24.0
	25,000	24.0	24.0	21.5	22.5
	50,000	24.0	17.5	20.0	14.5

		0.0 w/o Gd_2O_3		4.0 w/o Gd_2O_3	
	Exposure (MWD/MT)	Melt (kW/ft)	1% ε_p (kW/ft)	Melt (kW/ft)	1% ε_p (kW/ft)
Fuel Type BP8x8R					
BP8DRB299	0	24.0	24.0	21.5	24.0
	25,000	24.0	24.0	20.5	20.5
	50,000	23.5	15.5	19.0	12.0

NOTE
(1) Peak linear heat generation rates shown are minimum bounding values to the occurrence of the given condition.

VY CYCLE 13 FUEL PERFORMANCE

CORE AVERAGE GAP CONDUCTANCE

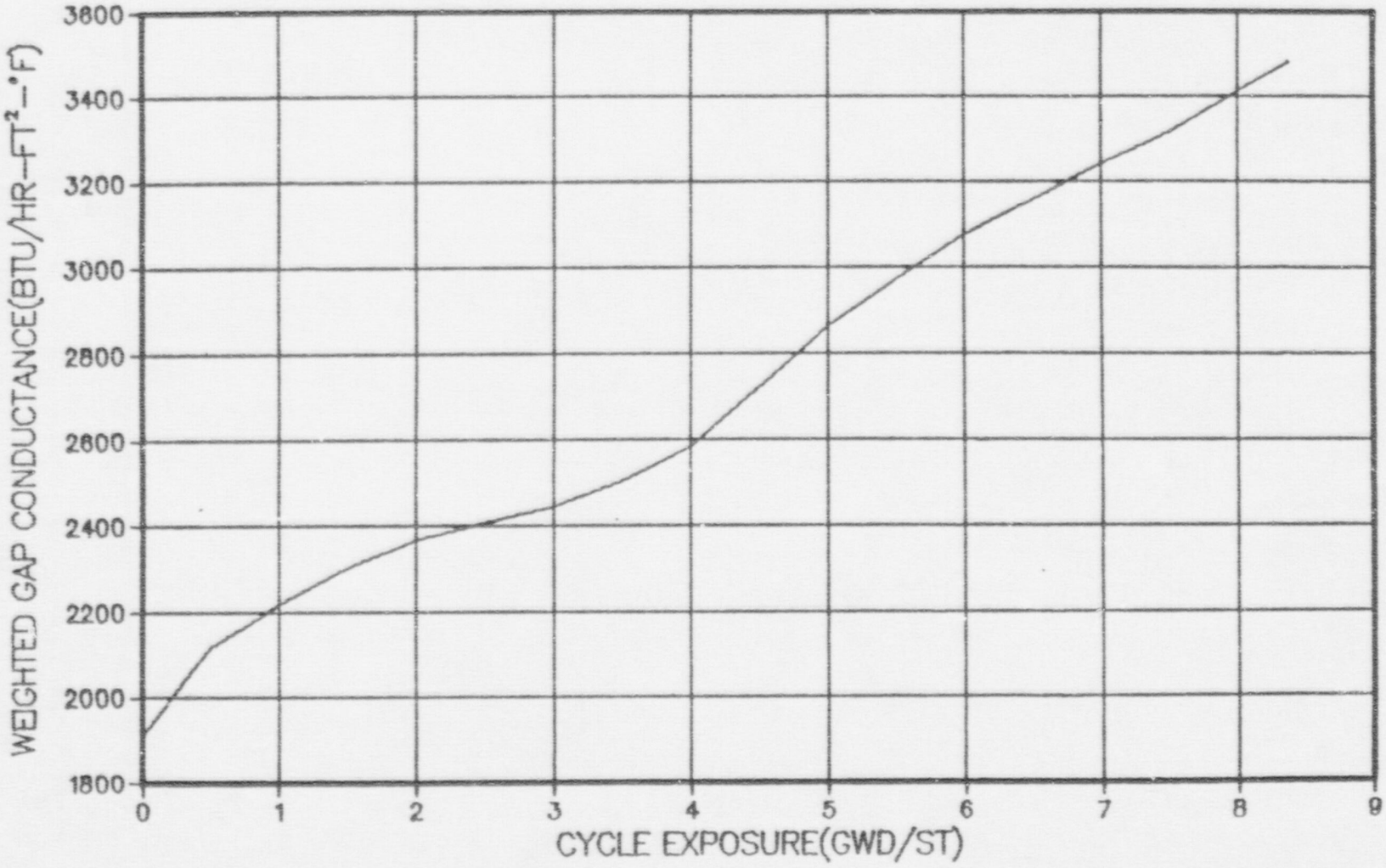

FIGURE 4.2.1

VY CYCLE 13 CORE AVERAGE GAP CONDUCTANCE VERSUS CYCLE EXPOSURE

VERMONT YANKEE – HOT CHANNEL GAP CONDUCTANCE

P8X8RB FUEL -- GAP CONDUCTANCE VS EXPOSURE

1.4 CHOPPED COSINE AXIAL POWER SHAPE WITH PEAK AT MAPLHGR

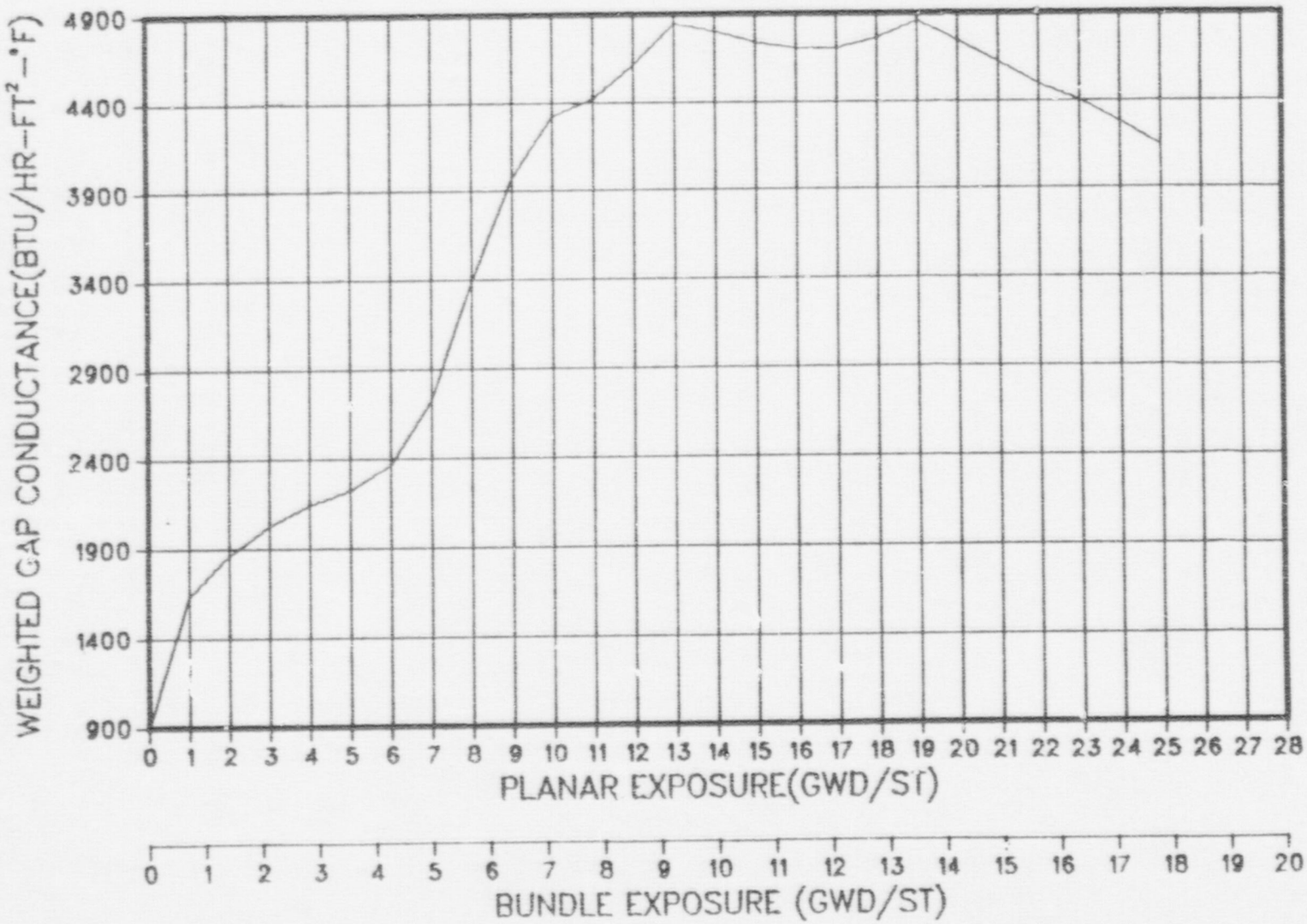

FIGURE 4.2.2

VY HOT CHANNEL GAP CONDUCTANCE FOR BP8X8R VERSUS EXPOSURE

5.0 NUCLEAR DESIGN

5.1 Core Power Distributions

The Reload Cycle was depleted using SIMULATE [4] to give both a rodded depletion and an All Rods Out (ARO) Haling depletion.

5.1.1 Haling Power Distribution

The Haling depletion serves as the basis for defining core reactivity characteristics for most transient evaluations. This is primarily because its flat power shape has conservatively weak scram characteristics.

The Haling power distribution is calculated in the ARO condition. The Haling iteration converges on a self-consistent power and exposure distribution for the burnup step to EOFPL. In principle, this should provide the overall minimum peaking power shape for the cycle. During the actual cycle, flatter power distributions might occasionally be achieved by shaping with control rods. However, such shaping would leave underburned regions in the core which would peak at another point in time. Figures 5.1.1 and 5.1.2 give the Haling radial and axial average power distributions for the Reload Cycle.

5.1.2 Rodded Depletion Power Distribution

The rodded depletion was used to evaluate the mislocated bundle error and the rod withdrawal error because it provides initializing rod patterns and it makes more realistic predictions of initial CPR values. It was also used in the rod drop worth and shutdown margin calculations because it burns the top of the core more realistically than the Haling.

To generate the rodded depletion, control rod patterns were developed which give critical eigenvalues at each point in the cycle and peaking similar to the Haling calculation. The resulting patterns were frequently more peaked than the Haling, but were below expected operating limits. However, as stated above, the underburned regions of the core can exhibit peaking in excess of the Haling peaking when pulling ARO at EOFPL. Figures 5.1.3 and 5.1.4 give the APO at EOFPL power distributions for the Reload Cycle rodded depletion.

Note, in Figure 5.1.4, that the average axial power at ARO for the rodded depletion is more bottom peaked than the Haling (Figure 5.1.2). The rodded depletion would result in better scram characteristics at EOFPL.

5.2 Core Exposure Distributions

The Reload Cycle exposures are summarized in Table 3.3.1. The projected BOC radial exposure distribution for the Reload Cycle is given in Figure 3.2.1. The Haling calculation produced the EOFPL radial exposure distribution given in Figure 5.2.1. Since the Haling power shape is constant, it can be held fixed by SIMULATE to give the exposure distributions at various mid-cycle points. BOC, EOFPL-2000 MWD/ST, EOFPL-1000 MWD/ST, and EOFPL exposure distributions were used to develop reactivity input for the core wide transient analyses.

The rodded depletion differs from the Haling during the cycle because the rods shape the power differently. However, rod sequences are swapped frequently and the overall exposure distribution at end of cycle is similar to the Haling. Figure 5.2.2 gives the EOFPL radial exposure distribution for the Reload Cycle rodded depletion.

5.3 Cold Core Reactivity and Shutdown Margin

The cold K_{eff} with ARO and the cold K_{eff} with All Rods Inserted (ARI) at BOC were calculated using the SIMULATE code [4,5] and are shown in Table 5.3.1. K_{eff} with ARO minus the cold critical K_{eff} is the amount of excess core reactivity. K_{eff} with ARI minus the K_{eff} with ARO is the worth of all the control rods.

The cold critical eigenvalue K_{eff} was defined as the average calculated critical eigenvalue minus a 95% confidence level uncertainty. Then all cold results were normalized to make the critical K_{eff} eigenvalue equal to 1.000.

Technical Specifications [8] state that, for sufficient shutdown margin, the core must be subcritical by at least 0.25% ΔK + R (defined below) with the strongest worth control rod withdrawn. Again, using SIMULATE, a search was made for the strongest worth control rod at various exposures in the cycle. This is necessary because rod worths change with exposure on adjacent assemblies. Then the cold K_{eff} with the strongest rod out was calculated at BOC and at the end of each control rod sequence. Subtracting each cold K_{eff} with the strongest rod out from the cold critical K_{eff} eigenvalue defines the shutdown margin as a function of exposure. Figure 5.3.1 shows the results. Because the local reactivity may increase with exposure, the shutdown margin (SDM) may decrease. To account for this, and other uncertainties, the value R is calculated. R is defined as R_1 plus R_2. R_1 is the difference between the cold K_{eff} with the strongest rod out at BOC and the maximum cold K_{eff} with the strongest rod out in the cycle. R_2 is a measurement uncertainty in the demonstration of SDM associated with the manufacture of past control blades. It is presently set at .07% ΔK. The shutdown margin results are summarized in Table 5.3.1.

5.4 Standby Liquid Control System Shutdown Capability

The shutdown capability of the Standby Liquid Control System (SLCS) is designed to bring the reactor from full power to cold, ARO, xenon free shutdown with at least 5% ΔK margin. Using SIMULATE [4], the ppm of boron was adjusted until the K_{eff} reached the cold critical K_{eff} minus .05. Each case assumed cold, xenon-free conditions, with All Rods Out. The cycle was searched to find the most reactive point in the cycle. This analysis found that the plant would be subcritical by 5% ΔK at the worst point in cycle with less than the 800 ppm of boron required by VY Technical Specifications [8]. Table 5.4.1 lists the amount of boron concentration and the corresponding shutdown capability of the SLCS.

5.5 Changes in Nuclear Design Methods

The computer code, CASMO-1 [5], had input limitations that did not allow adequate modelling of the new fuel type. Therefore, CASMO-2 [10] was

used to generate the cross sections for all fuel types used in Cycle 13. CASMO-1 and CASMO-2 use the same cross section library and are neutronically equivalent with one exception. The reflecting boundary condition for the two-dimensional bundle calculation has been revised in CASMO-2. CASMO-2 more accurately handles cases with high flux gradients close to the problem boundary.

Before utilizing the methodology of CASMO-2 with SIMULATE, Vermont Yankee Cycles 9 through 11, and most of the current Cycle 12 were benchmarked. The CASMO-2/SIMULATE model compared to the CASMO-1/SIMULATE model as follows: The average hot eigenvalue went up by +.0009. The average of the standard deviations went from $\pm$.00240 to $\pm$.00246. When comparing both models to actual plant Traversing Incore Probe (TIP) readings, the average absolute error for the four cycles increased from 1.53% to 1.58%. The cold critical data for the four cycles was also benchmarked. The 95% confidence, minimum cold critical eigenvalue went from .9926 to .9935. As can be seen by these results, the differences between the CASMO-2 and CASMO-1 were examined in detail and found to have minimal impact on the analyses.

TABLE 5.3.1

VY CYCLE 13

K_{eff} VALUES AND SHUTDOWN MARGIN CALCULATION

BOC K_{eff} - Uncontrolled	1.1220
BOC K_{eff} - Controlled	.9705
Cold Critical K_{eff} Eigenvalue	1.0000
BOC K_{eff} - Controlled With Strongest Worth Rod Withdrawn	.9887
Cycle Minimum Shutdown Margin Occurs at BOC With Strongest Worth Rod Withdrawn	1.13% ΔK
R_1, Maximum Increase in Cold K_{eff} With Exposure	.00% ΔK

TABLE 5.4.1

VY CYCLE 13

STANDBY LIQUID CONTROL SYSTEM SHUTDOWN CAPABILITY

ppm of Boron	Shutdown Margin
718	5.0% ΔK
800	6.6% ΔK

VERMONT YANKEE
CYCLE 13 HALING DEPLETION
EOFPL BUNDLE AVERAGE RELATIVE POWERS

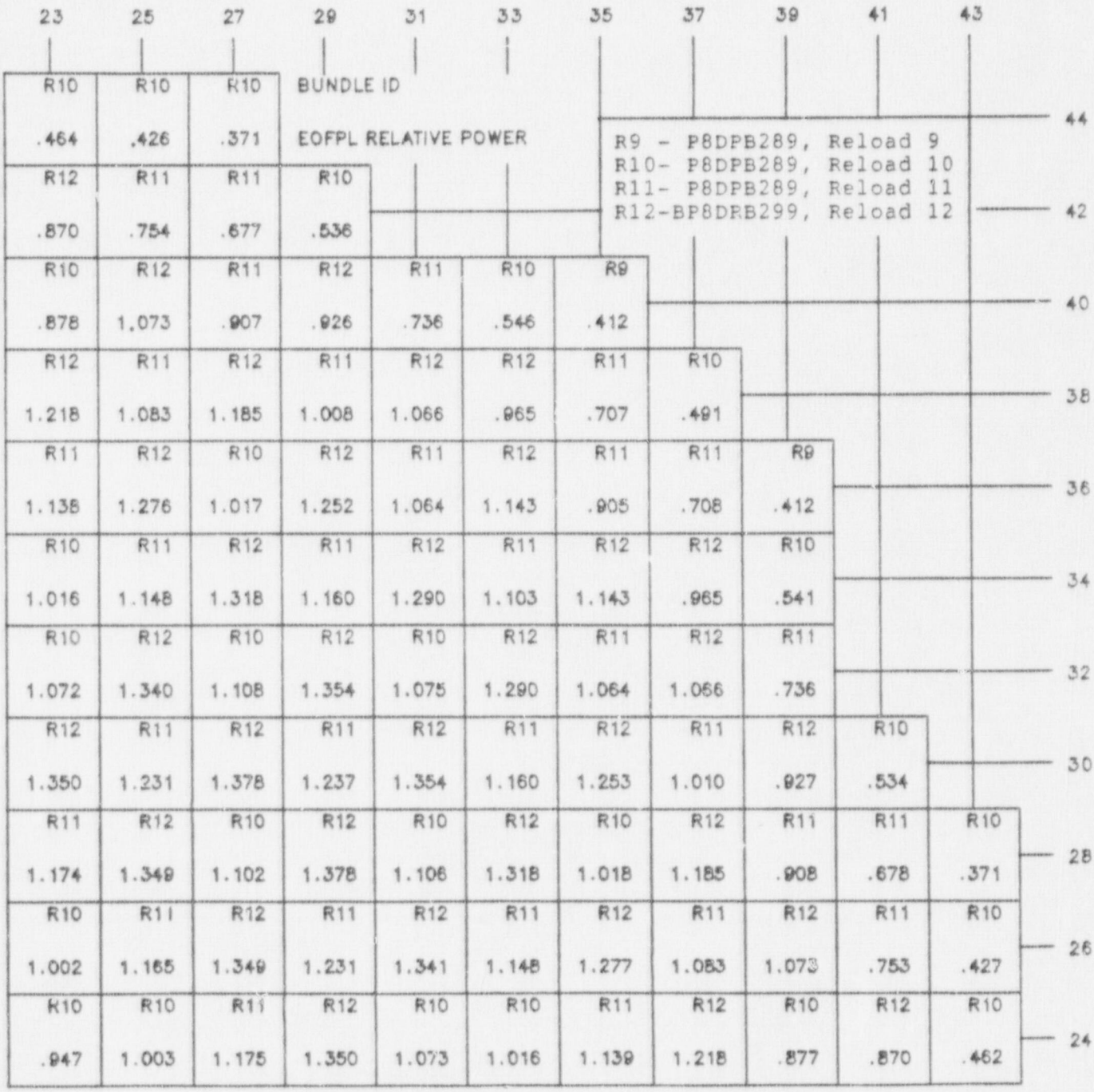

FIGURE 5.1.1

VY CYCLE 13 HALING DEPLETION, EOFPL BUNDLE AVERAGE RELATIVE POWERS

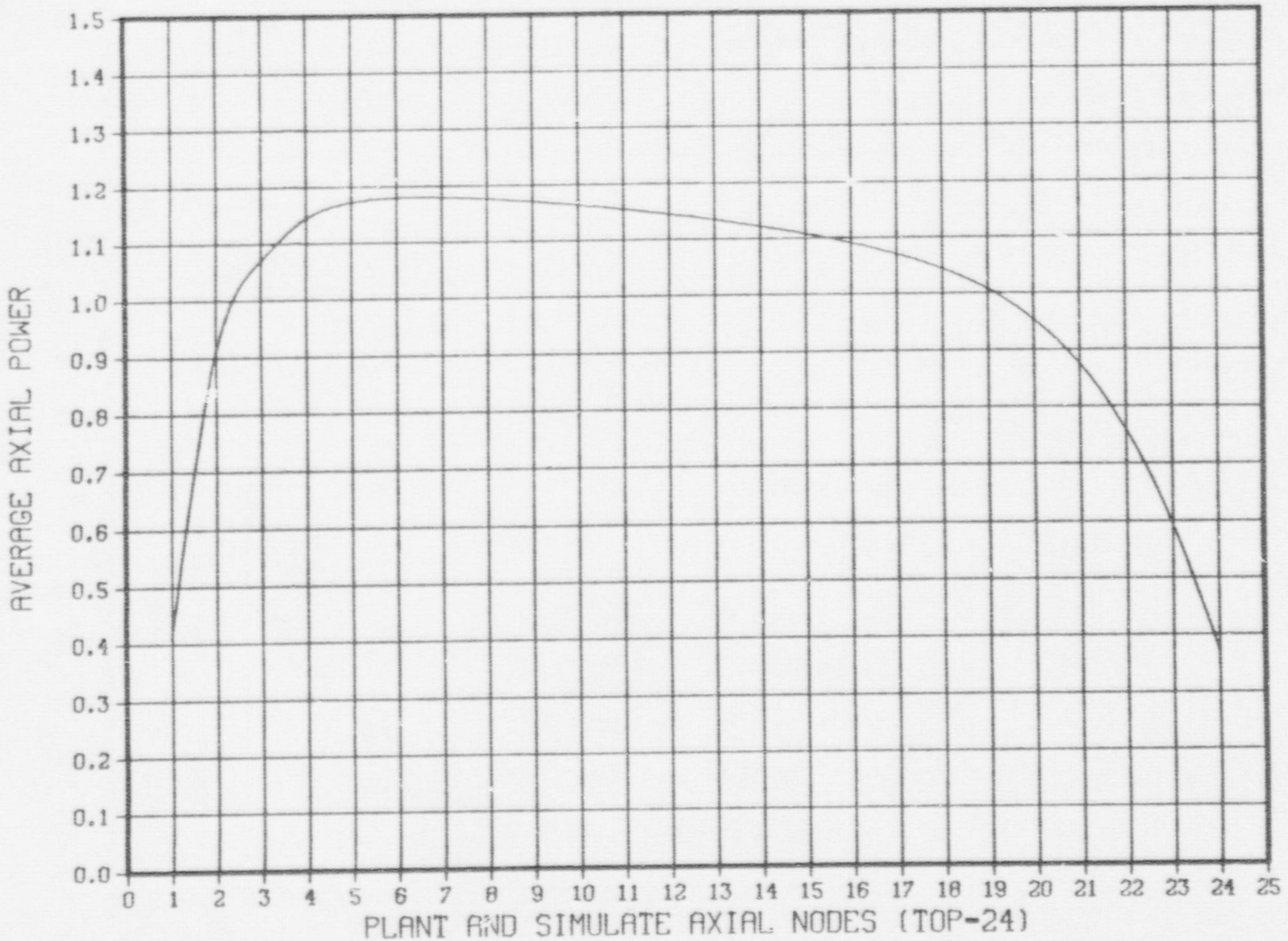

FIGURE 5.1.2

VY CYCLE 13 HALING DEPLETION, EOFPL CORE AVERAGE AXIAL POWER DISTRIBUTION

VERMONT YANKEE
CYCLE 13 RODDED DEPLETION
EOFPL BUNDLE AVERAGE RELATIVE POWERS

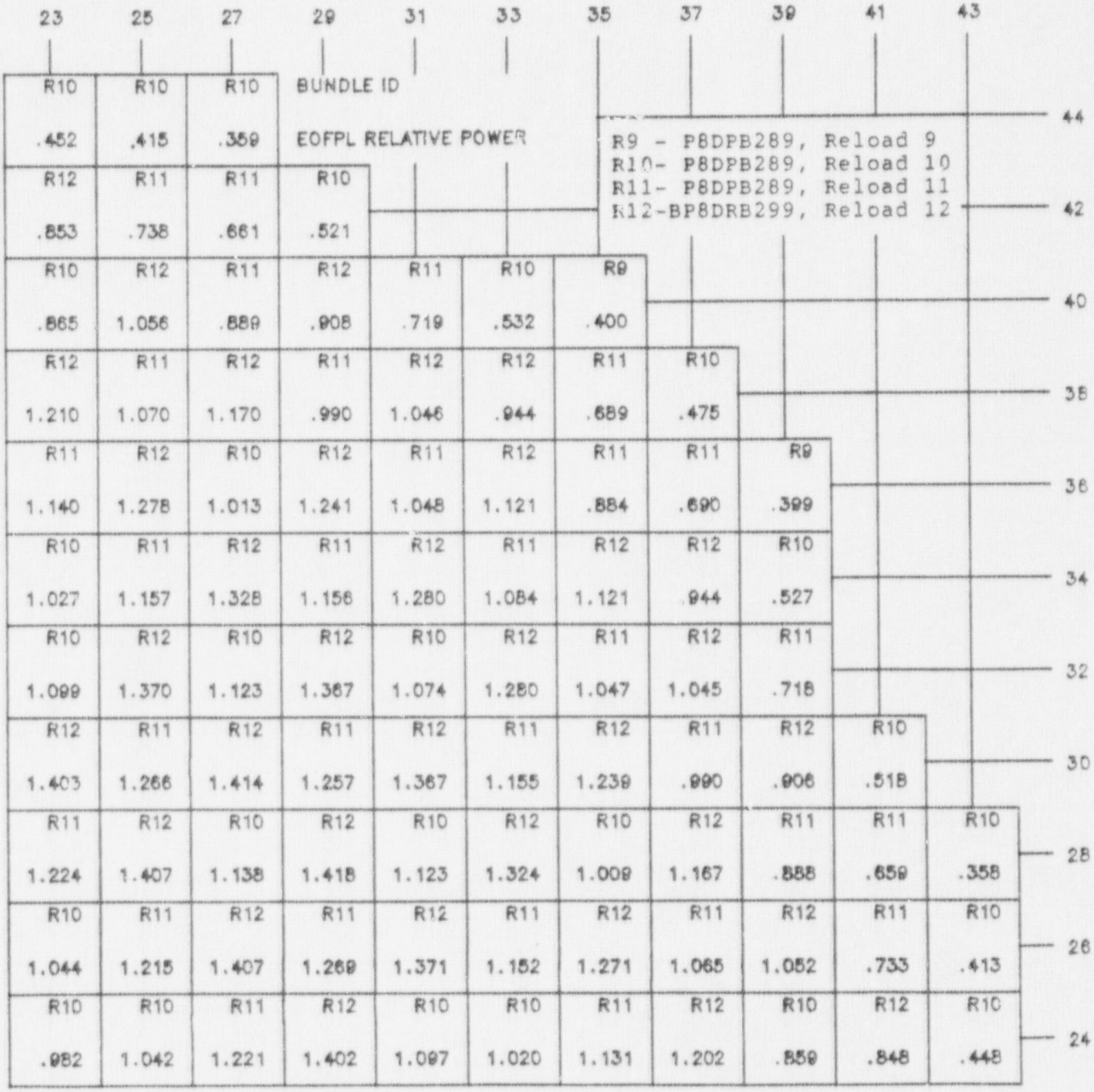

FIGURE 5.1.3
VY CYCLE 13 RODDED DEPLETION-ARO AT EOFPL, BUNDLE AVERAGE RELATIVE POWERS

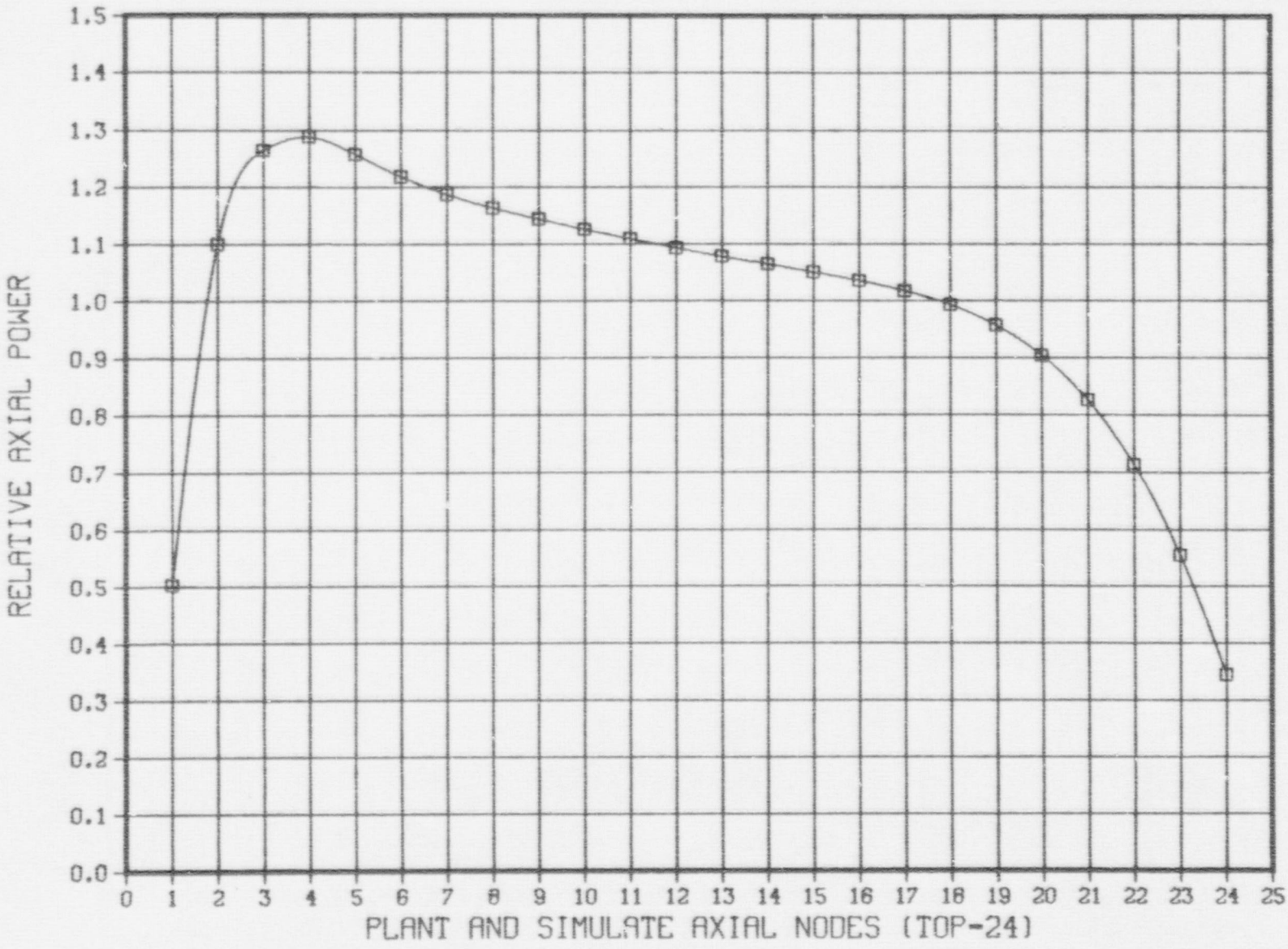

FIGURE 5.1.4

VY CYCLE 13 RODDED DEPLETION-ARO AT EOFPL, CORE AVERAGE AXIAL POWER DISTRIBUTION

VERMONT YANKEE
CYCLE 13 HALING DEPLETION
EOFPL BUNDLE AVERAGE EXPOSURES

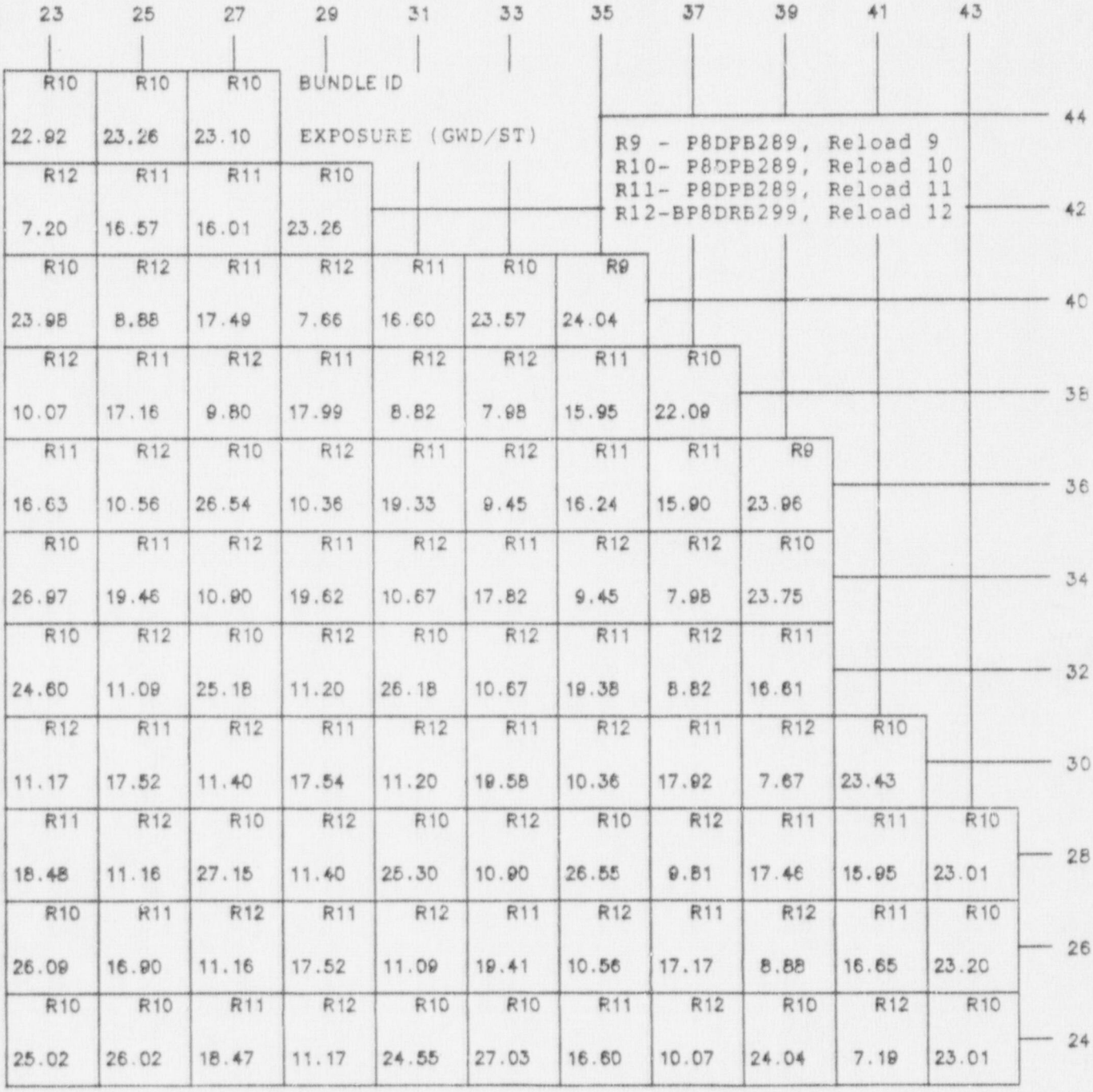

FIGURE 5.2.1

VY CYLCE 13 HALING DEPLETION, EOFPL BUNDLE AVERAGE EXPOSURES

VERMONT YANKEE
CYCLE 13 RODDED DEPLETION
EOFPL BUNDLE AVERAGE EXPOSURES

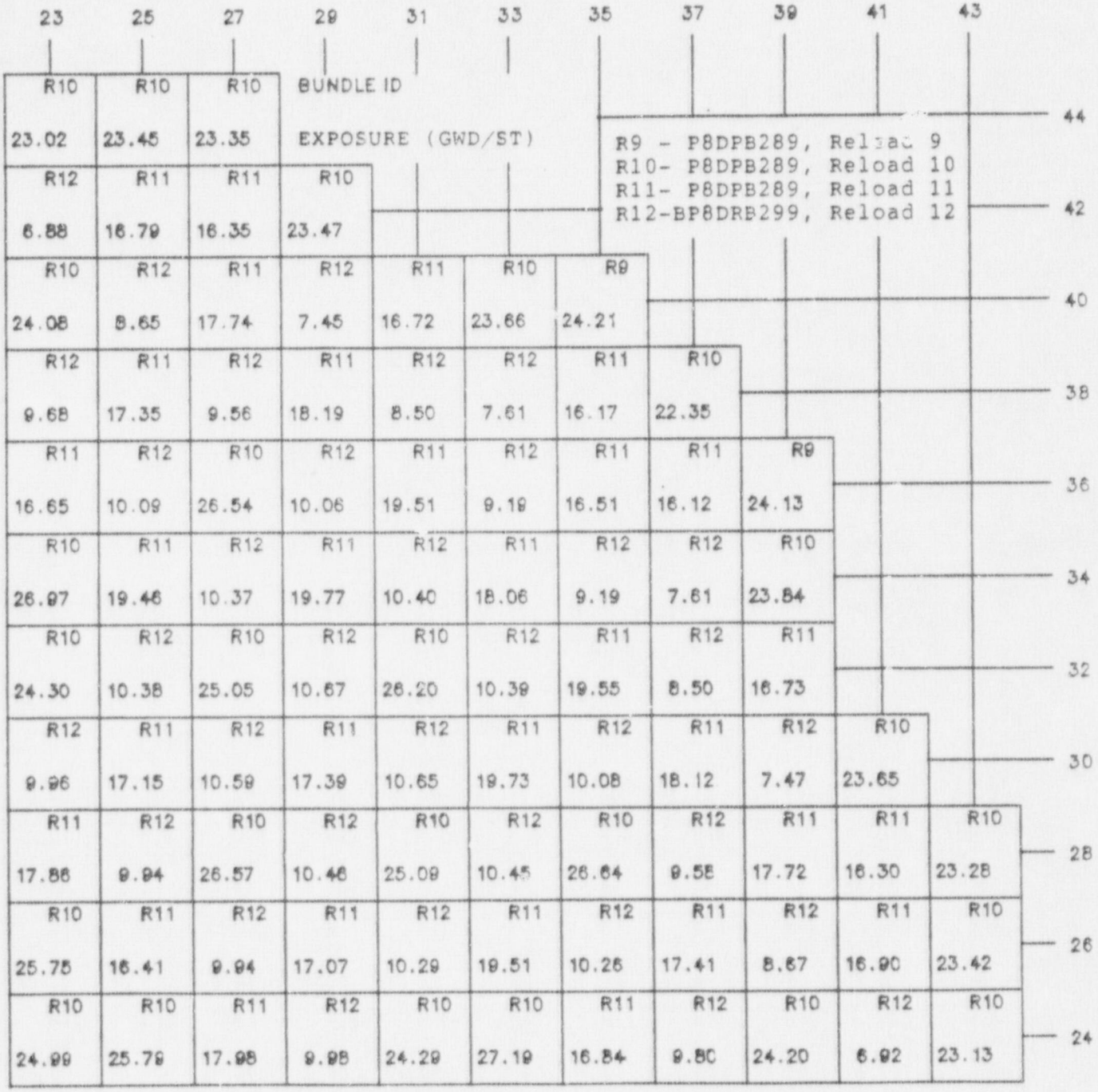

FIGURE 5.2.2

VY CYCLE 13 RODDED DEPLETION, EOFPL BUNDLE AVERAGE EXPOSURES

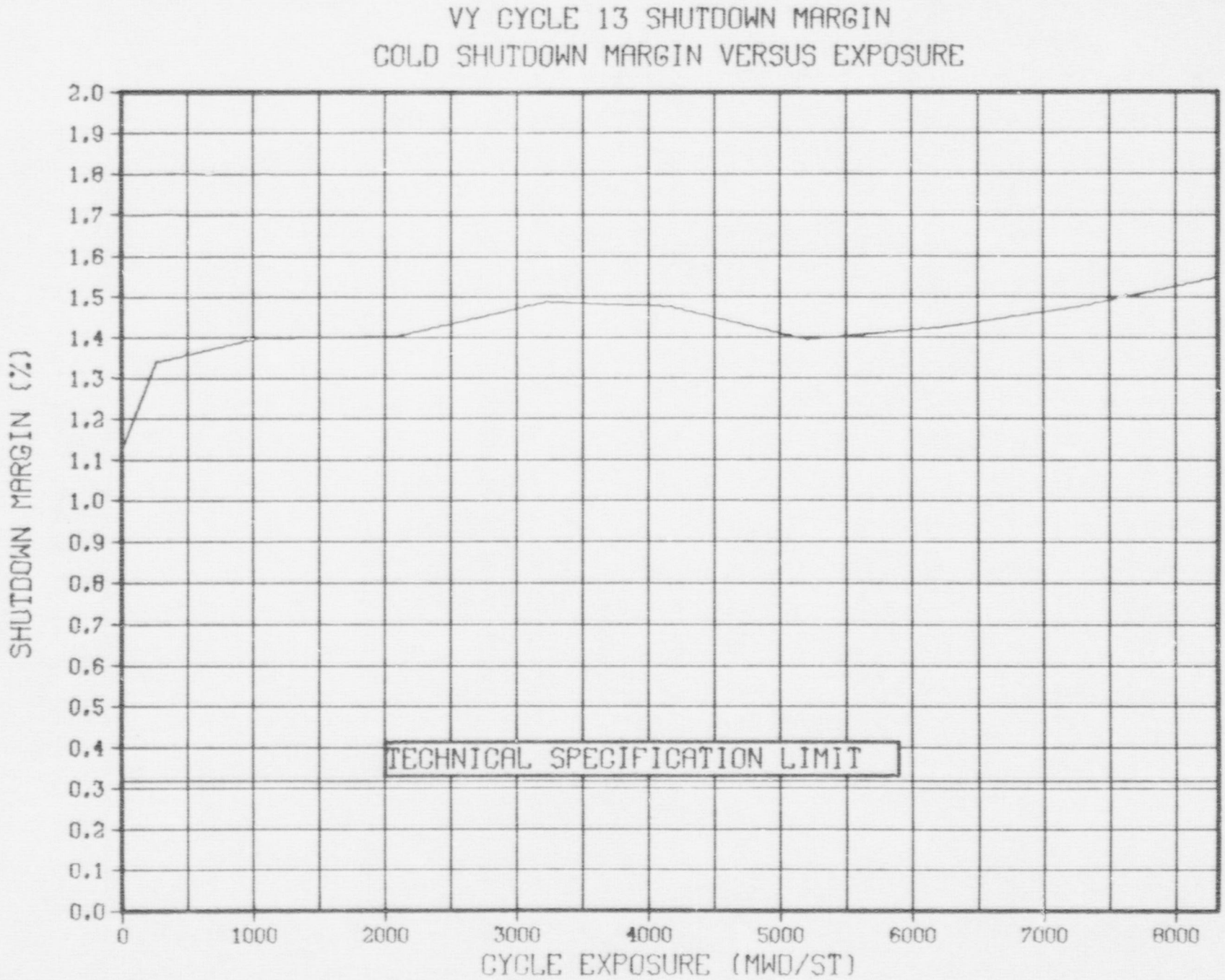

FIGURE 5.3.1

VY CYCLE 13 COLD SHUTDOWN DELTA K IN PERCENT VERSUS CYCLE EXPOSURE

6.0 THERMAL-HYDRAULIC DESIGN

The thermal-hydraulic evaluation of the Reload Cycle was performed using the methods described in the following section.

6.1 Steady-State Thermal Hydraulics

Core steady-state thermal-hydraulic analyses were performed using the FIBWR [11,12] computer code. The FIBWR code incorporates a detailed geometrical representation of the complex flow paths in a BWR core, and explicitly models the leakage flow to the bypass region. FIBWR calculates the core pressure drop and total bypass flow for a given total core flow. The power distribution, inlet enthalpy, and geometry are presumed known and are supplied to FIBWR. The power distribution is derived by SIMULATE [4]. Core pressure drop and total leakage flow predicted by the FIBWR code were used in setting the initial conditions for the system transient analysis model.

6.2 Reactor Limits Determination

The objective for normal operation and anticipated transient events is to maintain nucleate boiling. Avoiding a transition to film boiling protects the fuel cladding integrity. Based on Reference 3, the fuel cladding integrity safety limit for Vermont Yankee is a Lowest Allowable Minimum Critical Power Ratio (LAMCPR) of 1.07. Operating limits are specified to maintain adequate margin to onset of the boiling transition. The figure of merit utilized for plant operation is the Critical Power Ratio (CPR). This is defined as the ratio of the critical power (bundle power at which some point within the assembly experiences onset of boiling transition) to the operating bundle power. Thermal margin is stated in terms of the minimum value of the critical power ratio, MCPR, which corresponds to the most limiting fuel assembly in the core. Both the transient (safety) and normal operating thermal limits in terms of MCPR are derived based on the GEXL correlation as described in Reference 13.

Vermont Yankee Technical Specifications [8] limit the operation of the Reload Cycle fuel to a linear heat generation rate (LHGR) limit of 13.4 kW/ft. The basis for a MLHGR of 13.4 kW/ft can be found in Reference 3.

7.0 ACCIDENT ANALYSIS

7.1 Transient Analysis

Transient simulations are performed to assess the impact of certain transients on the heat transfer characteristics of the fuel. The figure of merit used is the Critical Power Ratio (CPR). It is the purpose of the analysis to determine the minimum critical power ratio (MCPR) such that the safety limit is not violated for the transients considered.

7.1.1 Methodology

The analysis requires two types of simulations. A system level simulation is performed to determine the overall plant response. Transient core inlet and exit conditions and normalized power from the system level calculation are used to perform detailed thermal-hydraulic simulations of the fuel, referred to as "hot channel calculations". The hot channel simulations provide the bundle transient ΔCPR (the initial bundle CPR minus the MCPR experienced during the transient).

The system level simulations are performed with the model documented in Reference 14.

The hot channel calculations are performed with the RETRAN [15] and TCPYA01 [16] computer codes. The GEXL correlation [13] is used in TCPYA01 to evaluate critical power ratio. The calculational procedure is outlined below.

The hot channel transient ΔCPR calculations employ a series of "inner" and "outer" iterations, as illustrated by the flow chart in Figure 7.1.1. The outer loop iterates on the hot channel initial power level. This is necessary because the ΔCPR for a given transient varies with Initial Critical Power Ratio (ICPR). However, only the ΔCPR corresponding to a transient MCPR equal to the safety limit (i.e., 1.07 + ΔCPR = ICPR) is appropriate. The approximate constancy of the ΔCPR/ICPR ratio is useful in these iterations. Each outer iteration requires a RETRAN hot channel run to

calculate the transient enthalpies, flows, pressure and saturation properties at each time step. These are required for input to the TCPYA01 code. TCYPA01 is then used to calculate a CPR at each time step during the transient, from which a transient ΔCPR is derived. The hot channel model assumes a chopped cosine axial power shape with a peak/average ratio of 1.4.

The inner loop iterates on the hot channel inlet flow. These iterations are necessary because the RETRAN hot channel model calculates the entrance loss coefficient when the initial power level, flow, and pressure drop are given. The pressure drop is assumed equal to the core average pressure drop, and the flow is varied for a given power level until the calculated entrance loss coefficient is correct. FIBWR [11, 12] is utilized to estimate the correct inlet flow for a particular power level and pressure drop.

7.1.2 Initial Conditions and Assumptions

The initial conditions for the system simulations are based on maximum turbine capacity of 105% of rated steam flow. The corresponding reactor conditions are 104.5% core thermal power and 100% core flow. The core axial power distribution for each of the exposure points is based on the 3-D SIMULATE predictions associated with the generation of the reactivity data (Section 7.1.3). The core inlet enthalpy is set so that the amount of carryunder from the steam separators and the quality in the liquid region outside the separators is as close to zero as possible. For fast pressurization transients, this maximizes the initial pressurization rate and predicts a more severe neutron power spike. A summary of the initial operating state used for the system simulations is provided in Table 7.1.1.

Assumptions specific to a particular transient are discussed in the section describing the transient. In general, the following assumptions are made for all transients:

1. Scram setpoints are at Technical Specification [8] limits.

2. Protective system logic delays are at equipment specification limits.

3. Safety/relief valve and safety valve capacities are based on Technical Specification [8] rated values.

4. Safety/relief valve and safety valve setpoints are modeled as being at the Technical Specification [8] upper limit. Valve responses are based on slowest specified response values.

5. Control rod drive scram speed is based on the Technical Specification limits. The analysis addresses a dual set of scram speeds, referred to as the "Measured" and the "67B" scram times. "Measured" refers to the faster scram times given in Section 3.3.C.1.1 of the Technical Specifications [8]. "67B" refers to the slower scram times given in Section 3.3.C.1.2 of the Technical Specifications [8].

7.1.3 Reactivity Functions

The methods used to generate the fuel temperature, moderator density, and scram reactivity functions are described in detail in Reference 17. The method is outlined below.

A complete set of reactivity functions, the axial power distribution, and the kinetics parameters are generated from base states established for EOFPL, EOFPL-1000 MWD/ST, EOFPL-2000 MWD/ST, and BOC exposure statepoints. These statepoints are characterized by exposure and void history distributions, control rod patterns, and core thermal-hydraulic conditions. The latter are consistent with the assumed system transient conditions provided in Table 7.1.1.

The BOC base state is established by shuffling from the previously defined Current Cycle endpoint into the Reload Cycle loading pattern. A criticality search provides an estimate of the BOC critical rod pattern. The

EOFPL and intermediate core exposure and void history distributions are calculated with a Haling depletion as described in Section 5.2. The EOFPL state is unrodded. As such, it is defined sufficiently. However, EOFPL-1000 MWD/ST and EOFPL-2000 MWD/ST exposure statepoints require base control rod patterns. These are developed to be as "black and white" as possible. That is, beginning with the rodded depletion configuration, all control rods which are more than half inserted are fully inserted, and all control rods which are less than half inserted are fully withdrawn. If the SIMULATE calculated parameters are within operating limits, then this configuration becomes the base case. If the limits are exceeded, a minimum number of control rods are adjusted a minimum number of notches until the parameters fall within limits. Using this method, the control rod patterns and resultant power distributions are established which minimize the scram reactivity function and maximize the core average moderator density reactivity coefficient. For the transients analyzed, this tends to maximize the power response.

At each exposure statepoint, reactivity function table sets are produced for the 12 core-volumes of the Vermont Yankee RETRAN model. The fuel temperature (Doppler) data set is generated by fixing the power distribution while varying the fuel temperature associated with that power. A moderator density table set is generated specifically for each transient type. The moderator density reactivity functions for the subcooling transient are generated by quasi-statically varying the inlet subcooling only. The moderator enthalpy source distribution is allowed to iterate with the calculated nuclear power until equilibrium is reached. The moderator density reactivity functions for the pressurization transients are generated by quasi-statically varying the core pressure. A series of calculations are performed for various inlet moderator temperatures. The moderator enthalpy source distribution is fixed at the base state case.

In order to qualitatively compare the core reactivity characteristics between different base configurations, core average reactivity coefficients at selected conditions are provided in Table 7.1.2. Calculated point kinetics parameters for RETRAN are also provided.

The reactivities versus scram insertion are calculated at constant, pretransient moderator conditions. These are fitted to yield highly detailed scram reactivity curves. The curves are combined with the appropriate rod position versus time data to generate the final RETRAN scram reactivity functions. Figures 7.1.2 through 7.1.4 display the inserted rod worths and rod positions as functions of scram time for the "Measured" scram time analysis. Figures 7.1.5 through 7.1.7 display similar curves for the "67B" scram time analysis.

7.1.4 Transients Analyzed

Past licensing analysis has shown that the transients which result in the minimum core thermal margins are:

1. Generator load rejection with complete failure of the turbine bypass system.

2. Turbine trip with complete failure of the turbine bypass system.

3. Loss of feedwater heating.

The "feedwater controller failure" (maximum demand) transient is not a limiting transient for Vermont Yankee, because of the plant's 110% steam flow bypass system. Past analyses have shown this transient to be considerably less limiting than any of the above for all exposure points. Brief descriptions and the results of the transients analyzed are provided in the following section.

7.2 Transient Analysis Results

The transients selected for consideration were analyzed at exposure points of EOFPL, EOFPL-1000 MWD/ST, and EOFPL-2000 MWD/ST; the loss of feedwater heating transient was also evaluated at BOC conditions. The transient results reported in Table 7.2.1 correspond to the limiting bundle type in the core.

7.2.1 Turbine Trip Without Bypass Transient (TTWOBP)

The transient is initiated by a rapid closure (0.1 second closing time) of the turbine stop valves. It is assumed that the steam bypass valves, which normally open to relieve pressure, remain closed. A reactor protection system signal is generated by the turbine stop valve closure switches. Control rod drive motion is conservatively assumed to occur 0.27 seconds after the start of turbine stop valve motion. The ATWS recirculation pump trip is assumed to occur at a setpoint of 1150 psig dome pressure. A pump trip time delay of 1.0 second is assumed to account for logic delay and M-G set generator field collapse. In simulating the transient, the bypass piping volume up to the valve chest is lumped into the control volume upstream of the turbine stop valves. Predictions of the salient system parameters at the three exposure points are shown in Figures 7.2.1 through 7.2.3 for the "Measured" scram time analysis.

7.2.2 Generator Load Rejection Without Bypass Transient (GLRWOBP)

The transient is initiated by a rapid closure (0.3 seconds closing time) of the turbine control valves. As in the case of the turbine trip transient, the bypass valves are assumed to fail. A reactor protection system signal is generated by the hydraulic fluid pressure switches in the acceleration relay of the turbine control system. Control rod drive motion is conservatively assumed to occur 0.28 seconds after the start of turbine control valve motion. The same modeling regarding the ATWS pump trip and bypass piping is used as in the turbine trip simulation. The influence of the accelerating main turbine generator on the recirculation system is simulated by specifying the main turbine generator electrical frequency as a function of time for the M-G set drive motors. The main turbine generator frequency curve is based on a 100% power plant startup test and is considered representative for the simulation. The system model predictions for the three exposure points are shown in Figures 7.2.4 through 7.2.6 for the "Measured" scram time analysis.

7.2.3 Loss of Feedwater Heating Transient (LOFWH)

A feedwater heater can be lost in such a way that the steam extraction line to the heater is shut off or the feedwater flow bypasses one of the heaters. In either case, the reactor will receive cooler feedwater, which will produce an increase in the core inlet subcooling, resulting in a reactor power increase.

The response of the system due to the loss of 100°F of the feedwater heating capability was analyzed. This represents the current licensing assumption for the maximum expected single heater or group of heaters that can be tripped or bypassed by a single event.

Vermont Yankee has a scram setpoint of 120% of rated power as part of the Reactor Protection System (RPS) on high neutron flux. In this analysis, no credit was taken for scram on high neutron flux, thereby allowing the reactor power to reach its peak without scram. This approach was selected to provide a bounding and conservative analysis for events initiated from any power level.

The transient response of the system was evaluated at several exposures during the cycle. The transient evaluation at EOFPL-1000 MWD/ST was found to be the limiting case between BOC to EOFPL. The results of the system response to a loss of 100°F feedwater heating capability evaluated at EOFPL-1000 MWD/ST as predicted by the RETRAN code are presented in Figure 7.2.7.

7.3 Overpressurization Analysis Results

Compliance with ASME vessel code limits is demonstrated by an analysis of the Main Steam Isolation Valves (MSIV) closing with failure of the MSIV position switch scram. EOFPL conditions were analyzed. The system model used is the same as that used for the transient analysis (Section 7.1.1). The initial conditions and modeling assumptions discussed in Section 7.1.2 are applicable to this simulation.

The transient is initiated by a simultaneous closure of all four MSIVs. A 3.0 second closing time, which is the Technical Specification [8] minimum, is assumed. A reactor scram signal is generated on APRM high flux. Control rod drive motion is conservatively assumed to occur 0.28 seconds after reaching the high flux setpoint. The system response is shown in Figure 7.3.1 for the "Measured" scram time analysis.

The maximum pressures at the bottom of the reactor vessel calculated for the "Measured" scram time analysis and for the "67B" scram time analysis are given in Table 7.3.1. These results are within the allowable code limit of 10% above vessel design pressure for upset conditions, or 1375 psig.

7.4 Local Rod Withdrawal Error Transient Results

The rod withdrawal error (RWE) is a local core transient caused by an operator erroneously withdrawing a control rod in the continuous withdrawal mode. If the core is operating at its operating limits for MCPR and LHGR at the time of the error, then withdrawal of a control rod could increase both local and core power levels with the potential for overheating the fuel.

There is a broad spectrum of core conditions and control rod patterns which could be present at the time of such an error. For most normal situations it would be possible to fully withdraw a control rod without exceeding 1% clad plastic strain or violating the CPR based fuel cladding integrity safety limit.

To bound the most severe of postulated rod withdrawal error events, a portion of the core MCPR operating limit envelope is specifically defined such that the cladding limits are not violated. The consequences of the error depend on the local power increase, the initial MCPR of the neighboring locations and the ability of the Rod Block Monitor (RBM) System to stop the withdrawing rod before MCPR reaches 1.07.

The most severe transient postulated begins with the core operating according to normal procedures and within normal operating limits. The

operator makes a procedural error and attempts to fully withdraw the maximum worth control rod at maximum withdrawal speed. The core limiting locations are close to the error rod. They experience the spatial power shape transient as well as the overall core power increase.

The core conditions and control rod pattern are conservatively modeled for the bounding case by specifying the following set of concurrent worst case assumptions:

1. The rod should have high reactivity worth. This is provided for by analysis of the core at several exposure points around the core peak reactivity. The test patterns are developed with xenon-free conditions. The xenon free condition and the additional control rod inventory needed to maintain criticality exaggerates the worth of the withdrawn control rod substantially when compared to normal operation with normal xenon levels.

2. The core is initially at 104.5% power and 100% flow.

3. The core power distribution is adjusted with the available control rods to place the locations within the four by four array of bundles around the error rod as close to the operating limits as possible.

4. Of the many patterns tested, the pattern with the highest ΔCPR results is selected as the bounding case.

The Rod Block Monitor System's ability to terminate the bounding case is evaluated on the following bases:

1. Technical Specifications [8] allow each of the separate RBM channels to remain operable if at least half of the Local Power Range Monitor (LPRM) inputs at every level are operable. For the interior RBM channels tested in this analysis, there are a maximum of four LPRM inputs per level. One RBM channel averages the inputs

from the A and C levels; the other channel averages the inputs from the B and D levels. Considering the inputs for a single channel, there are eleven failure combinations of none, one and two failed LPRM strings. The RBM channel responses are evaluated separately at these eleven input failure conditions. Then, for each channel taken separately, the lowest response as a function of error rod position is chosen for comparison to the RBM setpoint.

2. The event is analyzed separately in each of the four quadrants of the core due to the differing LPRM string physical locations relative to the error rod.

Technical Specifications require that both RBM channels be operable during normal operation. Thus, the first channel calculated to intercept the RBM setpoint is assumed to stop the rod. To allow for control system delay times, the rod is assumed to move two inches after the intercept and stop at the following notch.

The analysis is performed using SIMULATE [4]. Necessary properties of that model for use in this analysis are:

1. Accurate bundle power calculation as shown by the PDQ and gamma scan comparisons.

2. Accurate LPRM signal calculation as shown by the detailed TIP trace comparisons.

3. Accurate control rod worths and core power coefficient as shown by the consistent core eigenvalues.

Two separate cases are presented from numerous explicit SIMULATE analyses. The reactor conditions and case descriptions are shown in Figures 7.4.1 and 7.4.2. Case 1 analyzes the bounding event with zero xenon at the most reactive point in the cycle for the worst case abnormal rod pattern configuration. Case 2 is the worst of the 104.5% power conditions modeled

with more normal control rod patterns and equilibrium xenon. The transient results, the ΔCPR and maximum linear heat generation rate (MLHGR) values, are also shown in Figures 7.4.1 and 7.4.2. The ΔCPR values are evaluated such that the implied operating limit MCPR equals 1.07 + ΔCPR. This is done by conserving the figure of merit (ΔCPR/initial CPR) shown by the SIMULATE calculations. The use of this method provides valid ΔCPR values in the analysis of normal operating states where locations near the assumed error rod are not initially near the MCPR operating limit.

Case 2 is the worst of all the rod withdrawal transients analyzed from 104.5% power, full flow and normal rod pattern conditions. Case 2 is bounded by Case 1 with substantial MCPR margin. The Case 1 RBM channel responses are shown in Figures 7.4.3 and 7.4.4. They also show the control rod position at the point where the weakest RBM channel response first intercepts the RBM setpoint. For this same bounding case, the operating limit ΔCPR envelope component versus RBM setpoint is taken from Figure 7.4.1. The same figure shows the resultant LHGR assuming the limiting bundle is placed on the operating limit of 13.4 kW/ft prior to the withdrawal. The calculation includes the 2.2% power spiking penalty. The limiting bundle MLHGR demonstrates margin to the 1% plastic strain limit given the low exposure of the bundle. High exposure bundles which have low 1% plastic strain limits are never limiting.

7.5 Misloaded Bundle Error Analysis Results

7.5.1 Rotated Bundle Error

The primary result of a bundle rotation is a large increase in local pin peaking and R-factor as higher enrichment pins are placed adjacent to the surrounding wide water gaps. In addition, there may be a small increase in reactivity, depending on the exposure and void fraction states. The R-factor increase results in a CPR reduction, while the local pin peaking factor increase results in a higher pin LHGR. The objective of the analysis is to insure that in the worst possible rotation, the LHGR and CPR safety limits are not violated with the most limiting monitored bundles on their operating limits.

To analyze the CPR response, rotated bundle R-factors as a function of exposure are developed by adding the largest possible ΔR-factor resulting from a rotation to the exposure dependent R-factors of the properly oriented bundles [13]. Using these rotated bundle R-factors, the MCPR values resulting from a bundle rotation are determined using SIMULATE. This is done for each control rod sequence throughout the cycle. The process is repeated with the K-infinity of the limiting bundle modified slightly to account for the increase in reactivity resulting from the rotation. For each sequence, the MCPR for the properly oriented bundles is adjusted by a ratio necessary to place the corresponding rotated CPR on its 1.07 safety limit. The maximum of these adjusted MCPR's is the rotated bundle operating limit.

To determine the MLHGR resulting from a rotation, the ratios of the maximum rotated bundle local peaking factor to the maximum properly oriented bundle local peaking are determined for the expected range of exposure and void conditions. The maximum of this ratio is applied to the LHGR operating limit of 13.4 kW/ft. This maximum rotated bundle LHGR is, in addition, modified to account for the possible reactivity increase resulting from the rotation. It is also increased by the 2.2% power spiking penalty.

The results of the rotated bundle analysis are given in Table 7.5.1. Given the low exposure of the bundle, there is sufficient margin to the 1% plastic strain limit.

7.5.2 Mislocated Bundle Error

Misloading a high reactivity assembly into a region of high neutron importance results in a location of high relative assembly average power. Since the assembly is assumed to be properly oriented (not rotated), R-factors used for the misloaded bundle are the standard values for the fuel type.

The analysis uses multiple SIMULATE [4] cases to examine the effects of explicitly mislocating every older interior assembly in a quarter core with a fresh assembly. Because of symmetry, the results apply to the whole core. Edge bundles are not examined because they are never limiting, due to neutron leakage.

The effect of the successive mislocations is examined for every control rod sequence throughout the cycle. For each sequence, the MCPR for the properly loaded core is compared to the misloaded core at the misloaded location. The MCPR for the properly loaded core is adjusted by a ratio necessary to place the mislocated assembly on the 1.07 safety limit. The maximum of these adjusted MCPRs is the mislocated bundle operating limit.

Using the above procedure, all possible mislocations result in calculated operating limits well below that set by the rotated bundle analysis. This makes the mislocated bundle analysis less limiting than the rotated bundle analysis given in Section 7.5.1.

7.6 Control Rod Drop Accident Results

The control rod sequences are a series of rod withdrawal and banked withdrawal instructions specifically designed to minimize the worths of individual control rods. The sequences are examined so that, in the event of the uncoupling and subsequent free fall of the rod, the incremental rod worth is acceptable. Incremental rod worth refers to the fact that rods beyond Group 2 are banked out of the core and can only fall the increment from all in to the rod drive withdrawal position. Acceptable worth is one which produces a maximum fuel enthalpy less than 280 calories/gram.

Some out-of-sequence control rods could accrue potentially high worths. However, the Rod Worth Minimizer (RWM) will prevent withdrawing an out-of-sequence rod, if accidentally selected. The RWM is functionally tested before each startup.

The sequence in the RWM will take the plant from All Rods In (ARI) to well above 20% core thermal power. Above 20% power even multiple operator errors will not create a potential rod drop situation above 280 calories per gram [18, 19, and 20]. Below 20% power, however, the sequences must be examined for incremental rod worth. This is done throughout the cycle using the full core, xenon-free SIMULATE model [4].

Both the A and B sequences were examined. It was found that the highest worth rod was the first rod of the second group. Any of the first four rod arrays shown in Figures 7.6.1 and 7.6.2 may be designated as the first group pulled. However, a specific second group must follow as Table 7.6.1 illustrates. For added conservatism, the highest worth rod in the second group was deliberately assigned to be the first rod pulled. This assures that in any sequence the worths will always be less than those calculated here. The results of the calculations, as presented in Table 7.6.2, fit under the bounding analysis.

Beyond Group 2, procedures [21] apply which severely reduce the rod incremental worths. Therefore, the xenon-free, hot standby worths are much less than the cold, xenon-free worths [9].

TABLE 7.1.1

VY CYCLE 13 SUMMARY OF SYSTEM TRANSIENT MODEL
INITIAL CONDITIONS FOR TRANSIENT ANALYSES

Core Thermal Power (MWth)	1664.0
Turbine Steam Flow (% NBR)	105
Total Core Flow (10^6lbm/hr)	48.0
Core Bypass Flow (10^6lbm/hr)	5.3
Core Inlet Enthalpy (BTU/lbm)	520.9
Steam Dome Pressure (psia)	1034.7
Turbine Inlet Pressure (psia)	986.0
Total Recirculation Flow (10^6lbm/hr)	23.4
Core Plate Differential Pressure (psi)	18.5
Narrow Range Water Level (in.)	35
Average Fuel Gap Conductance	(See Section 4.2)

TABLE 7.1.2

VY CYCLE 13 TRANSIENT ANALYSIS REACTIVITY COEFFICIENTS AT SELECTED CONDITIONS

Calculated Parameter	Cycle Exposure Point (MWD/ST) EOFPL	EOFPL-1000	EOFPL-2000	BOC
Axial Shape Index(1)	-0.0852	-0.2013	-0.2176	-0.1371
Moderator Density Coefficient (Subcooling), ¢/Δu(2) Pressure = 1050 psia Subcooling = 30 BTU/lbm	21.18	21.90	23.44	19.65
Moderator Density Coefficient (Pressurization), ¢/Δu Pressure = 1050 psia Inlet Enthalpy = 520 BTU/lbm	23.31	23.36	24.82	(3)
Fuel Temperature Coefficient at 1130°F, ¢/°F	-0.292	-0.294	-0.297	-0.270
Effective Delayed Neutron Fraction	0.005421	0.005505	0.005571	0.006115
Prompt Neutron Generation Time in Microseconds	41.46	41.48	40.72	38.24

Notes: (1) Axial Shape Index (ASI) = $\frac{P_T - P_B}{P_T + P_B}$

(2) Δu = change in density, in percent

(3) Pressurization transients are not calculated at BOC

TABLE 7.2.1

VY CYCLE 13 TRANSIENT ANALYSIS RESULTS

Transient	Exposure	Peak Prompt Power (Fraction of Initial Value)	Peak Avg. Heat Flux (Fraction of Initial Value)	ΔCPR
Turbine Trip Without Bypass, "Measured" Scram Time	EOFPL	2.732	1.236	.20
	EOFPL-1000	2.155	1.152	.14
	EOFPL-2000	1.409	1.023	.03
Turbine Trip Without Bypass, "67B" Scram Time	EOFPL	3.026	1.278	.25
	EOFPL-1000	2.518	1.208	.20
	EOFPL-2000	1.760	1.077	.07
Generator Load Rejection Without Bypass, "Measured" Scram Time	EOFPL	2.695	1.224	.19
	EOFPL-1000	2.116	1.141	.13
	EOFPL-2000	1.333	1.003	.01
Generator Load Rejection Without Bypass, "67B" Scram Time	EOFPL	3.101	1.280	.25
	EOFPL-1000	2.565	1.210	.20
	EOFPL-2000	1.742	1.065	.06
Loss of 100°F Feedwater Heating	EOFPL	1.213	1.205	.17
	EOFPL-1000	1.222	1.214	.18
	EOFPL-2000	1.223	1.216	.18
	BOC	1.211	1.203	.17

TABLE 7.3.1

VY CYCLE 13 OVERPRESSURIZATION ANALYSIS RESULTS

Conditions	Maximum Pressure at Reactor Vessel Bottom (psia)
"Measured" Scram Time	1265
"67B" Scram Time	1282

TABLE 7.5.1

VY CYCLE 13 ROTATED BUNDLE ANALYSIS RESULTS

Initial MCPR	Resulting MCPR	Resulting LHGR (Kw/ft)
1.20	1.07	17.20

TABLE 7.6.1

CONTROL ROD DROP ANALYSIS - ROD ARRAY PULL ORDER

The order in which rod arrays are pulled is specific once the choice of first group is made.

First Group Pulled is:	Second Group Pulled Must Be:	Successive Group Is Banked Out
Array 1	Array 2	Array 3 or 4
Array 2	Array 1	Array 3 or 4
Array 3	Array 4	Array 1 or 2
Array 4	Array 3	Array 1 or 2

TABLE 7.6.2

VY CYCLE 13 CONTROL ROD DROP ANALYSIS RESULTS

Maximum Incremental Rod Worth Calculated Cold, Xenon Free	.79% ΔK
Bounding Analysis Worth for Enthalpy Less than 280 Calories per Gram (References 18, 19, and 20)	1.30% ΔK

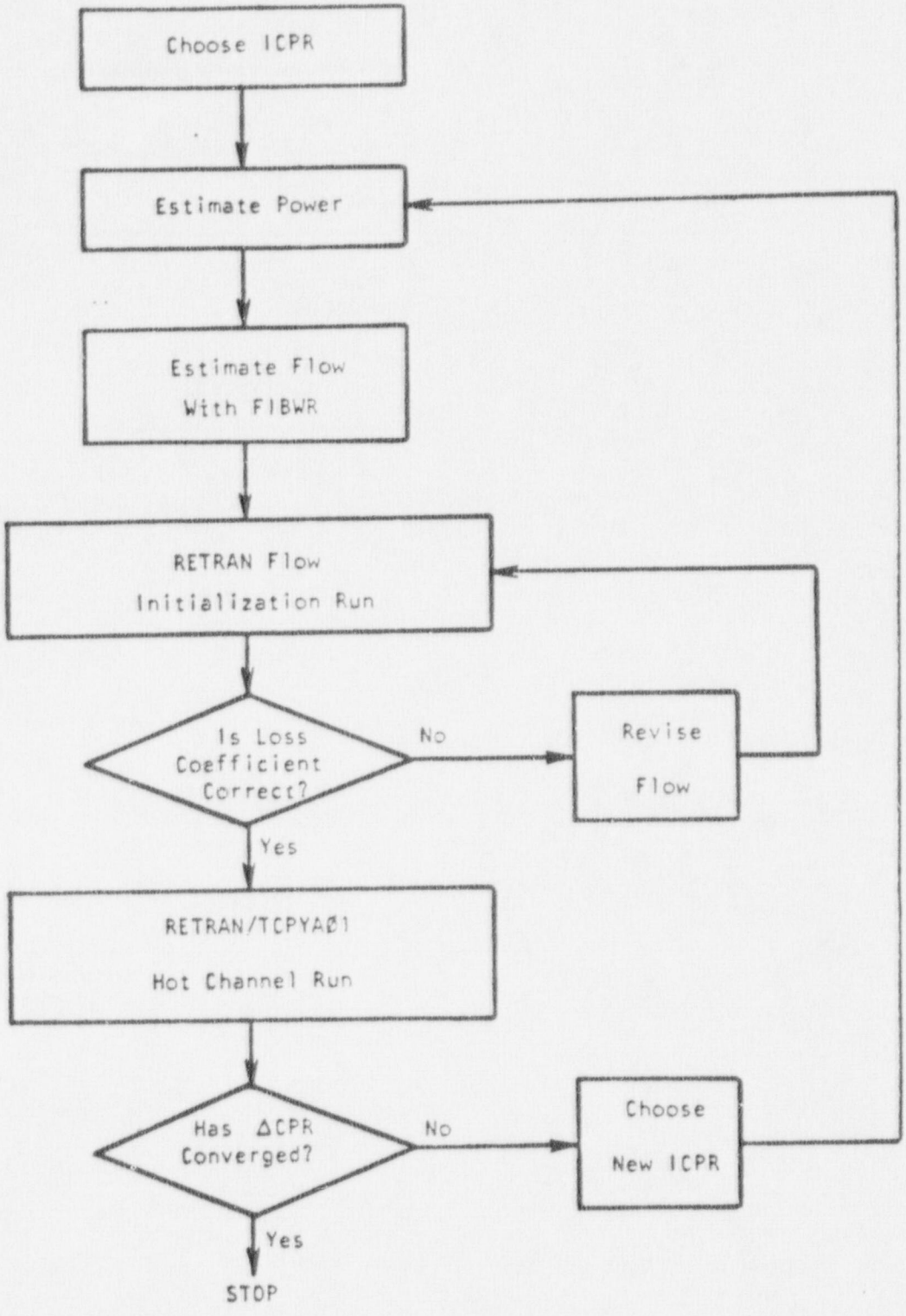

FIGURE 7.1.1

FLOW CHART FOR THE CALCULATION OF ΔCPR USING THE RETRAN/TCPYA01 CODES

VY CYCLE 13 - MST, EOFPL

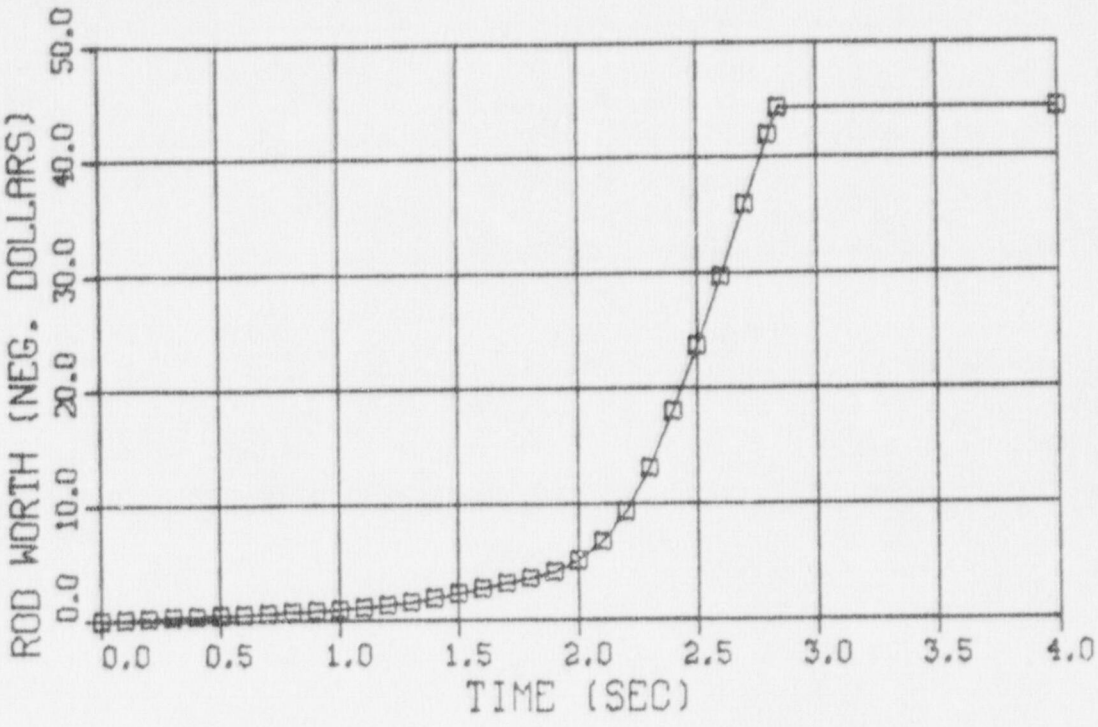

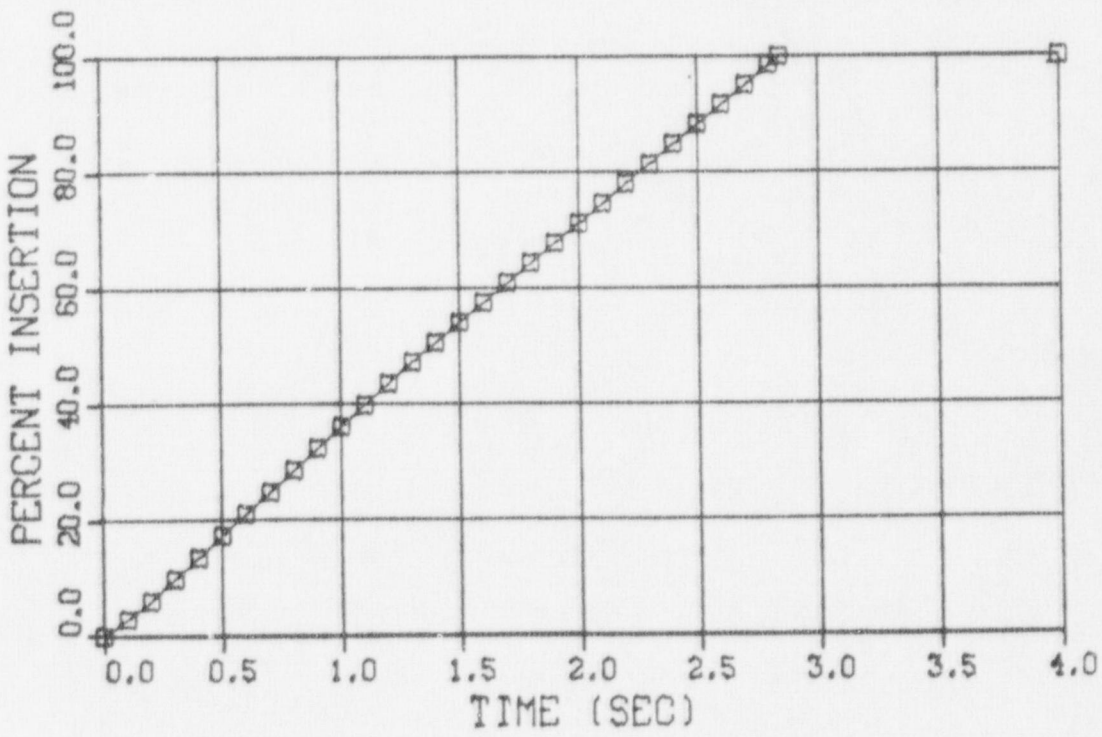

FIGURE 7.1.2
INSERTED ROD WORTH AND ROD POSITION VERSUS TIME FROM INITIAL ROD MOVEMENT AT EOFPL13, "MEASURED" SCRAM TIME

VY CYCLE 13 - MST, EOFPL-1

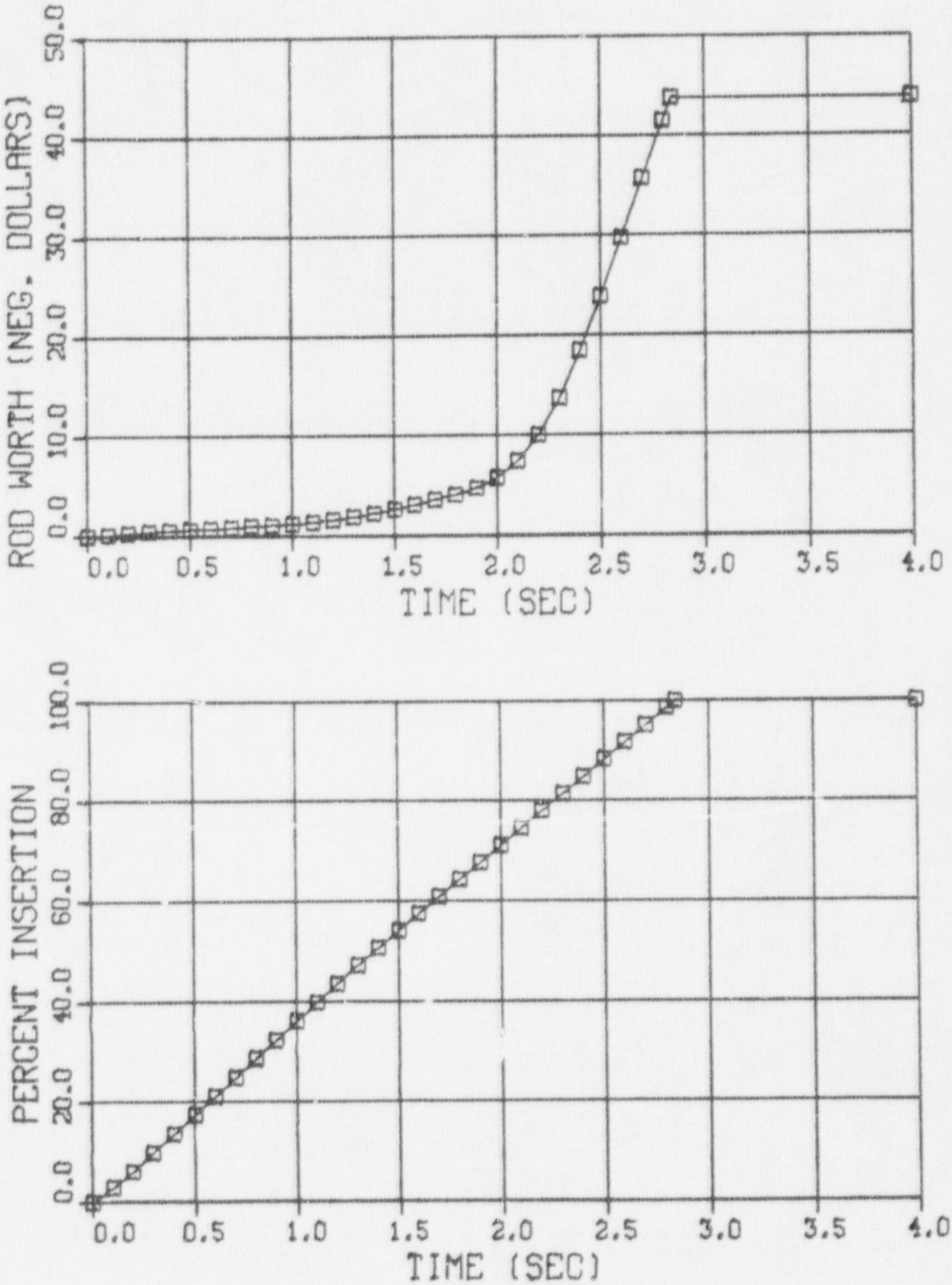

FIGURE 7.1.3
INSERTED ROD WORTH AND ROD POSITION VERSUS TIME FROM INITIAL ROD MOVEMENT AT EOFPL13-1000 MWD/ST "MEASURED" SCRAM TIME

VY CYCLE 13 - MST, EOFPL-2

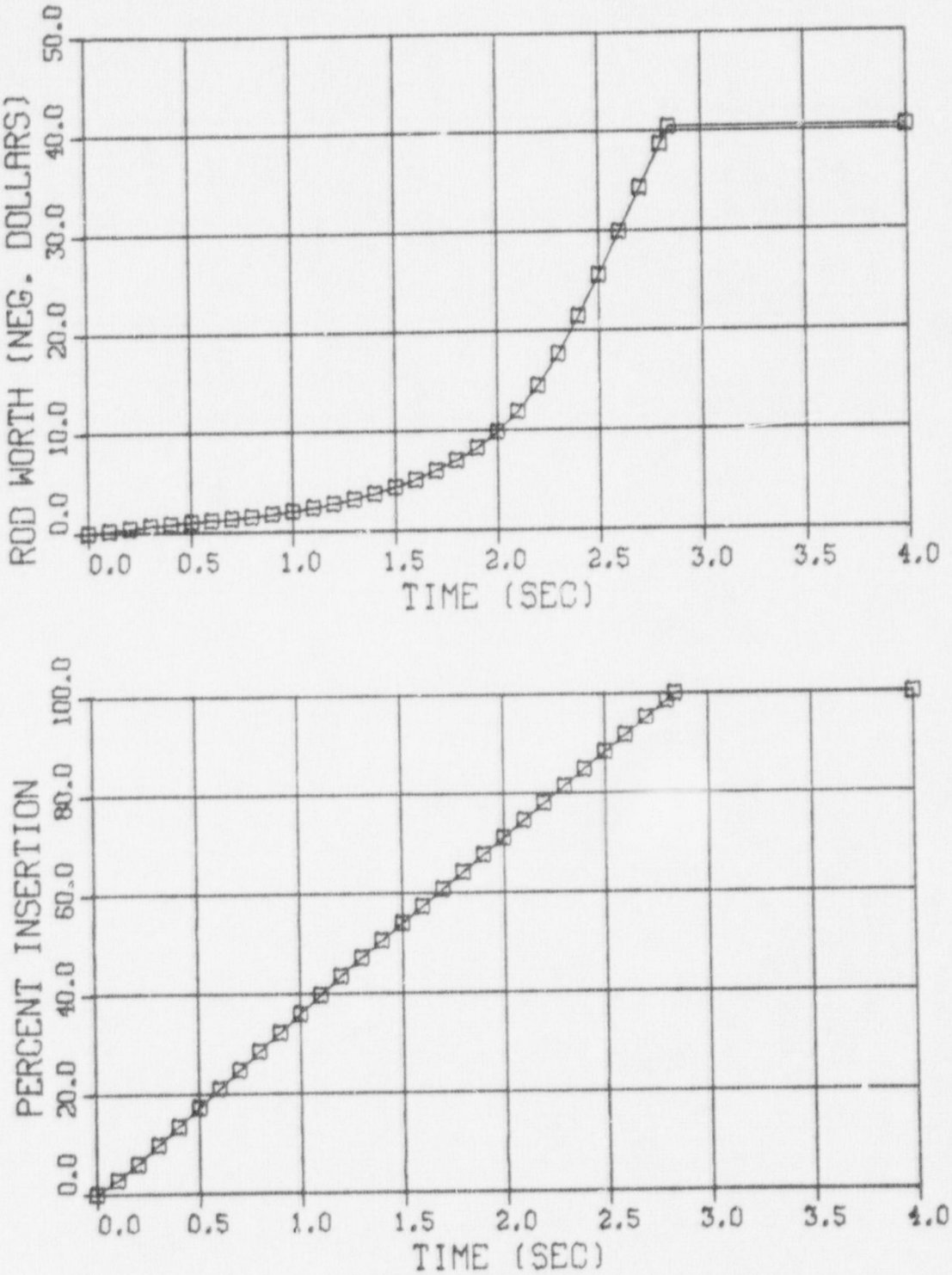

FIGURE 7.1.4
INSERTED ROD WORTH AND ROD POSITION VERSUS TIME FROM
INITIAL ROD MOVEMENT AT EOFPL13-2000 MWD/ST
"MEASURED" SCRAM TIME

VY CYCLE 13 - 67B SCRAM, EOFPL

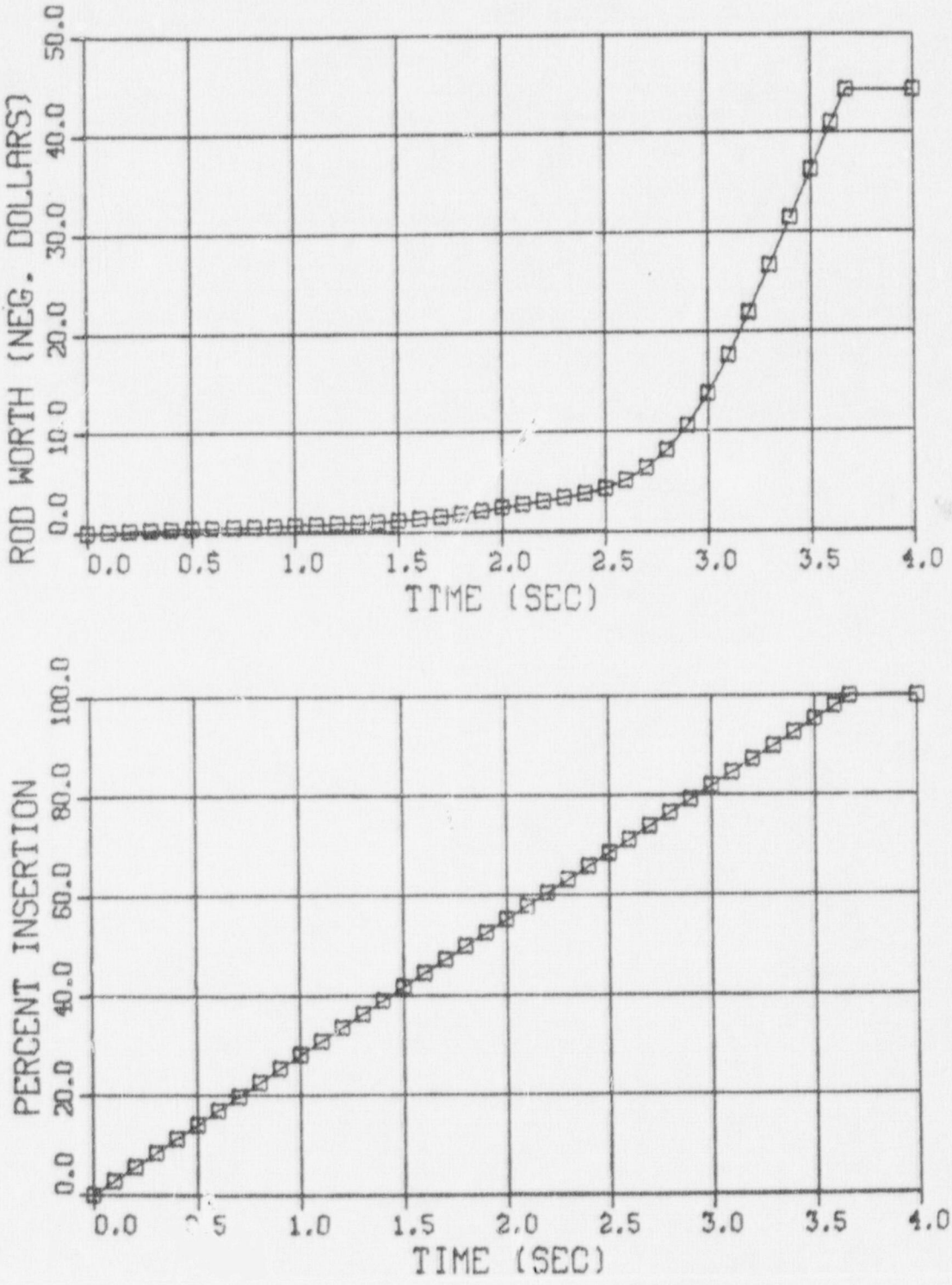

FIGURE 7.1.5
INSERTED ROD WORTH AND ROD POSITION VERSUS TIME FROM INITIAL ROD MOVEMENT AT EOFPL13, "67B" SCRAM TIME

VY CYCLE 13 - 67B SCRAM, EOFPL-1

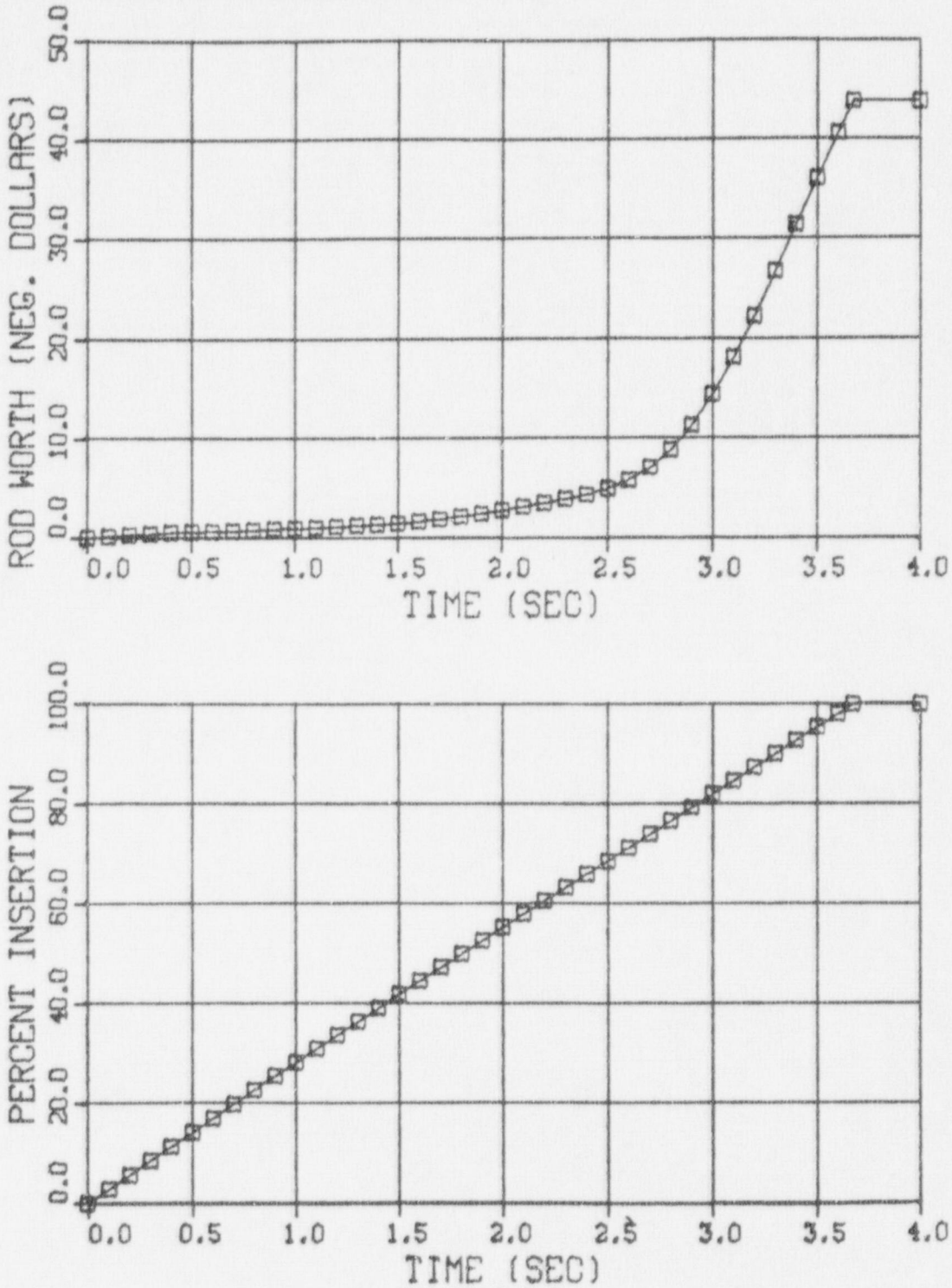

FIGURE 7.1.6

INSERTED ROD WORTH AND ROD POSITION VERSUS TIME FROM INITIAL ROD MOVEMENT AT EOFPL13-1000 MWD/ST

"67B" SCRAM TIME

VY CYCLE 13 - 67B SCRAM, EOFPL-2

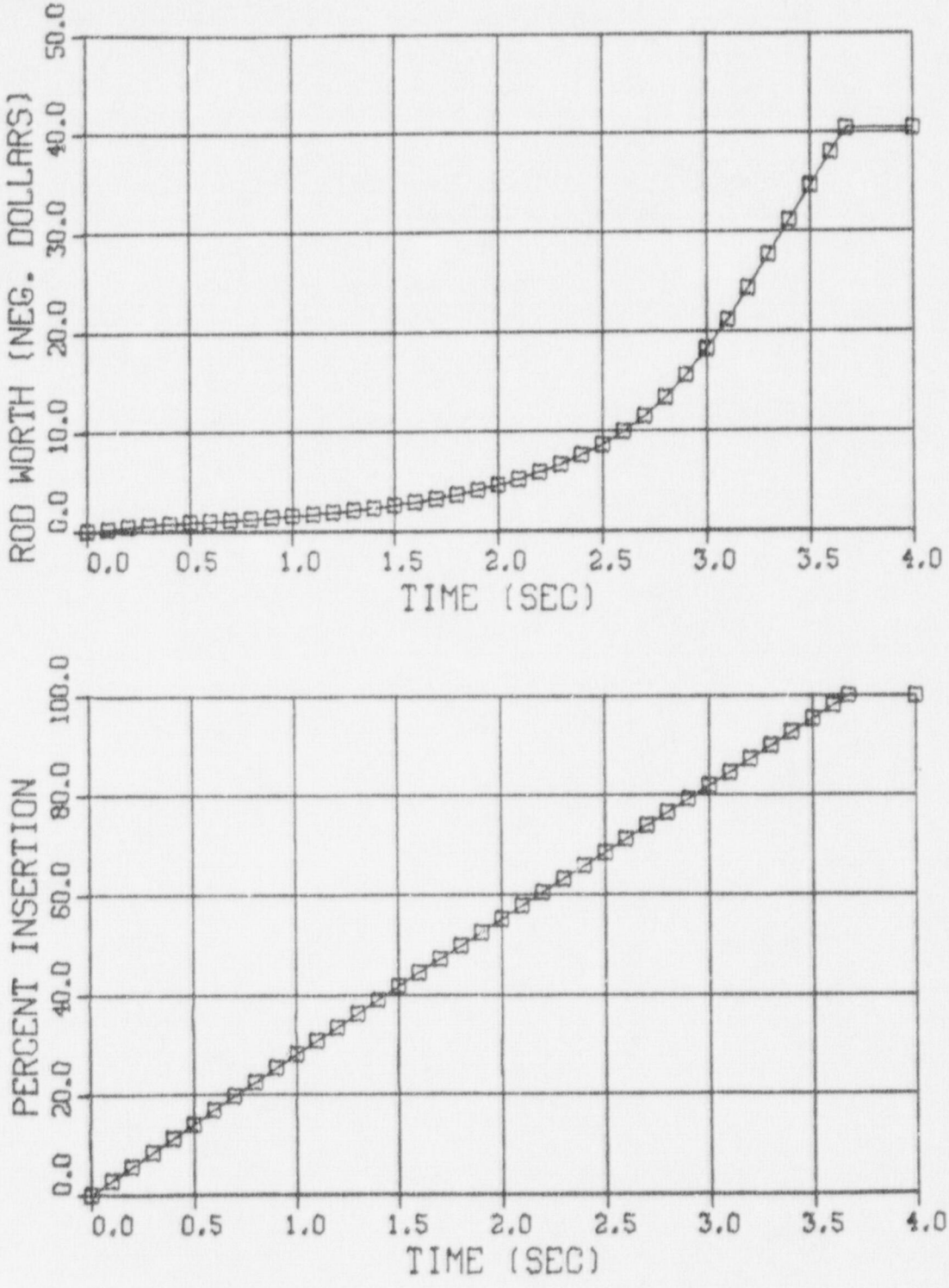

FIGURE 7.1.7
INSERTED ROD WORTH AND ROD POSITION VERSUS TIME FROM
INITIAL ROD MOVEMENT AT EOFPL13-2000 MWD/ST
"67B" SCRAM TIME

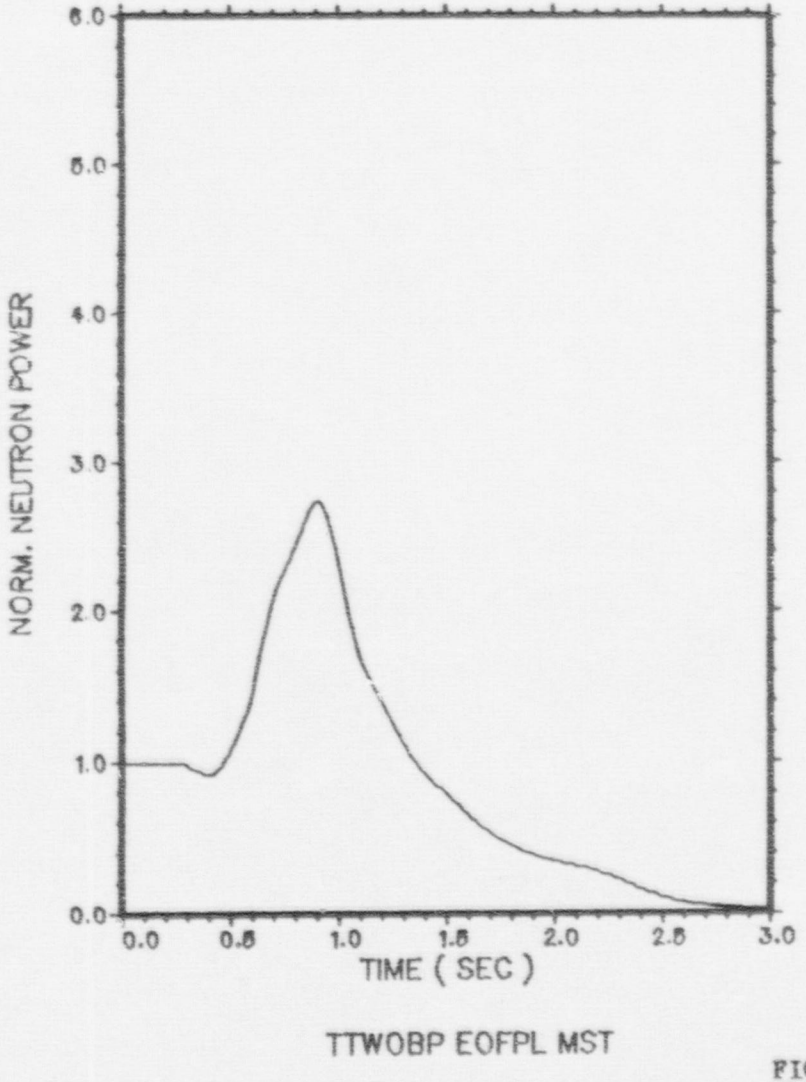

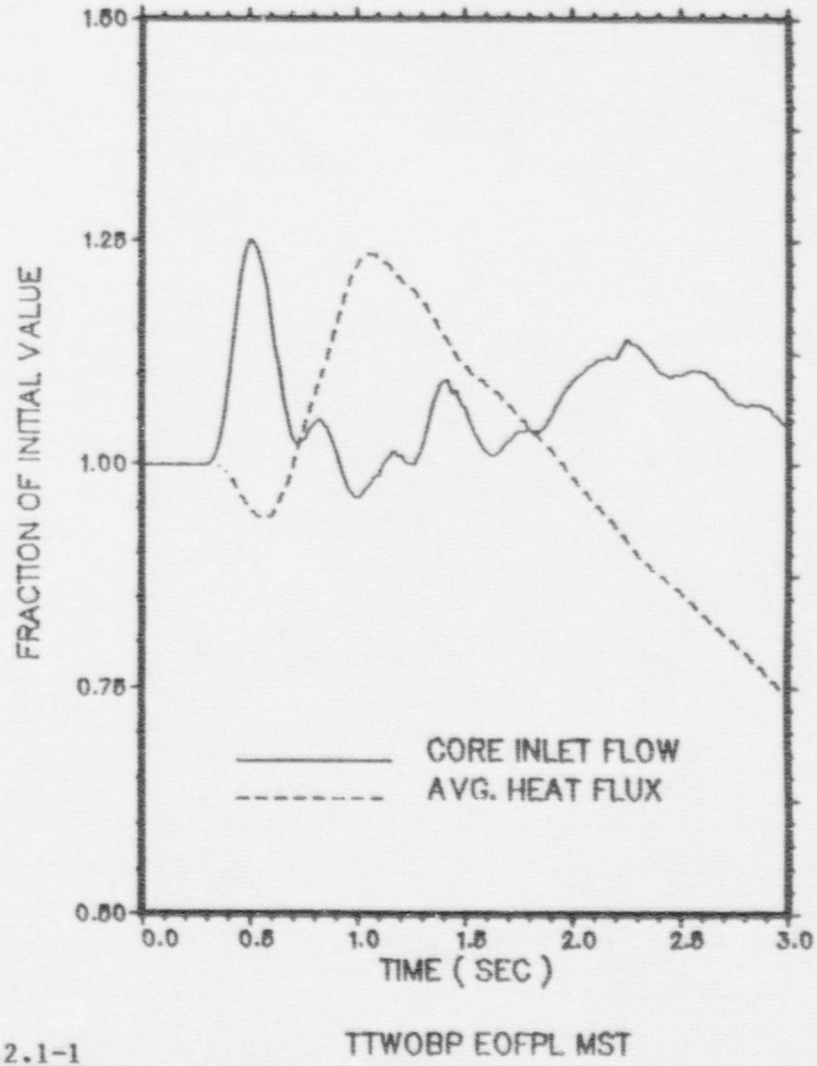

FIGURE 7.2.1-1

TURBINE TRIP WITHOUT BYPASS, EOFPL13

TRANSIENT RESPONSE VERSUS TIME, "MEASURED" SCRAM TIME

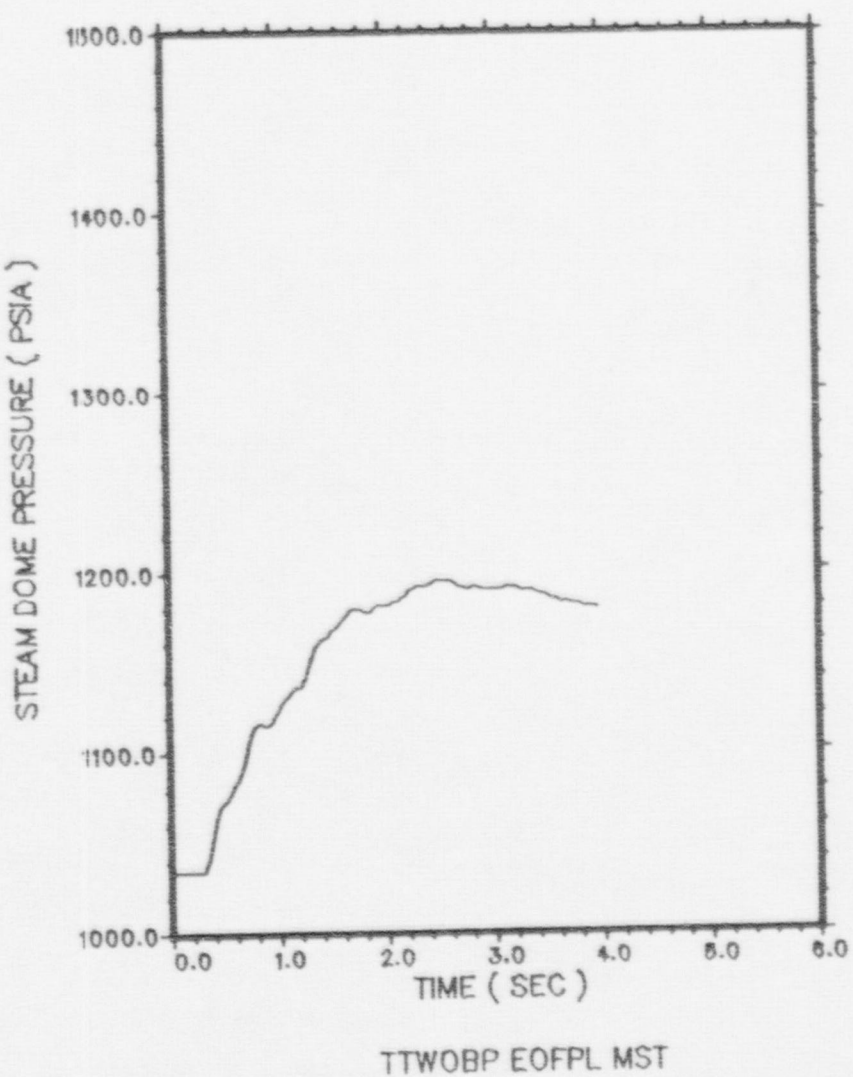

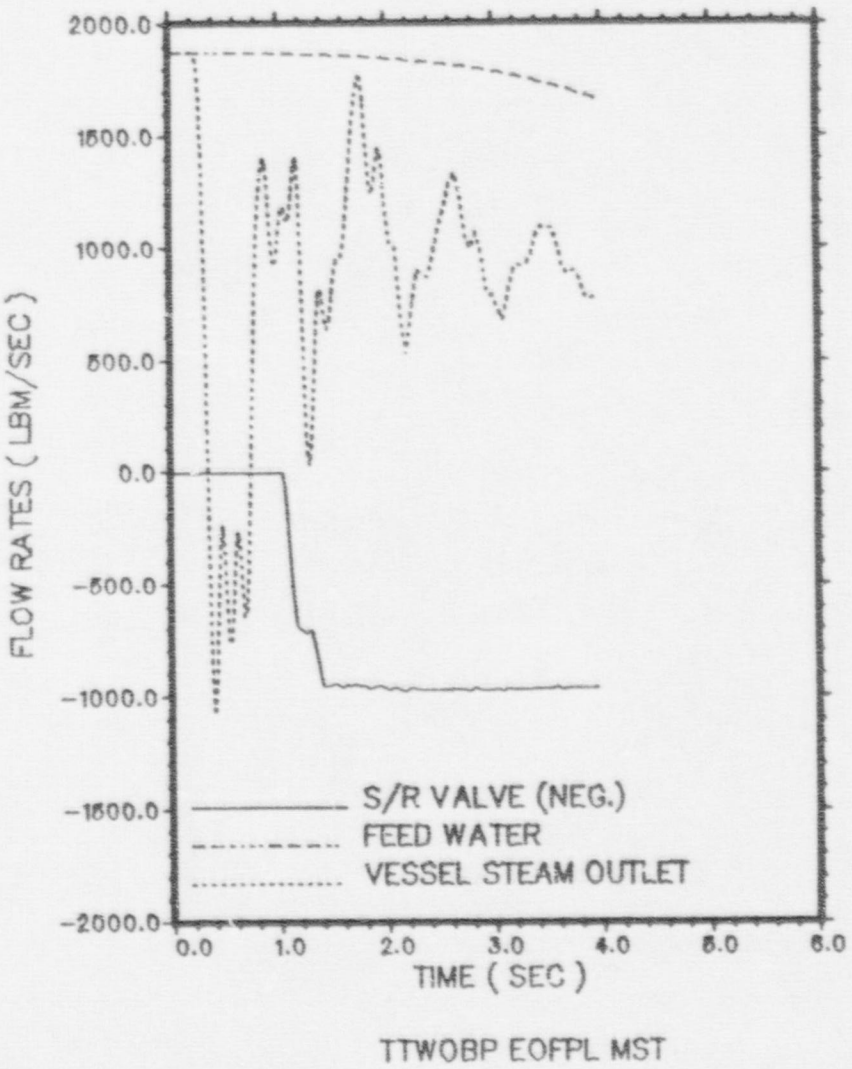

FIGURE 7.2.1-2
TURBINE TRIP WITHOUT BYPASS, EOFPL13
TRANSIENT RESPONSE VERSUS TIME, "MEASURED" SCRAM TIME

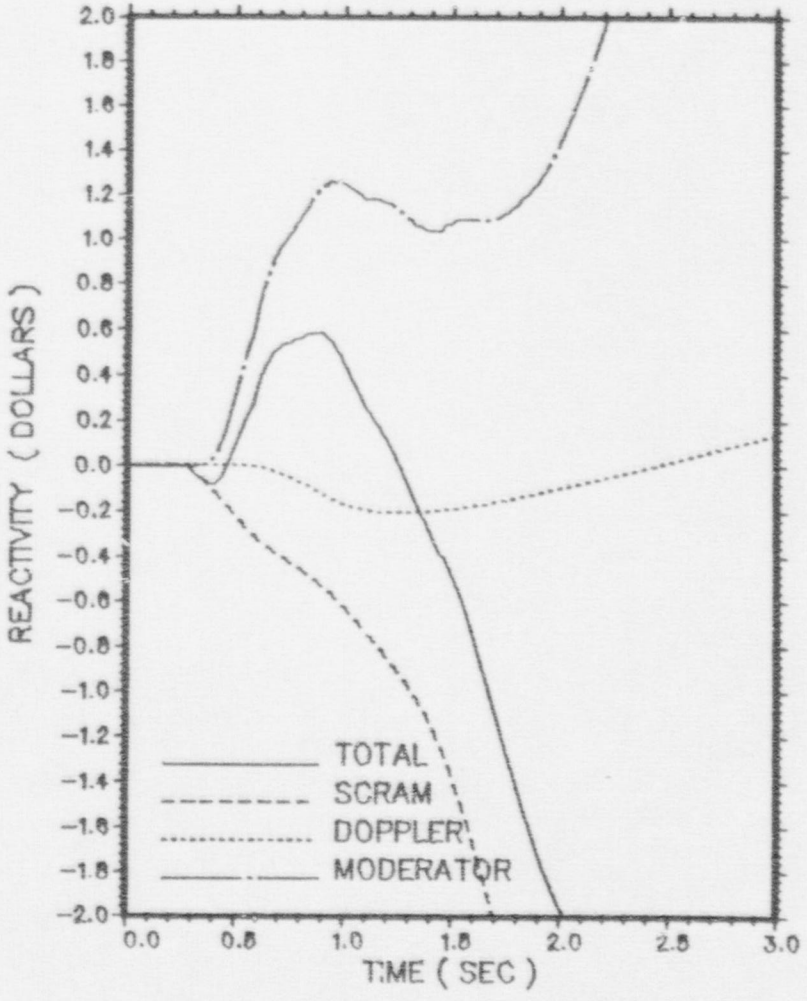

FIGURE 7.2.1-3
TURBINE TRIP WITHOUT BYPASS, EOFPL13
TRANSIENT RESPONSE VERSUS TIME, "MEASURED" SCRAM TIME

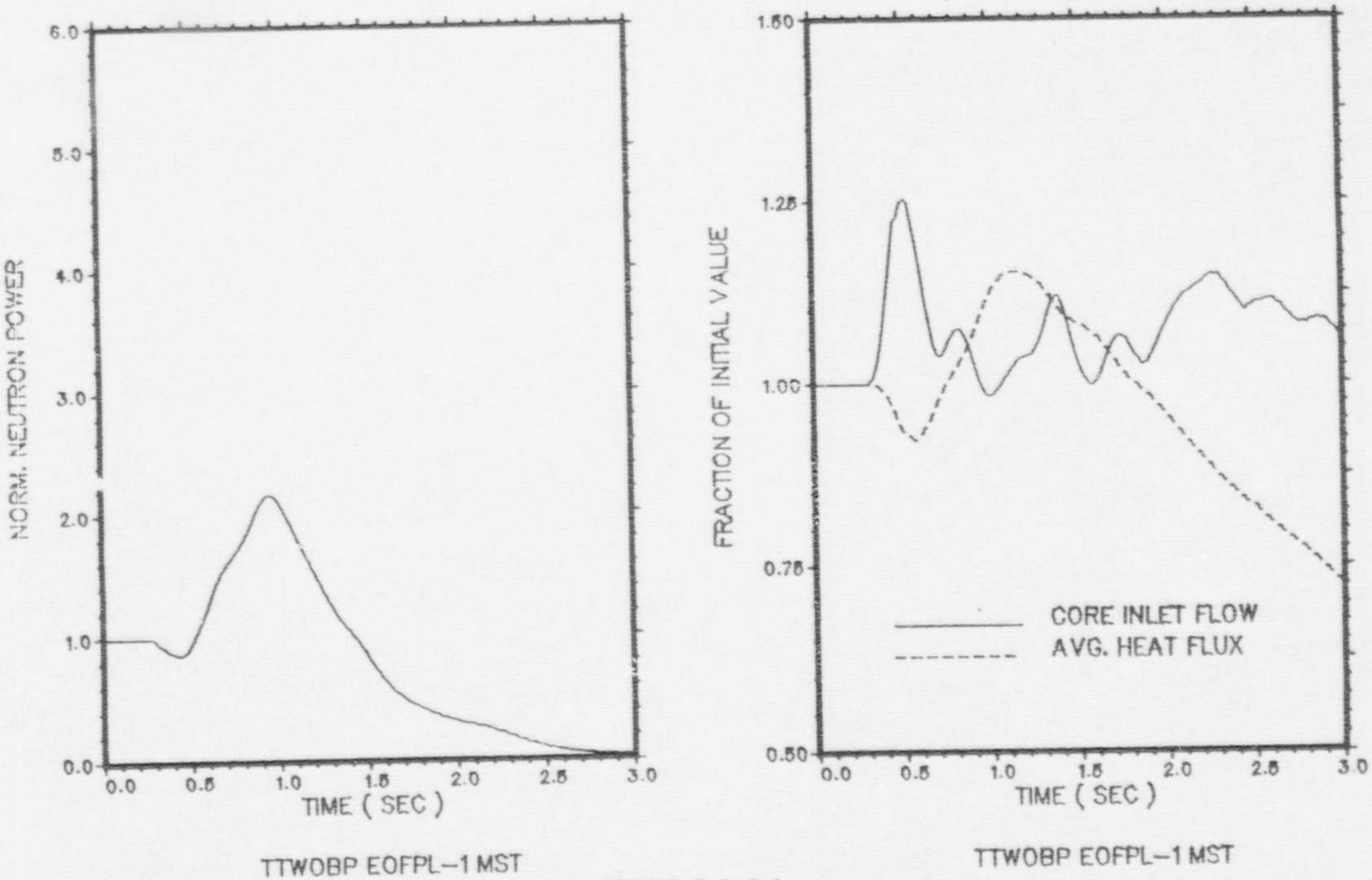

FIGURE 7.2.2-1
TURBINE TRIP WITHOUT BYPASS, EOFPL13-1000 MWD/ST
TRANSIENT RESPONSE VERSUS TIME, "MEASURED" SCRAM TIME

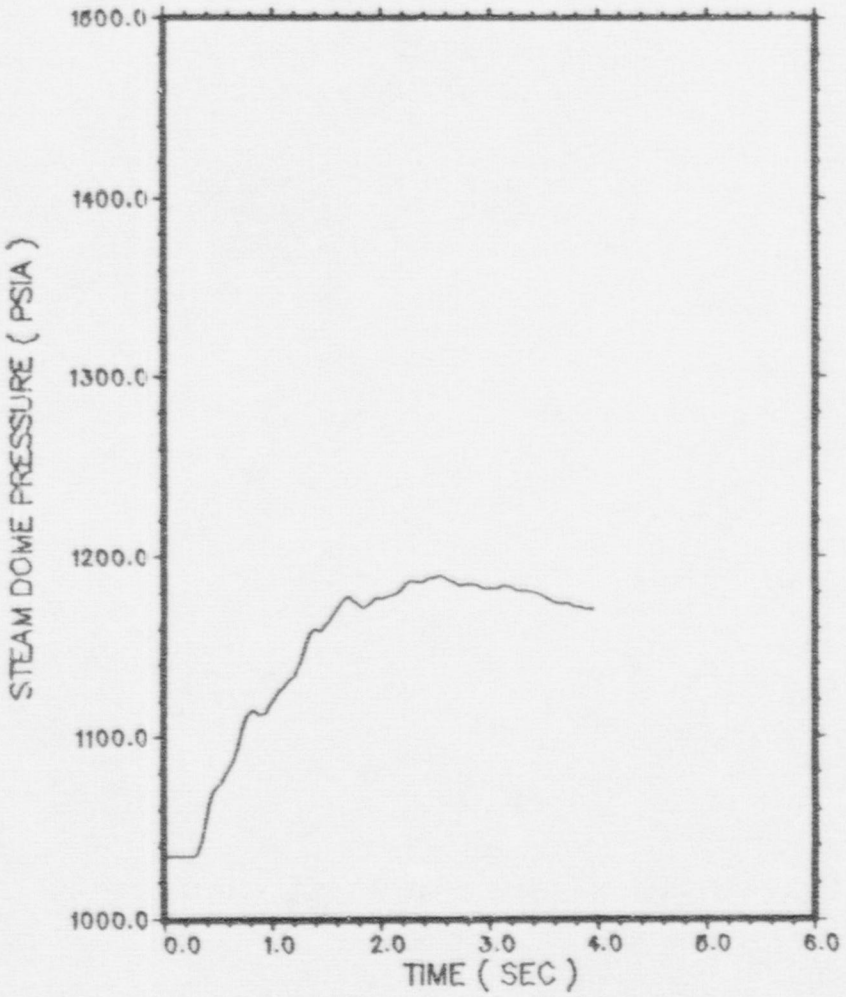

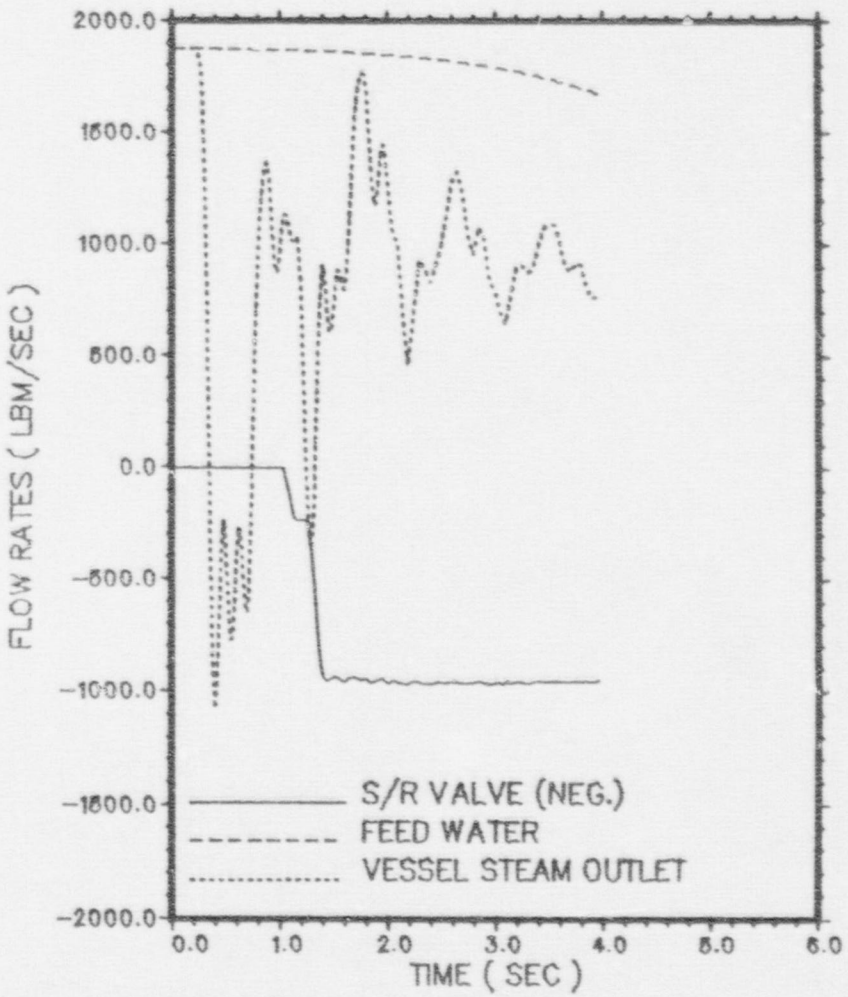

FIGURE 7.2.2-2
TURBINE TRIP WITHOUT BYPASS, EOFPL13-1000 MWD/ST
TRANSIENT RESPONSE VERSUS TIME, "MEASURED" SCRAM TIME

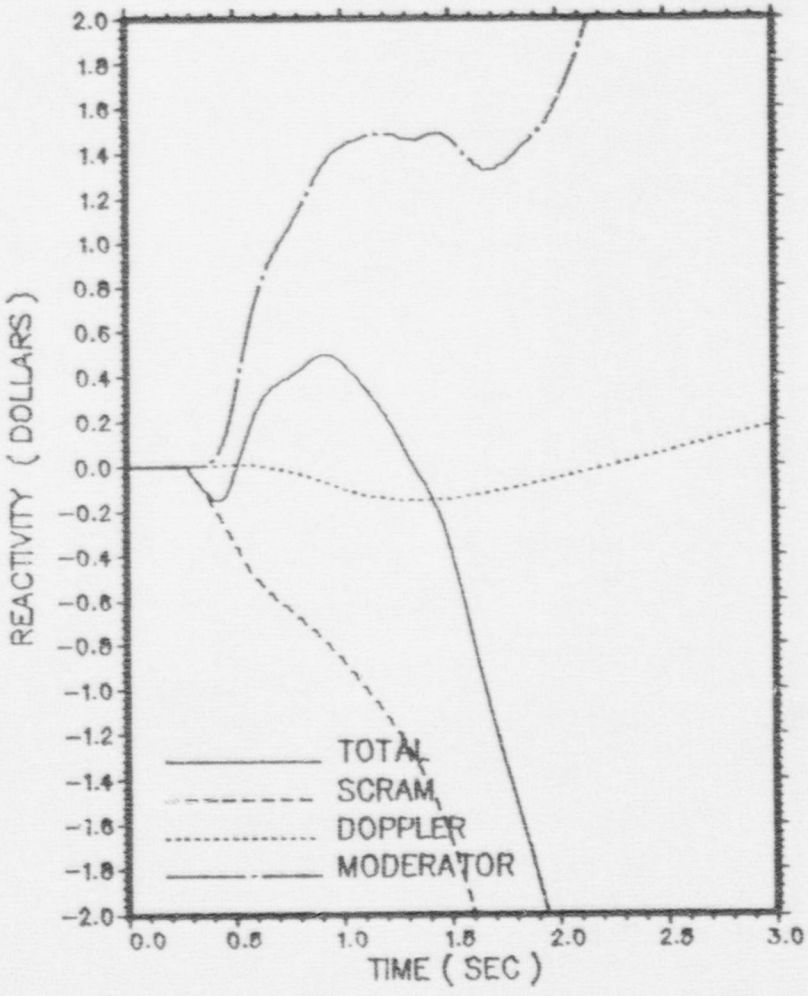

FIGURE 7.2.2-3
TURBINE TRIP WITHOUT BYPASS, EOFPL13-1000 MWD/ST
TRANSIENT RESPONSE VERSUS TIME "MEASURED" SCRAM TIME

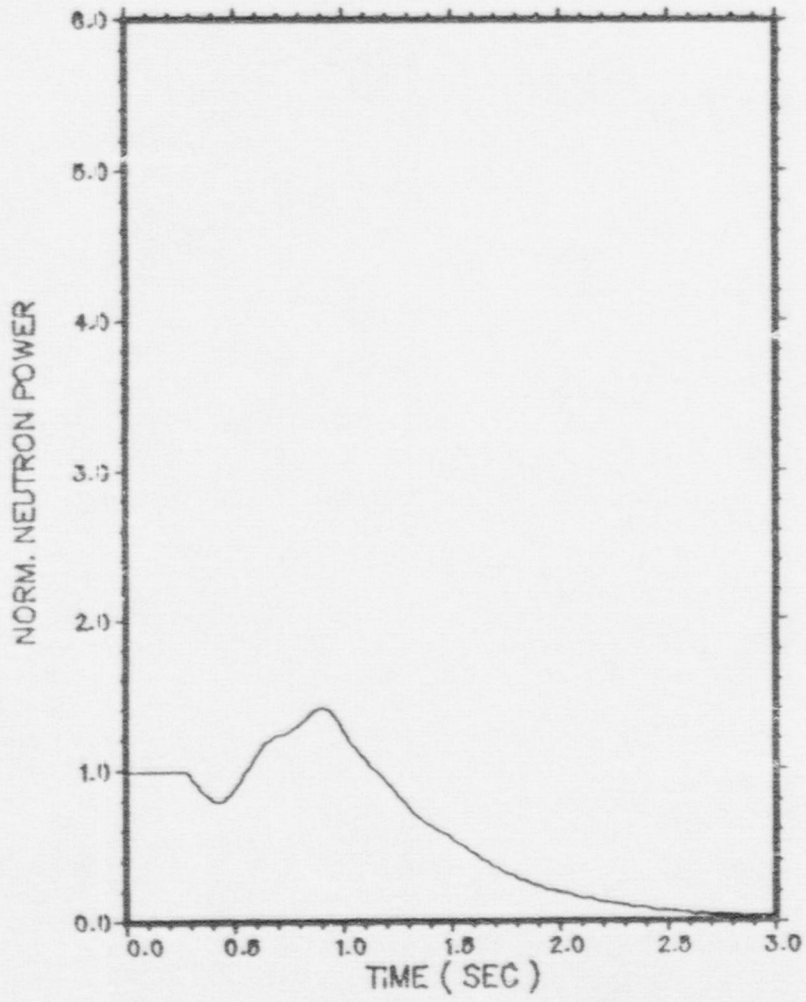

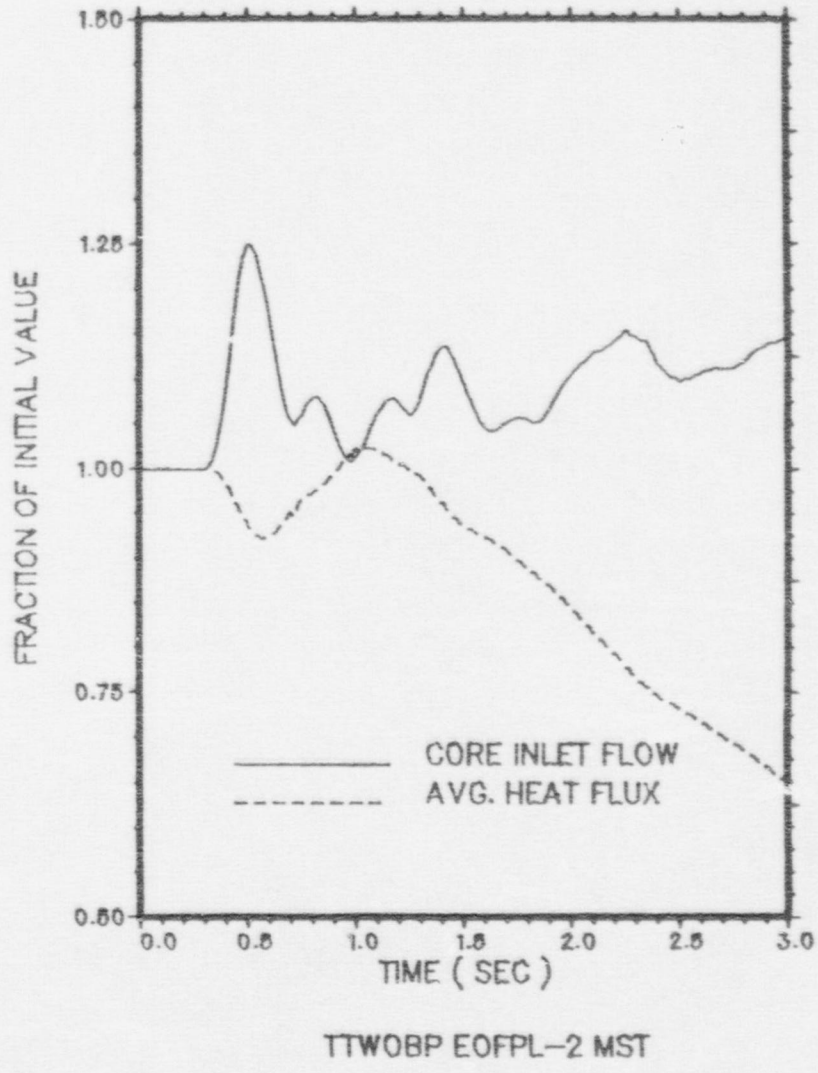

FIGURE 7.2.3-1
TURBINE TRIP WITHOUT BYPASS, EOFPL13-2000 MWD/ST
TRANSIENT RESPONSE VERSUS TIME, "MEASURED" SCRAM TIME

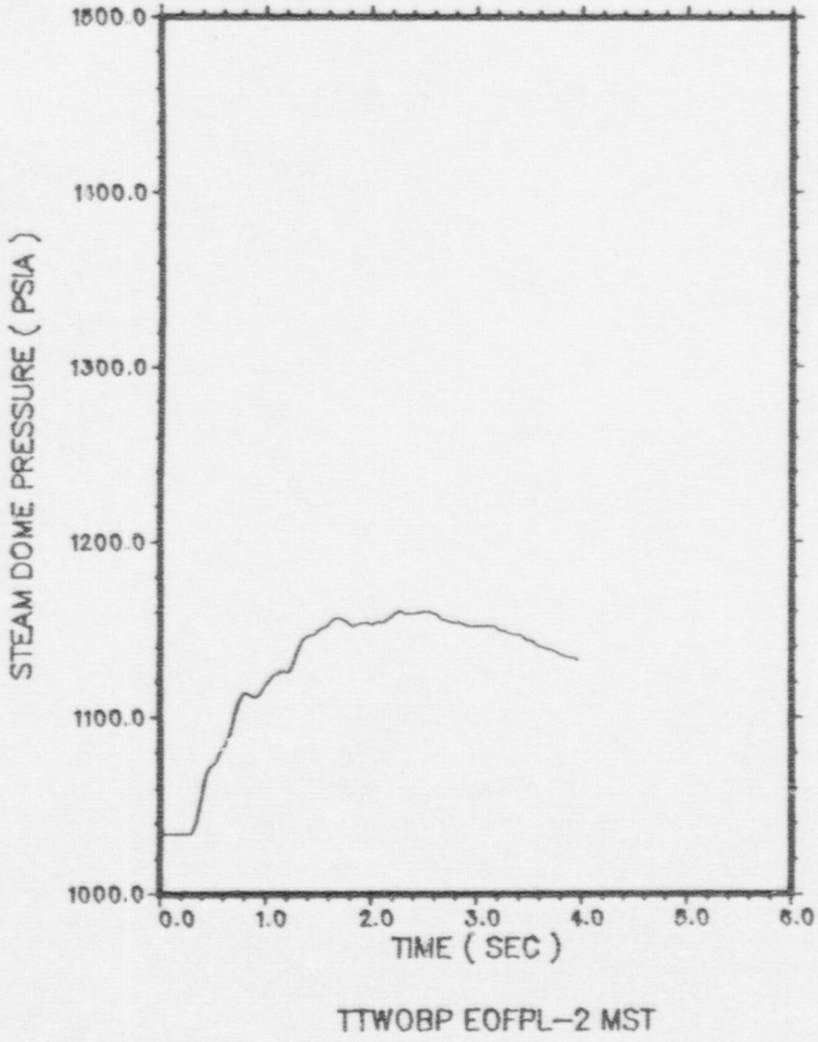

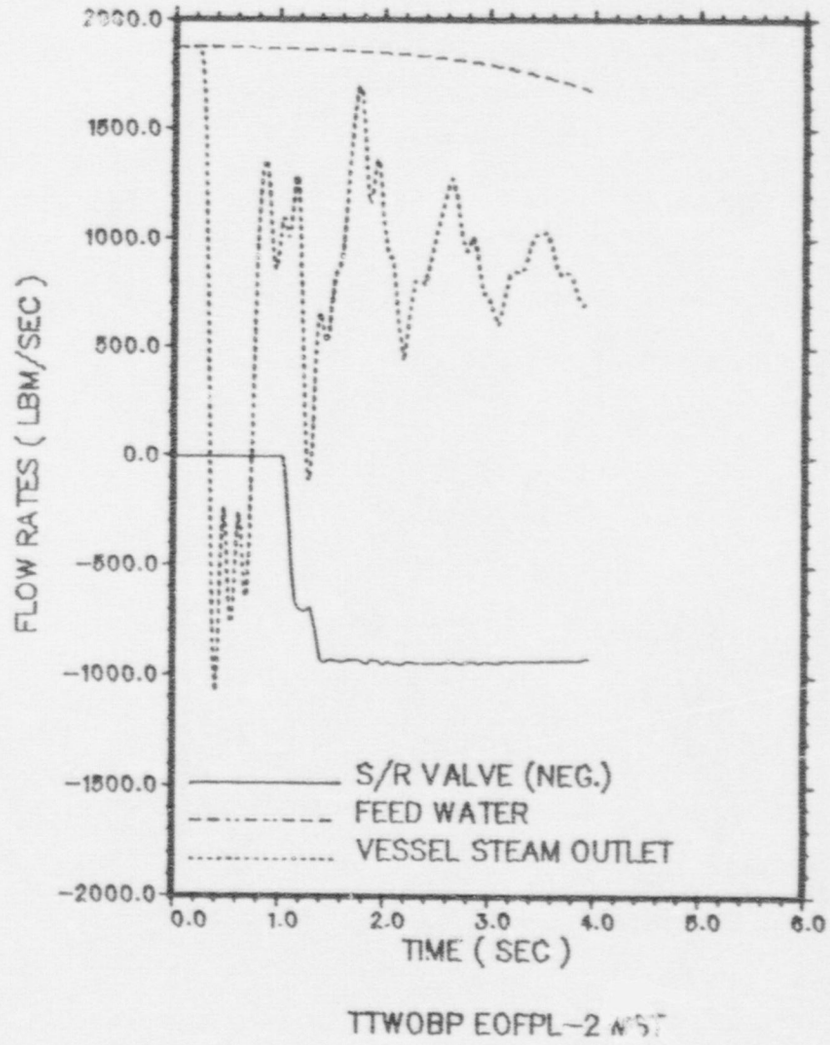

FIGURE 7.2.3-2
TURBINE TRIP WITHOUT BYPASS, EOFPL13-2000 MWD/ST
TRANSIENT RESPONSE VERSUS TIME, "MEASURED" SCRAM TIME

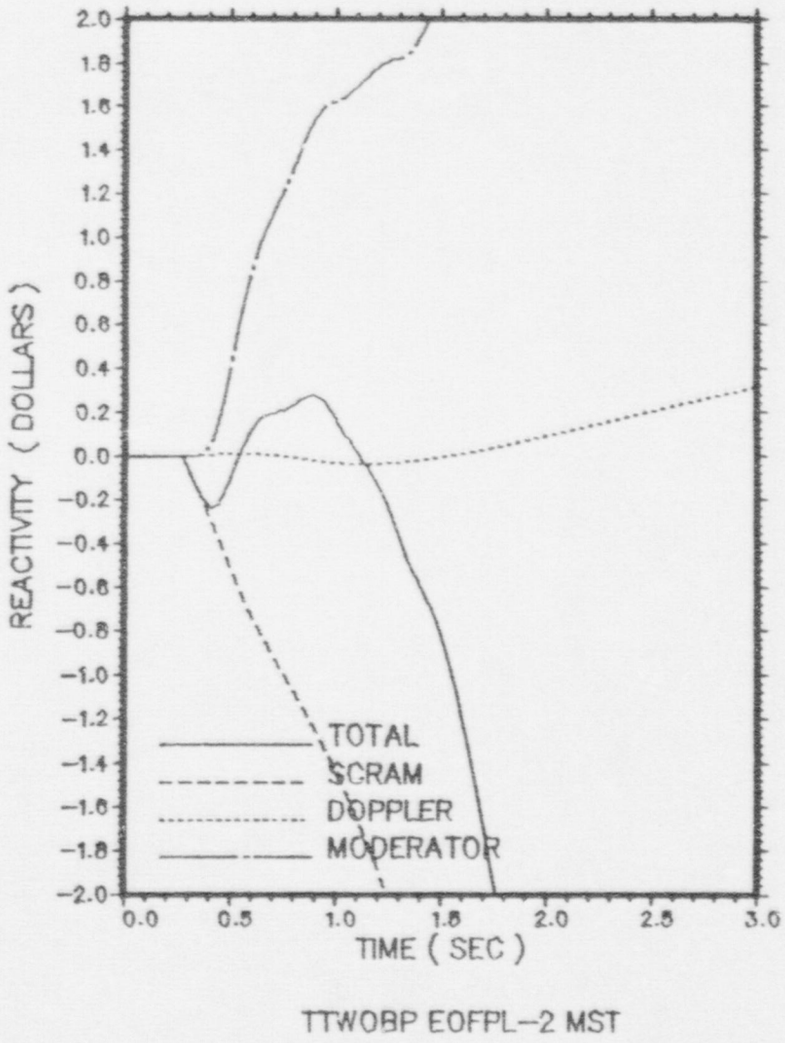

FIGURE 7.2.3-3

TURBINE TRIP WITHOUT BYPASS, EOFPL13-2000 MWD/ST
TRANSIENT RESPONSE VERSUS TIME, "MEASURED" SCRAM TIME

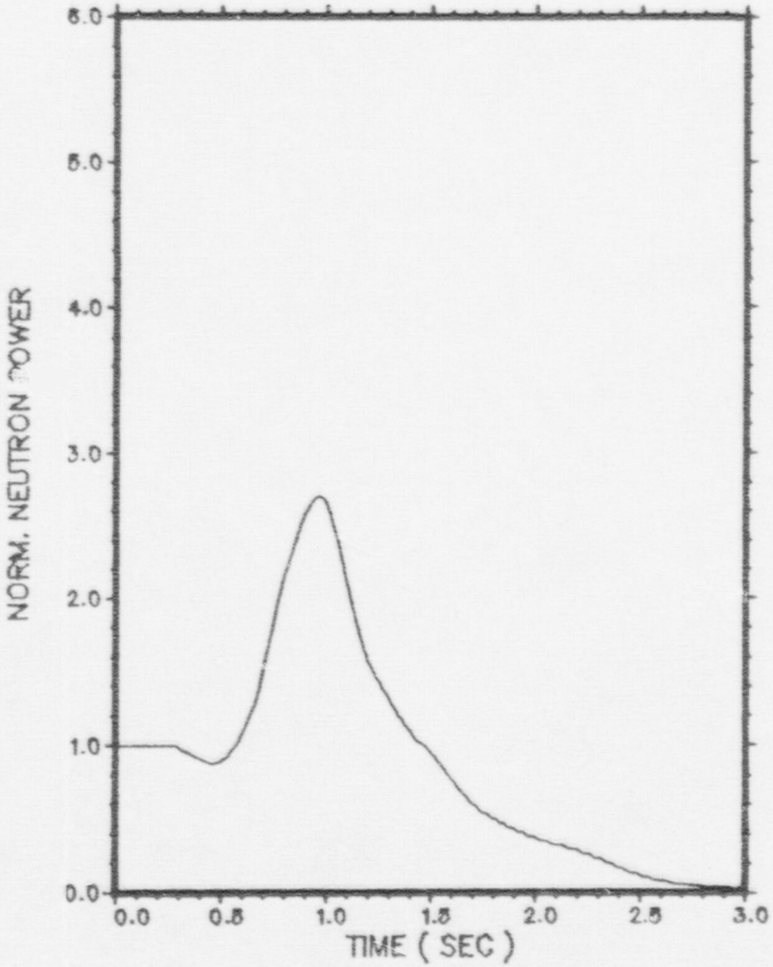

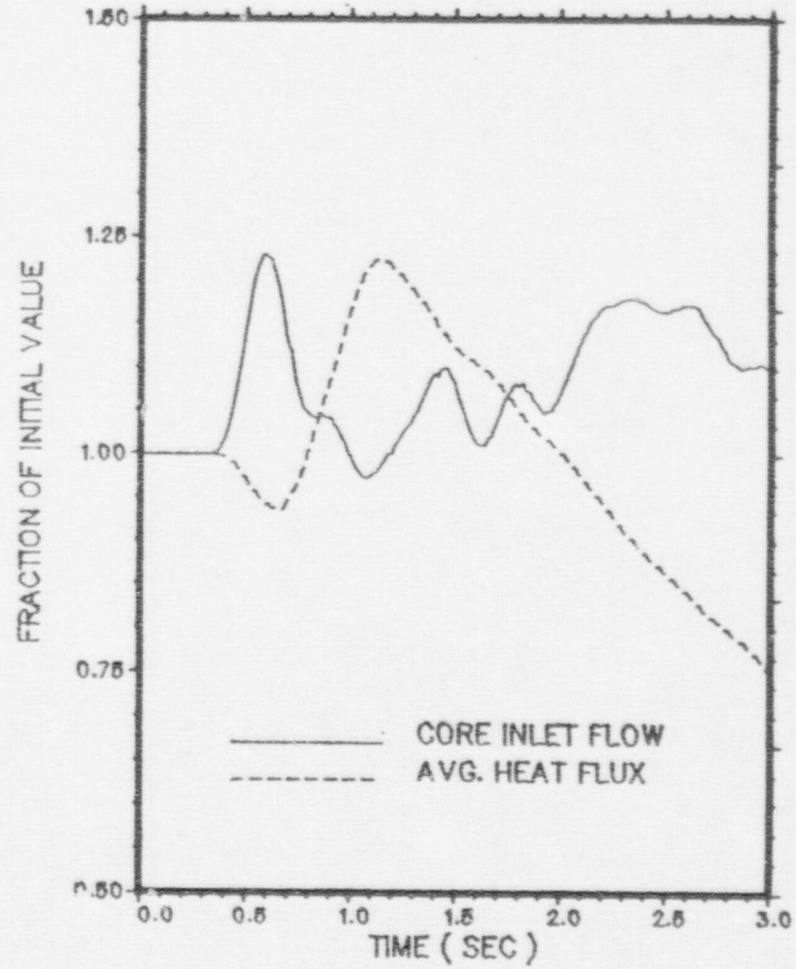

FIGURE 7.2.4-1
GENERATOR LOAD REJECTION WITHOUT BYPASS, EOFPL13
TRANSIENT RESPONSE VERSUS TIME, "MEASURED" SCRAM TIME

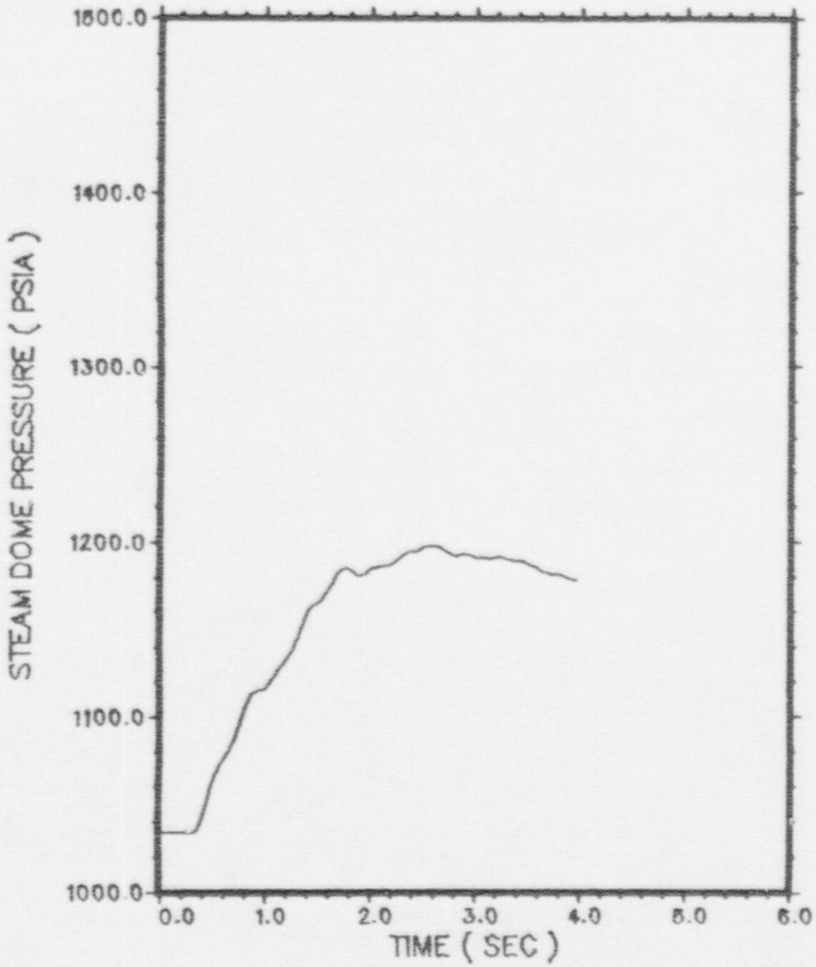

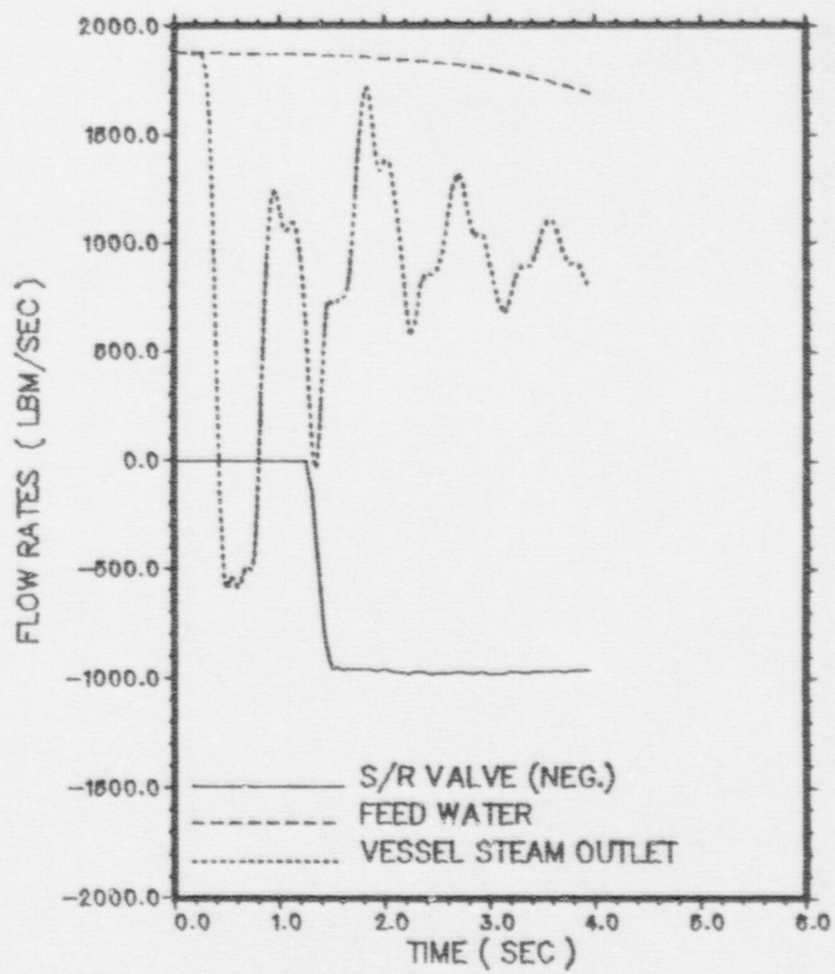

FIGURE 7.2.4-2
GENERATOR LOAD REJECTION WITHOUT BYPASS, EOFPL13
TRANSIENT RESPONSE VERSUS TIME, "MEASURED" SCRAM TIME

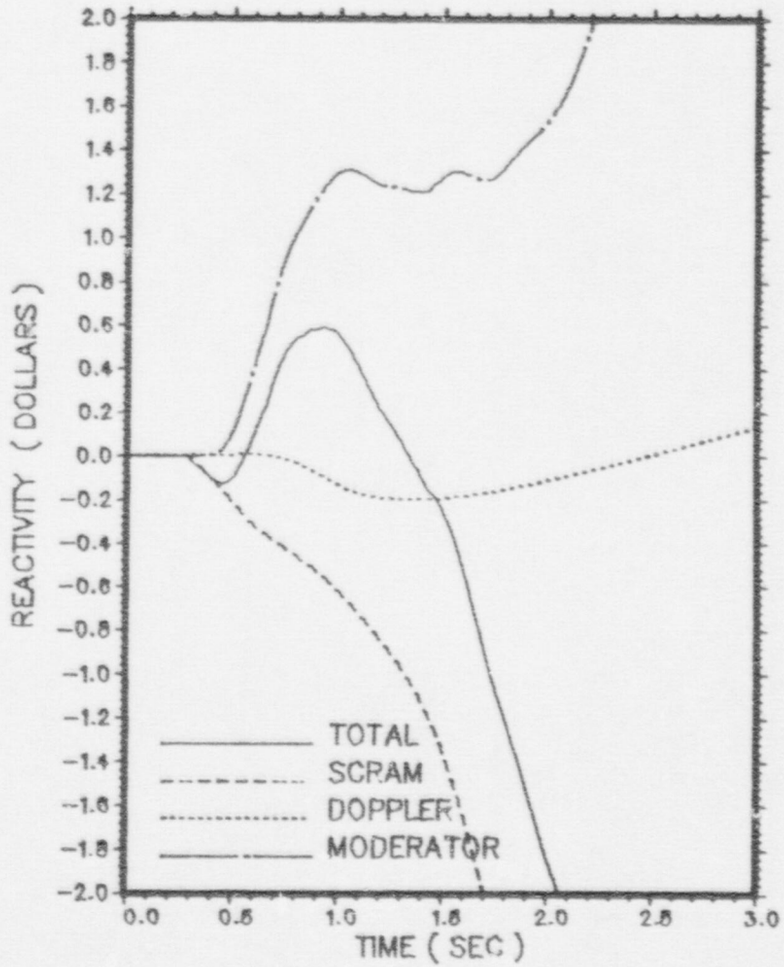

FIGURE 7.2.4-3
GENERATOR LOAD REJECTION WITHOUT BYPASS, EOFPL13
TRANSIENT RESPONSE VERSUS TIME, "MEASURED" SCRAM TIME

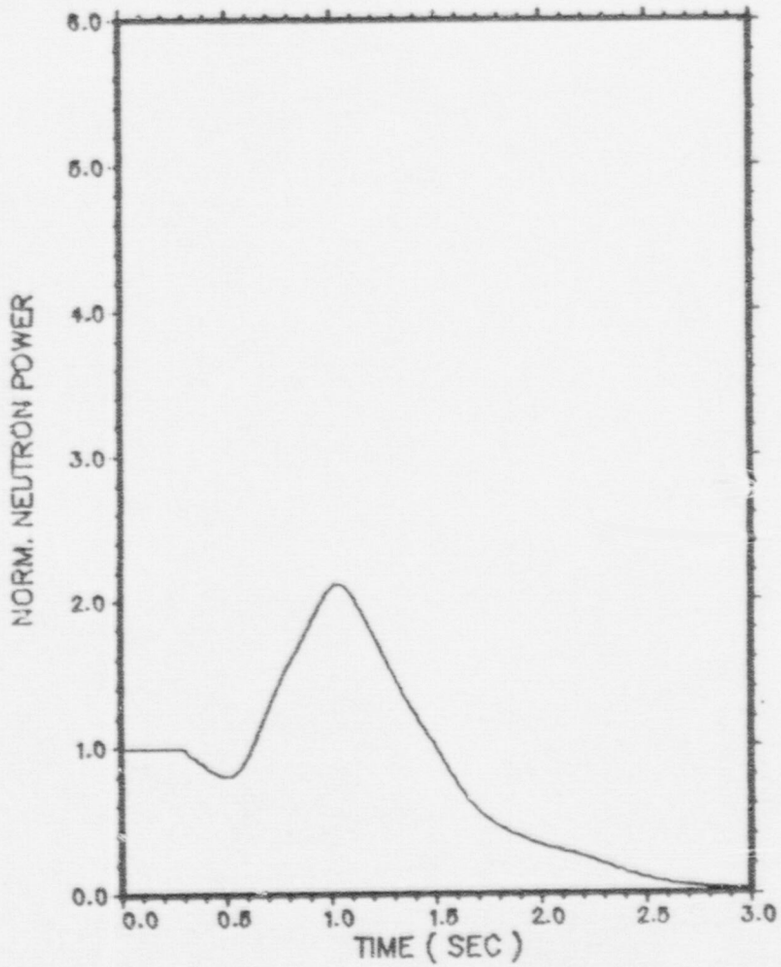

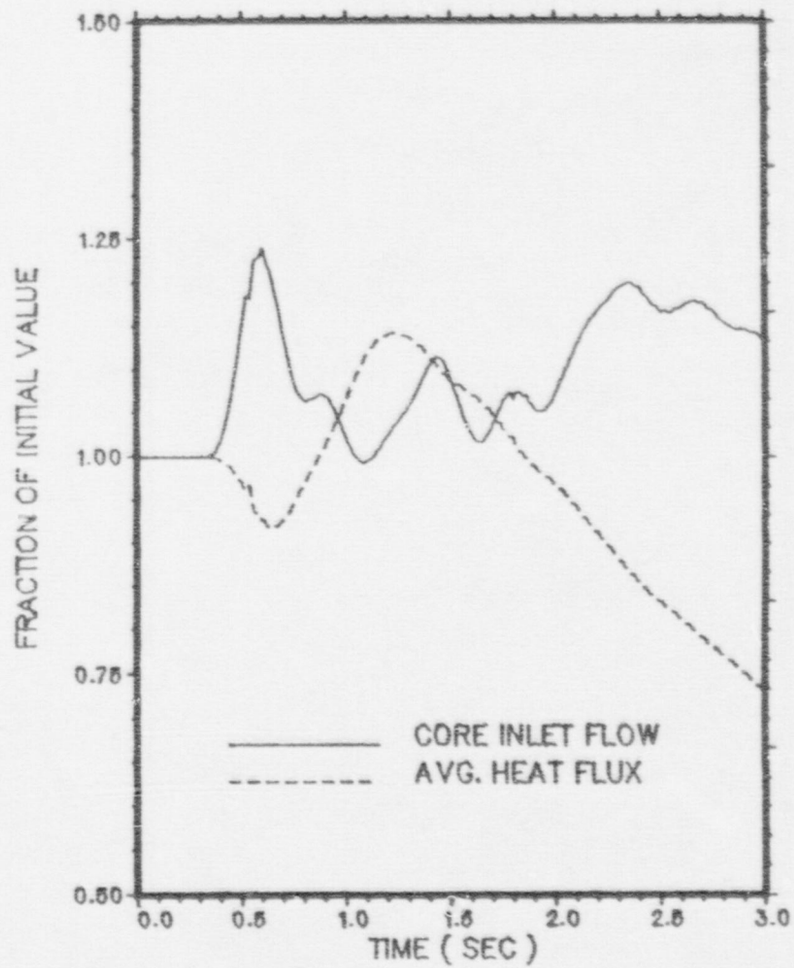

FIGURE 7.2.5-1

GENERATOR LOAD REJECTION WITHOUT BYPASS, EOFPL13-1000 MWD/ST
TRANSIENT RESPONSE VERSUS TIME, "MEASURED" SCRAM TIME

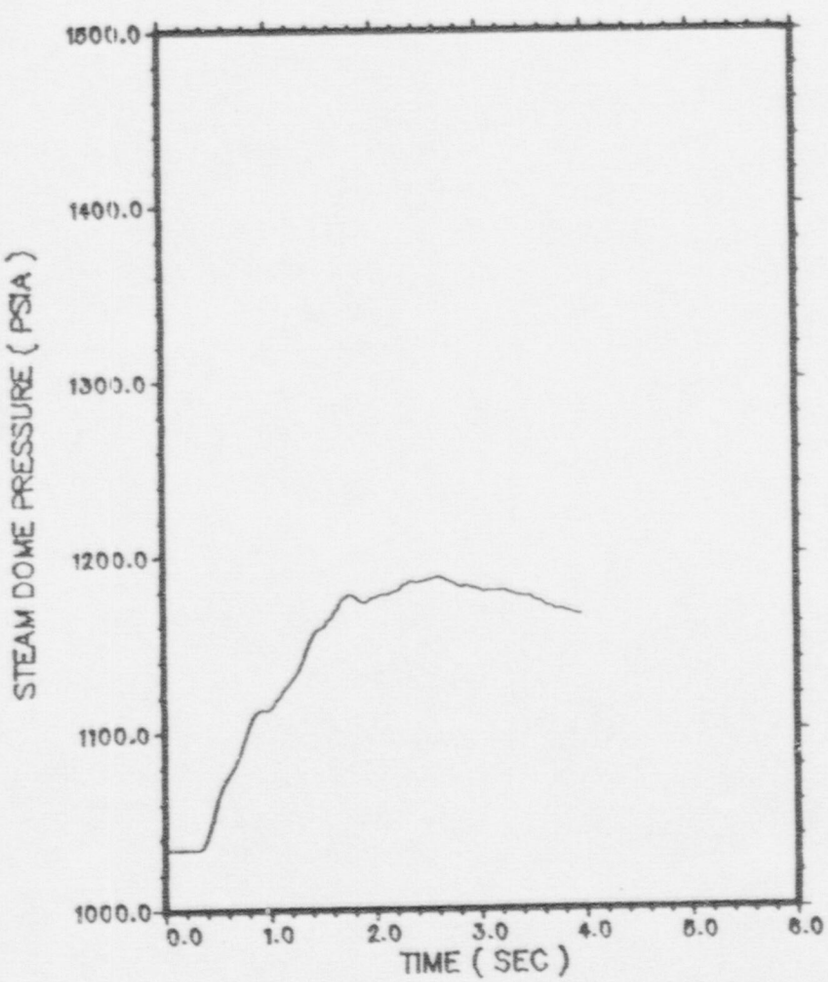

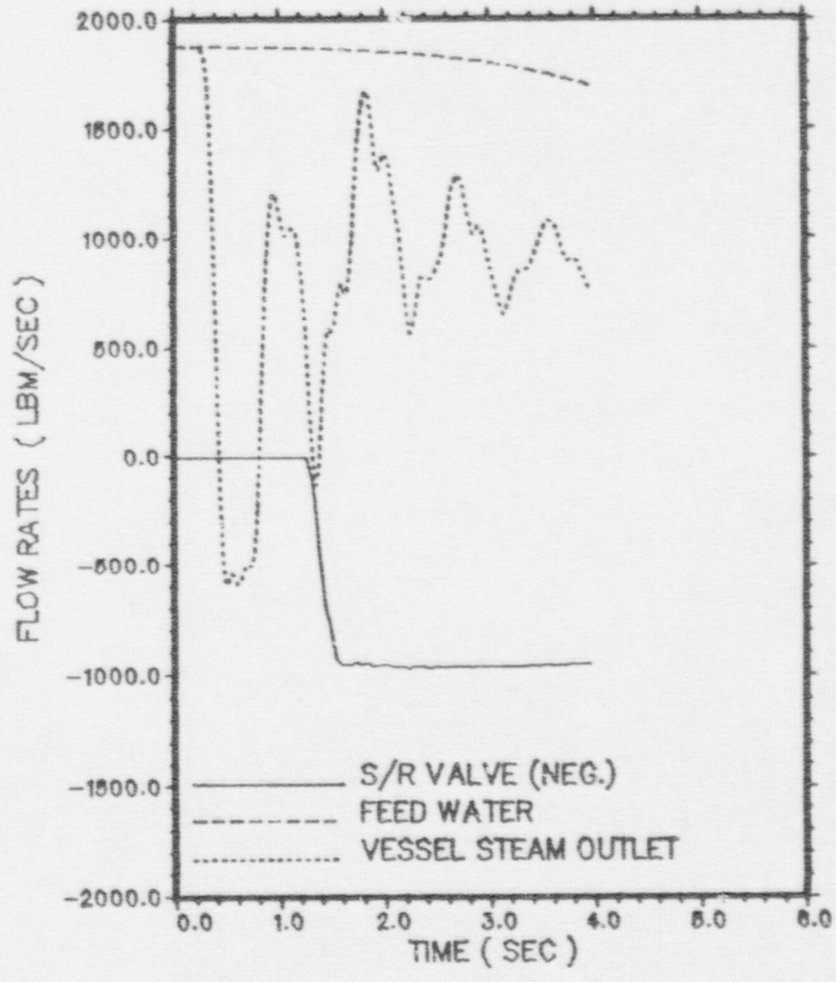

FIGURE 7.2.5-2

GENERATOR LOAD REJECTION WITHOUT BYPASS, EOFPL13-1000 MWD/ST
TRANSIENT RESPONSE VERSUS TIME, "MEASURED" SCRAM TIME

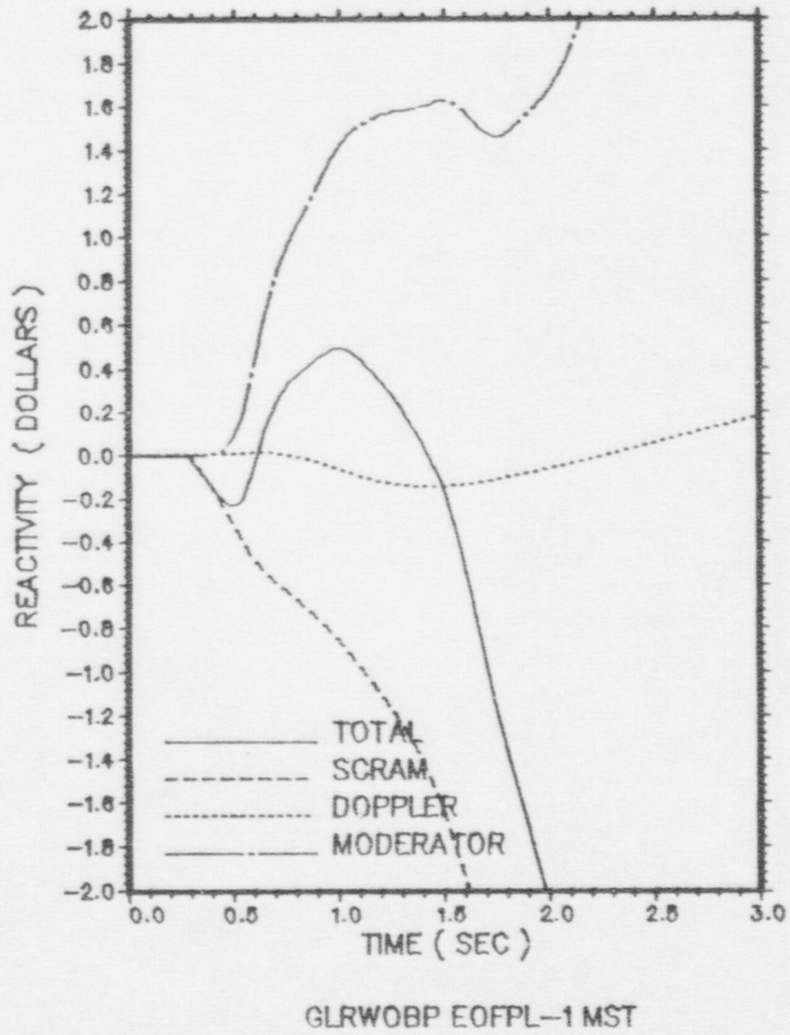

FIGURE 7.2.5-3
GENERATOR LOAD REJECTION WITHOUT BYPASS, EOFPL13-1000 MWD/ST
TRANSIENT RESPONSE VERSUS TIME, "MEASURED" SCRAM TIME

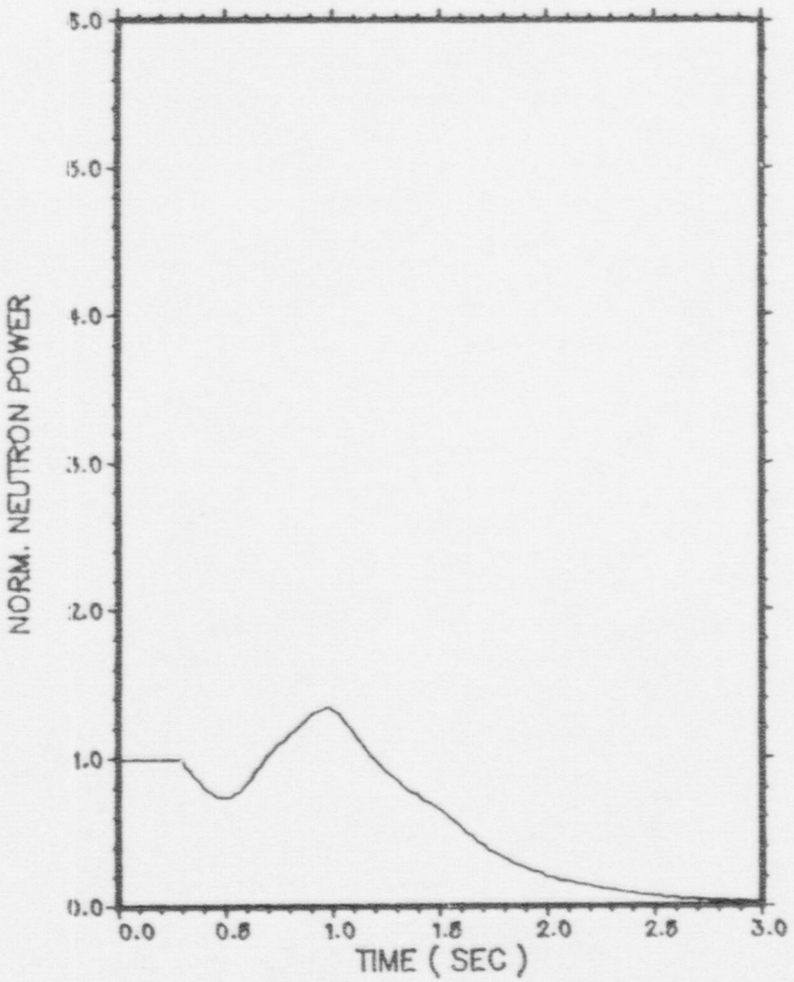

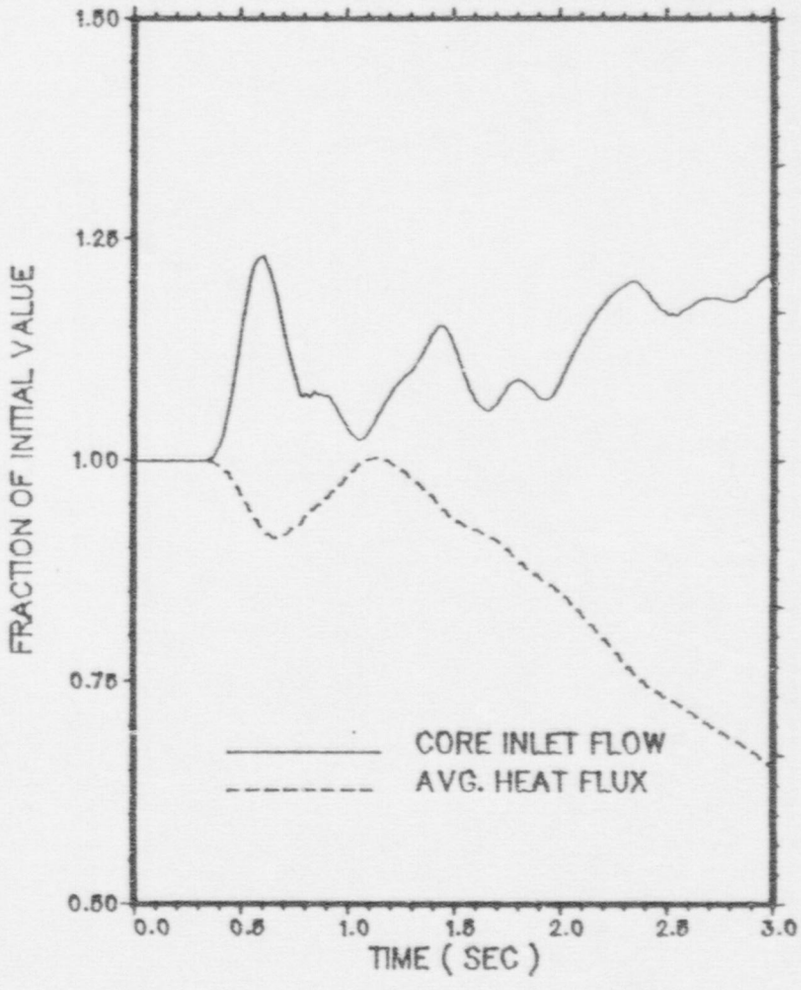

FIGURE 7.2.6-1

GENERATOR LOAD REJECTION WITHOUT BYPASS, EOFPL13-2000 MWD/ST

TRANSIENT RESPONSE VERSUS TIME, "MEASURED"SCRAM TIME

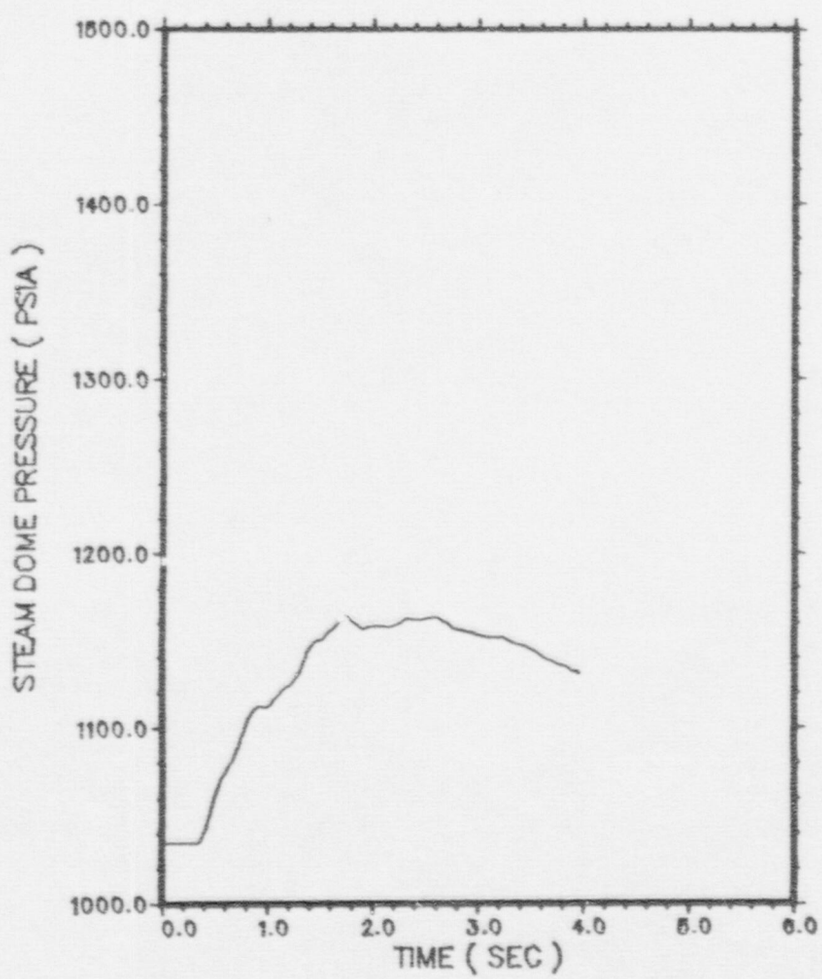

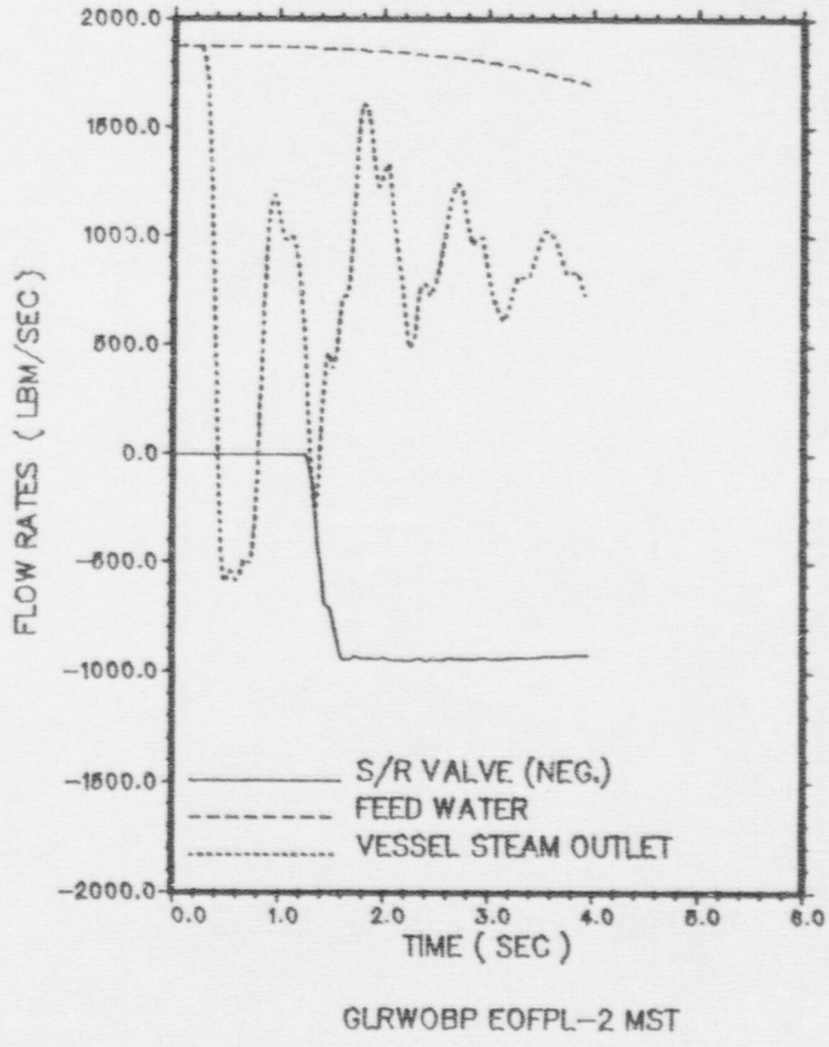

FIGURE 7.2.6-2
GENERATOR LOAD REJECTION WITHOUT BYPASS, EOFPL3-2000 MWD/ST
TRANSIENT RESPONSE VERSUS TIME, "MEASURED" SCRAM TIME

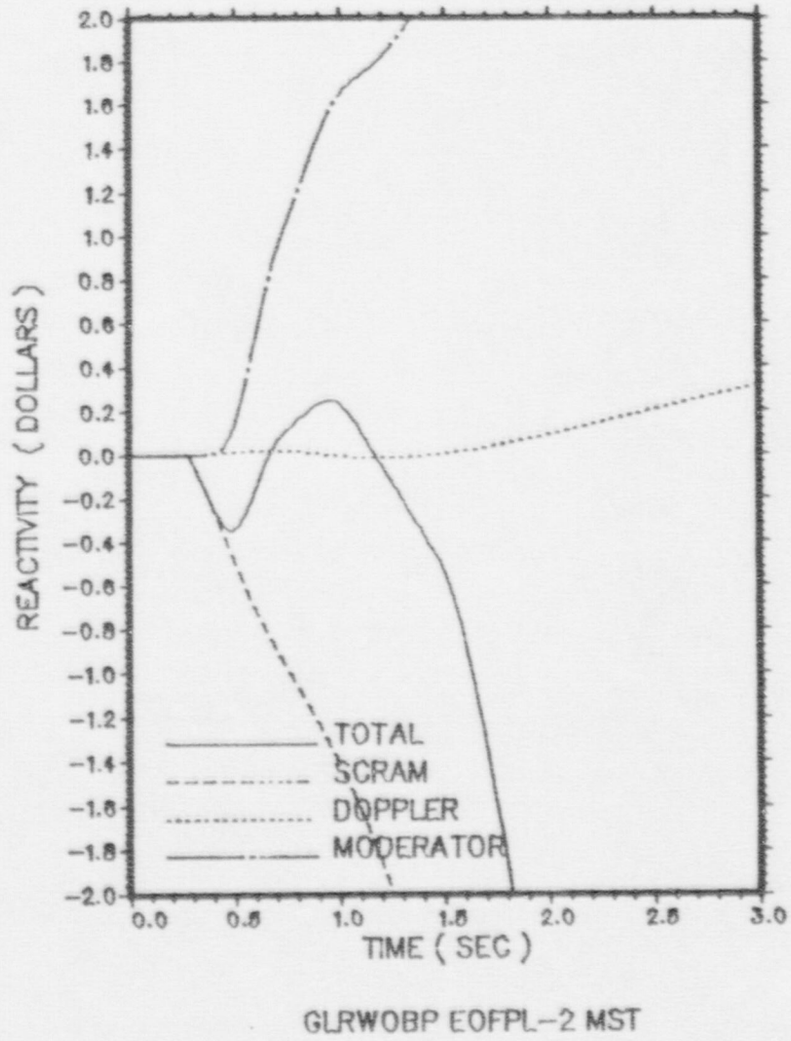

FIGURE 7.2.6-3
GENERATOR LOAD REJECTION WITHOUT BYPASS, EOFPL13-2000 MWD/ST
TRANSIENT RESPONSE VERSUS TIME, "MEASURED" SCRAM TIME

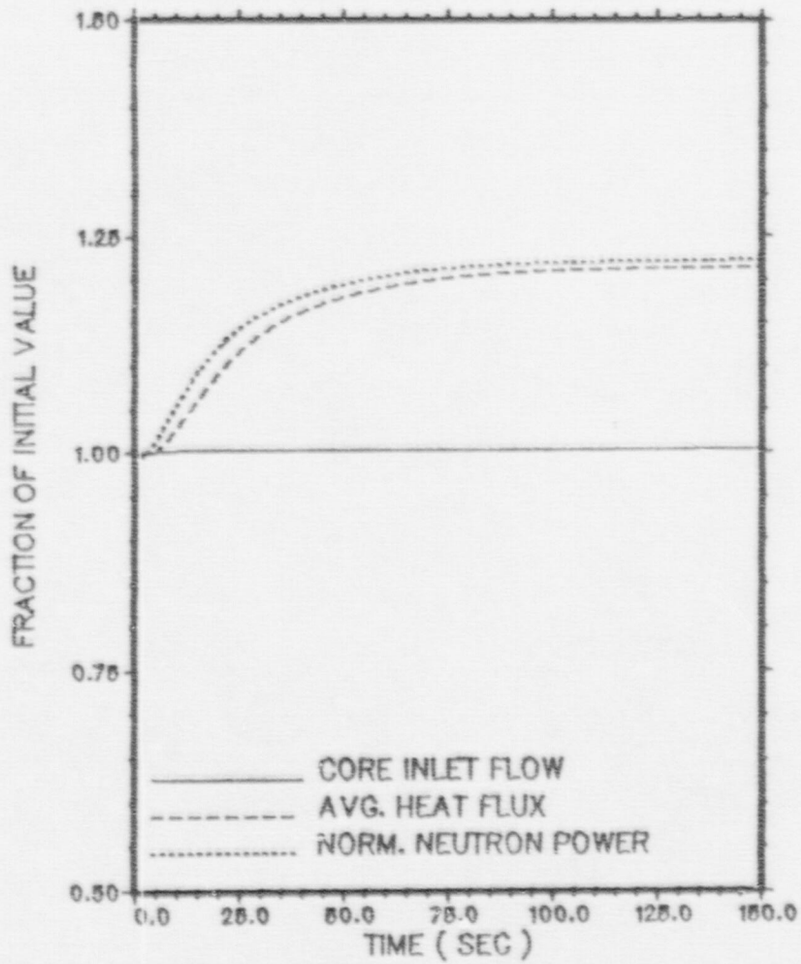

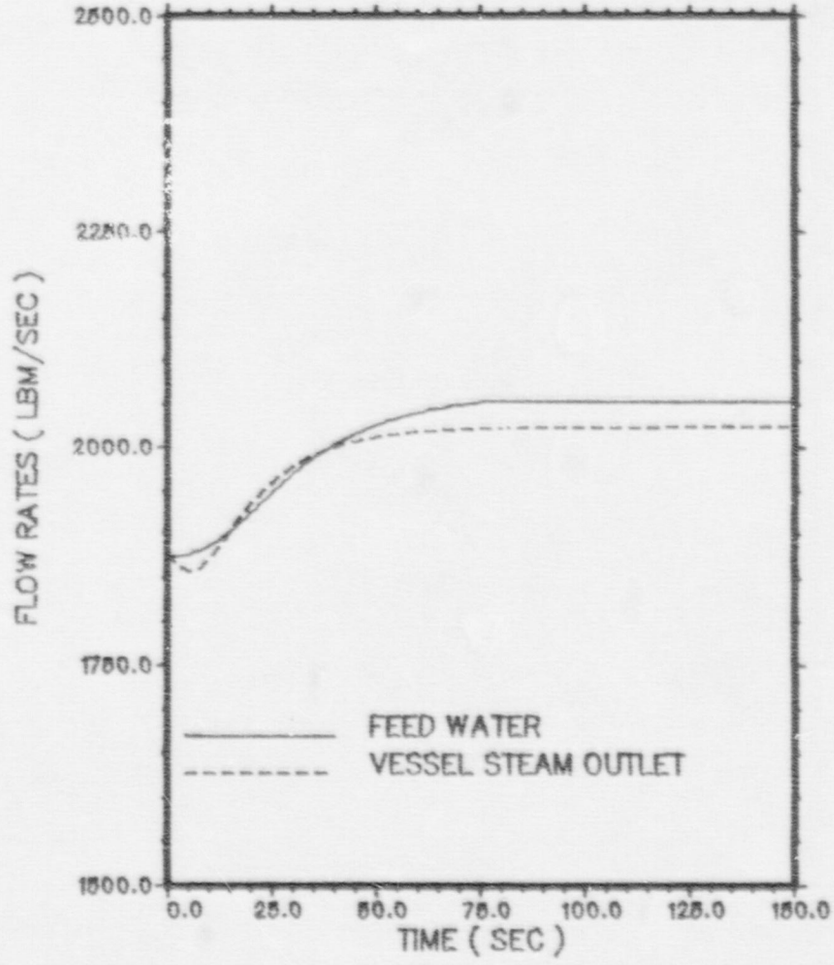

FIGURE 7.2.7-1
LOSS OF 100°F FEEDWATER HEATING, EOFPL13-1000 MWD/ST (LIMITING CASE)
TRANSIENT RESPONSE VERSUS TIME

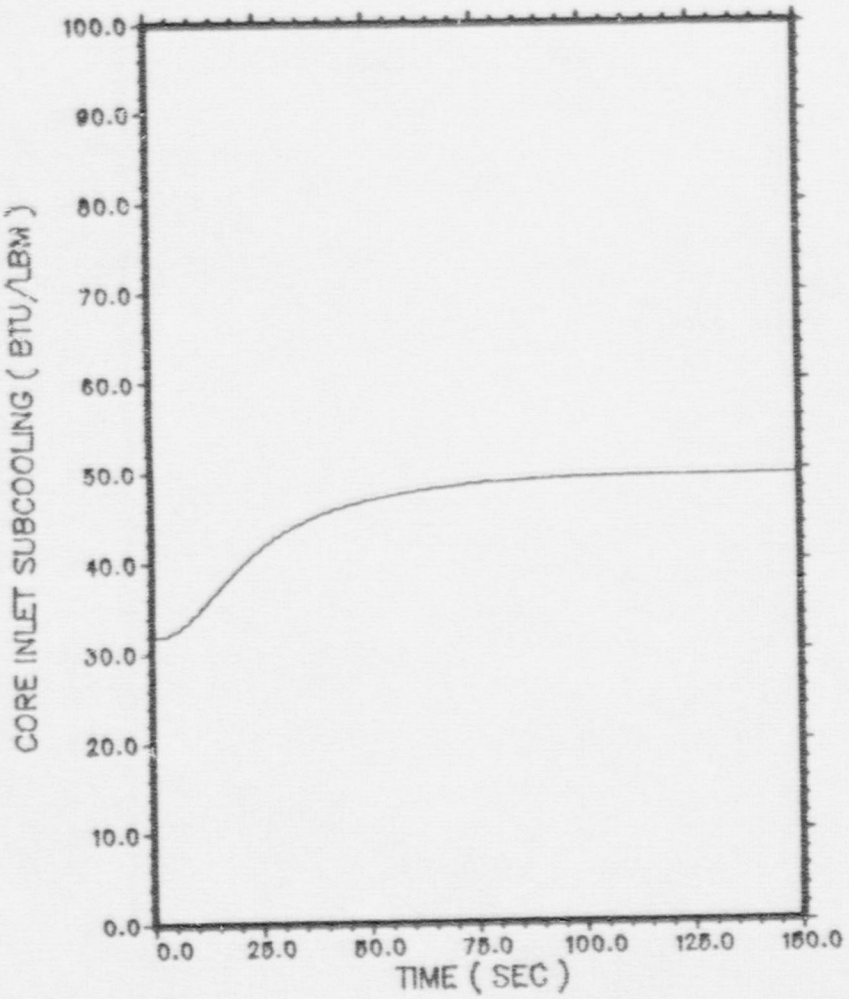

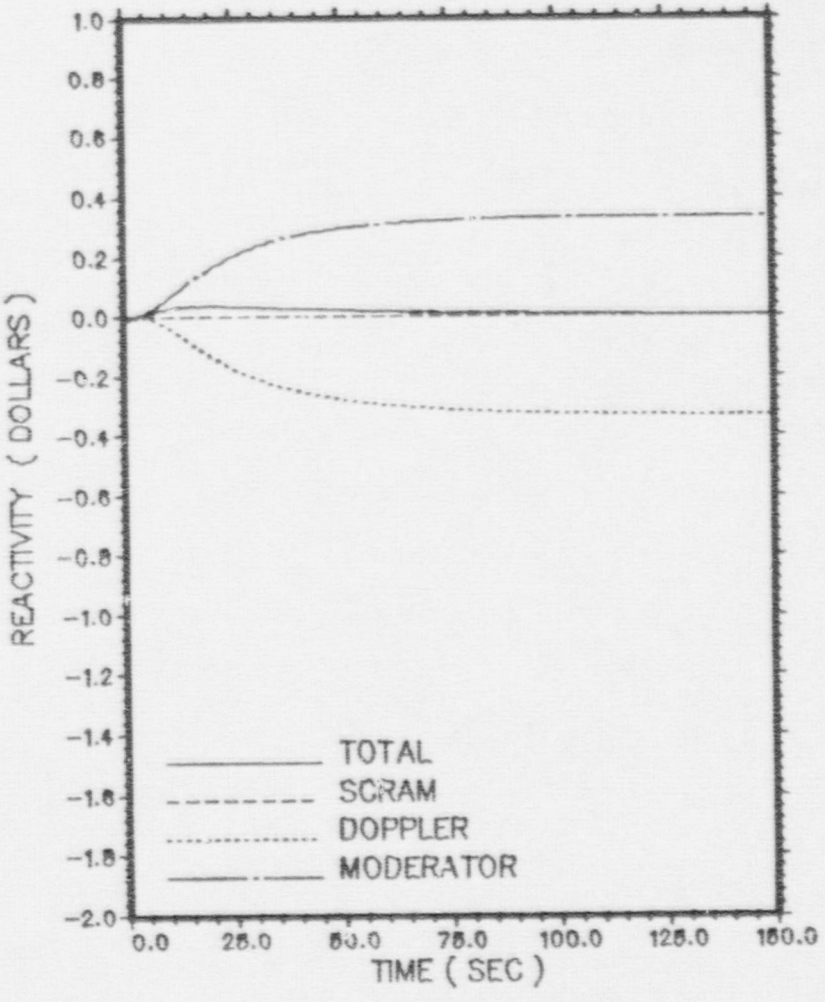

FIGURE 7.2.7-2

LOSS OF 100°F FEEDWATER HEATING, EOFPL13-1000 MWD/ST (LIMITING CASE)

TRANSIENT RESPONSE VERSUS TIME

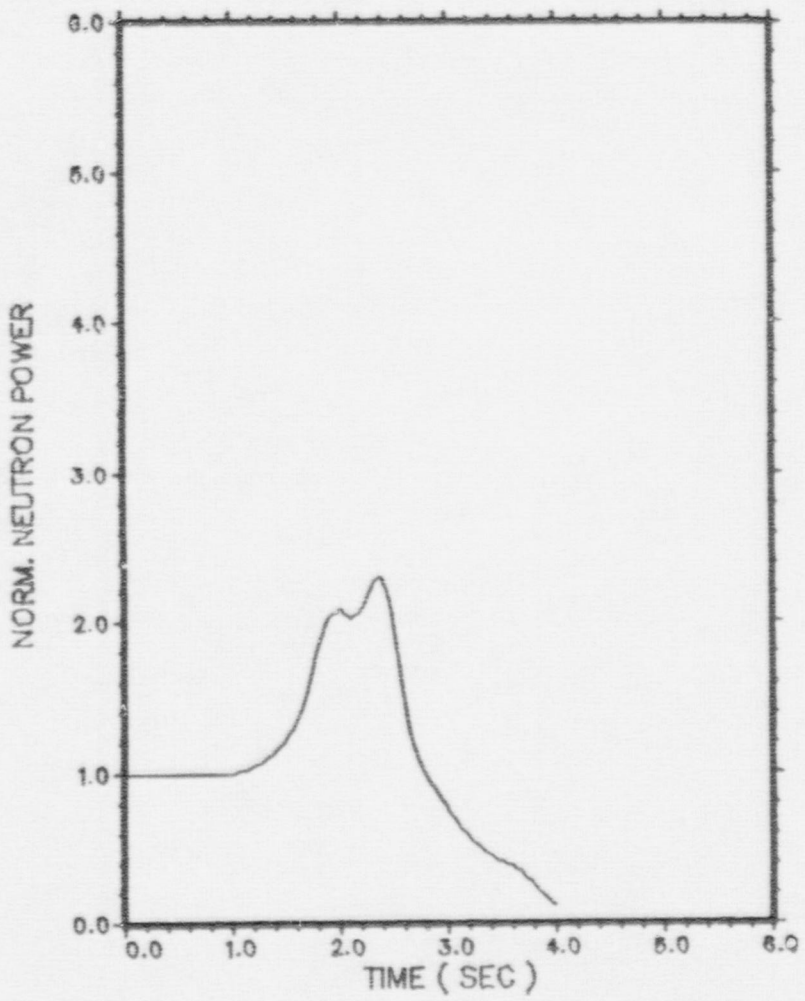

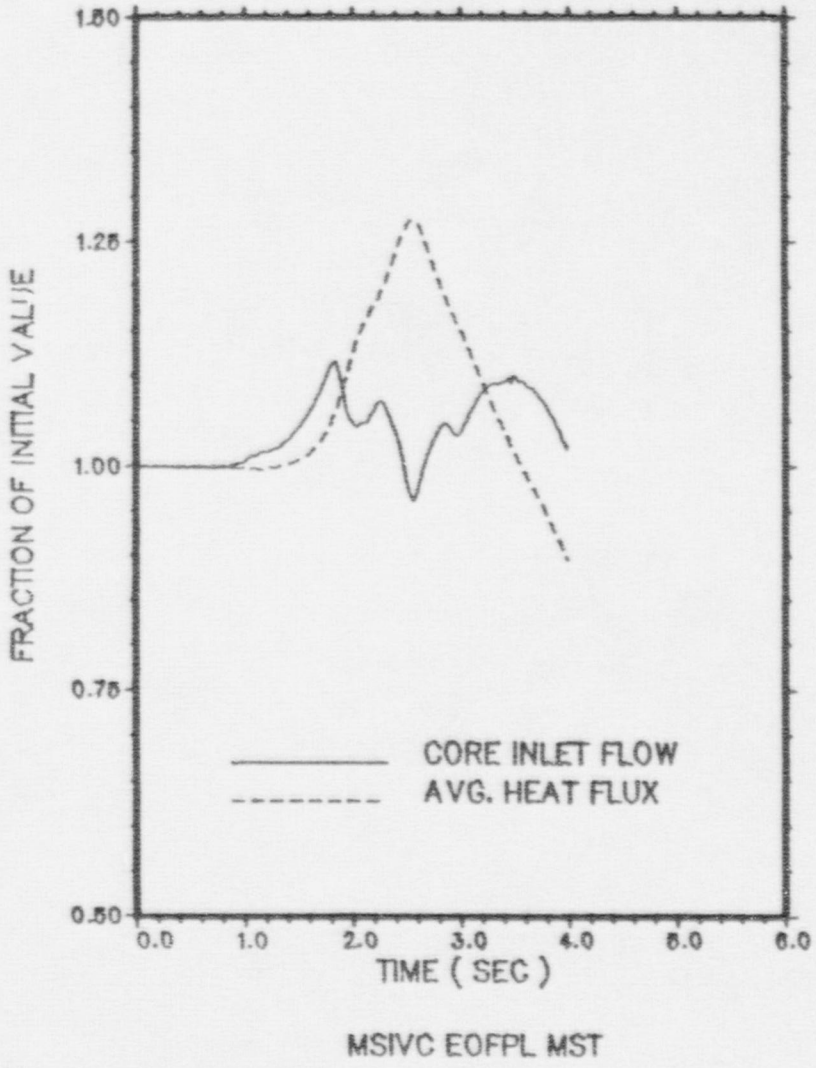

FIGURE 7.3.1-1
MSIV CLOSURE, FLUX SCRAM, EOFPL13
TRANSIENT RESPONSE VERSUS TIME, "MEASURED" SCRAM TIME

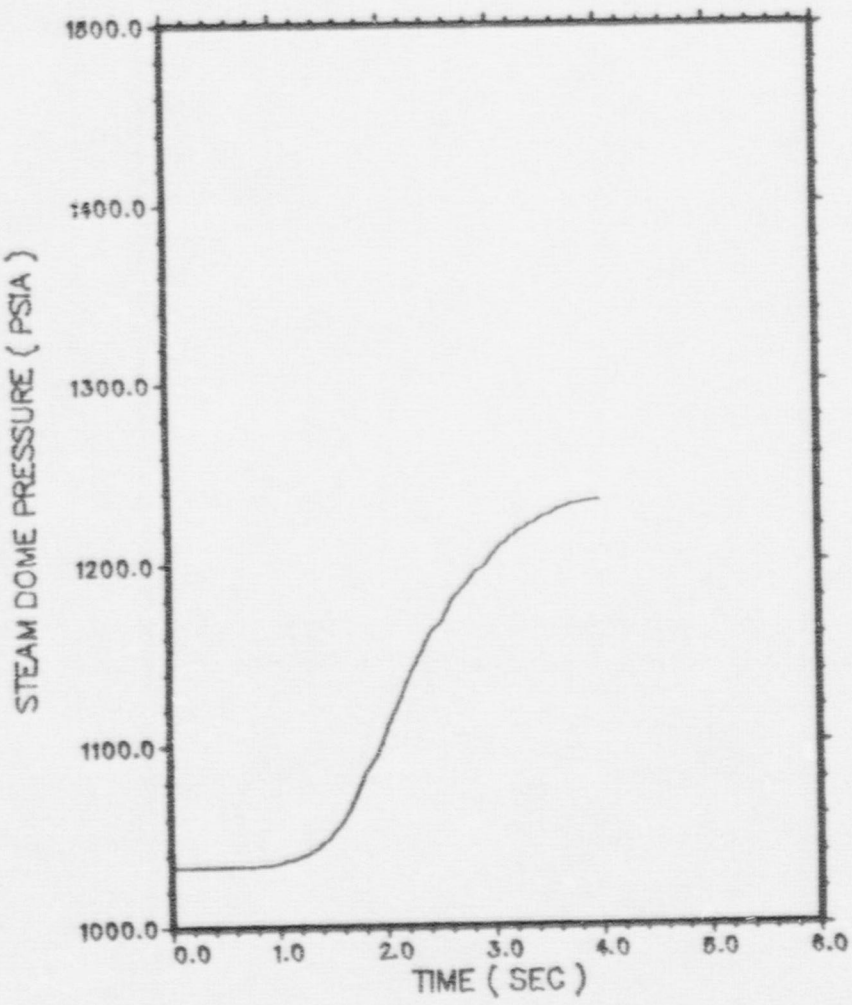

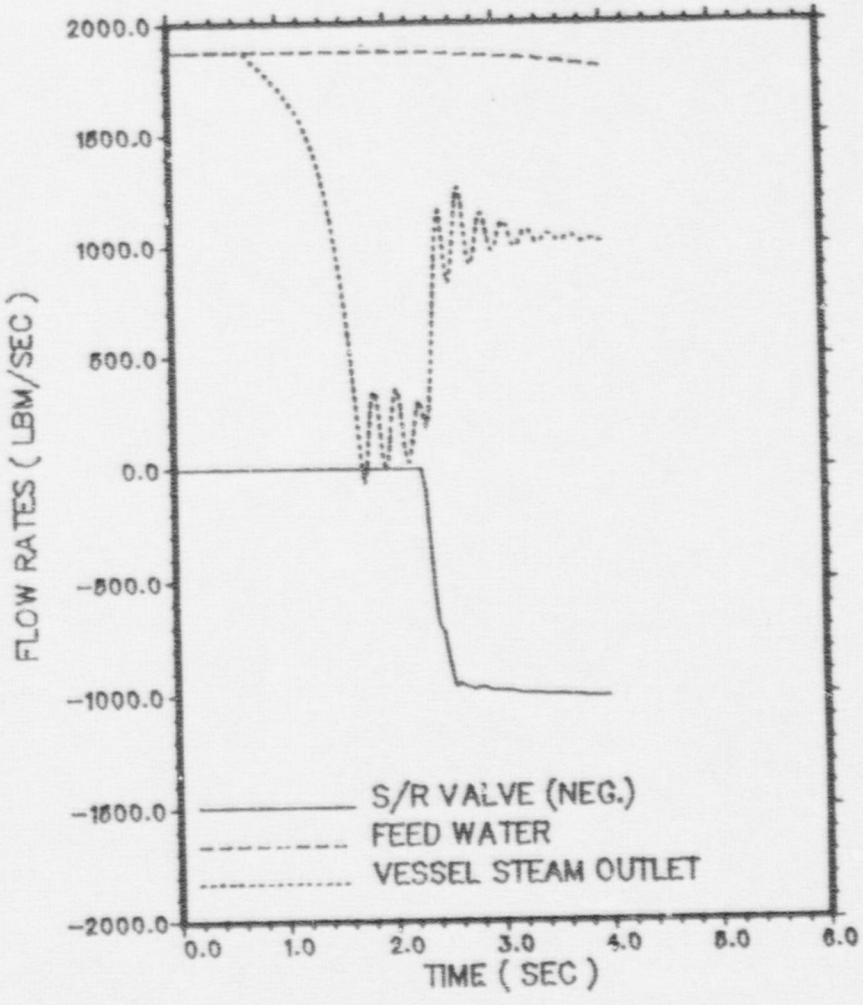

FIGURE 7.3.1-2
MSIV CLOSURE, FLUX SCRAM EOFPL13
TRANSIENT RESPONSE VERSUS TIME, "MEASURED" SCRAM TIME

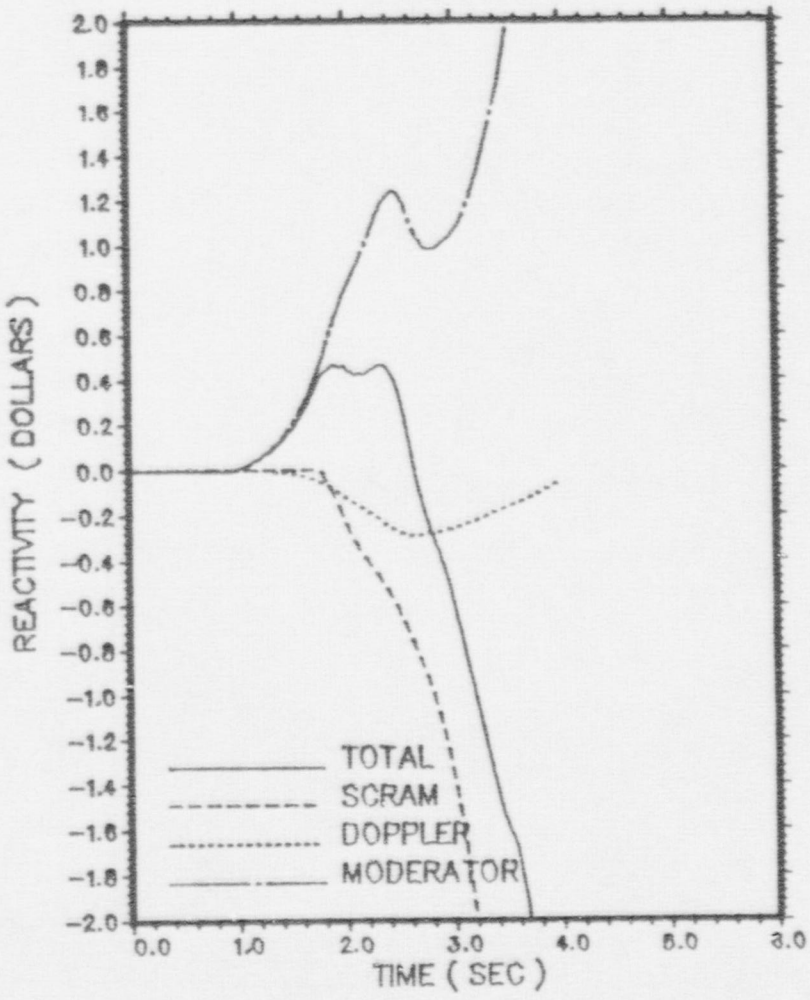

FIGURE 7.3.1-3
MSIV CLOSURE, FLUX SCRAM, EOFPL13
TRANSIENT RESPONSE VERSUS TIME, "MEASURED" SCRAM TIME

INITIAL CONDITIONS

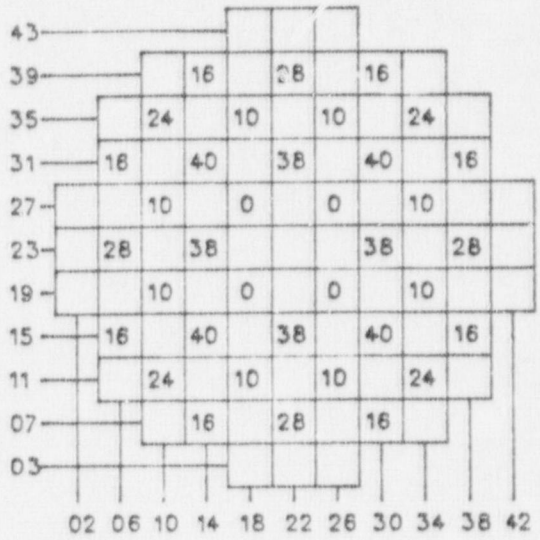

Core Thermal Power = 1664 MWt
Core Flow = 48 Mlb/hr
Cycle Exposure = 8240 MWd/st
Xenon Free

Core Average Pressure = 1042 psia
Initial MCPR = 1.287
Initial MLHGR = 13.4 kw/ft
RWE Control Rod = 26-27

TRANSIENT SUMMARY

RBM Setpoint	Rod Position	ΔCPR	MLHGR (kw/ft)
104	10	0.13	13.9
105	10	0.13	13.9
106	12	0.16	14.4
107	14	0.18	15.0
108	16	0.21	15.6

FIGURE 7.4.1

REACTOR INITIAL CONDITIONS AND TRANSIENT SUMMARY

FOR THE VY CYCLE 13 ROD WITHDRAWAL ERROR CASE 1

INITIAL CONDITIONS

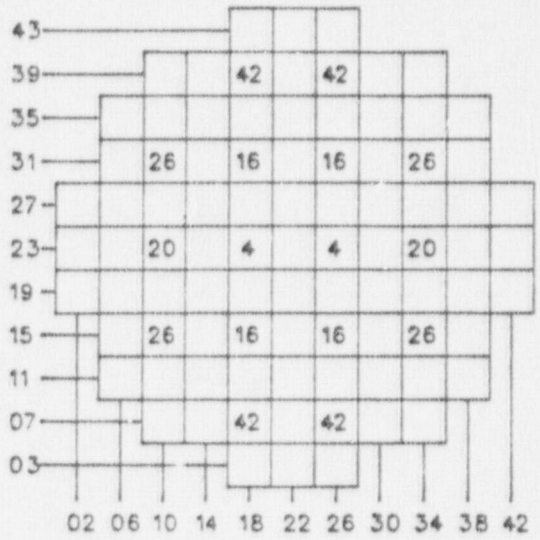

Core Thermal Power = 1664 MWt
Core Flow = 48 Mlb/hr
Cycle Exposure = 4160 MWd/st
Equilibrium Xenon

Core Average Pressure = 1042 psia
Initial MCPR = 1.414
Initial MLHGR = 12.1 kw/ft
RWE Control Rod = 26-23

TRANSIENT SUMMARY

RBM Setpoint	Rod Position	ΔCPR	MLHGR (kw/ft)
104	12	0.07	12.8
105	12	0.07	12.8
106	16	0.11	14.0
107	20	0.14	14.7
108	26	0.17	14.6

FIGURE 7.4.2

REACTOR INITIAL CONDITIONS AND TRANSIENT SUMMARY

FOR THE VY CYCLE 13 ROD WITHDRAWAL ERROR CASE 2

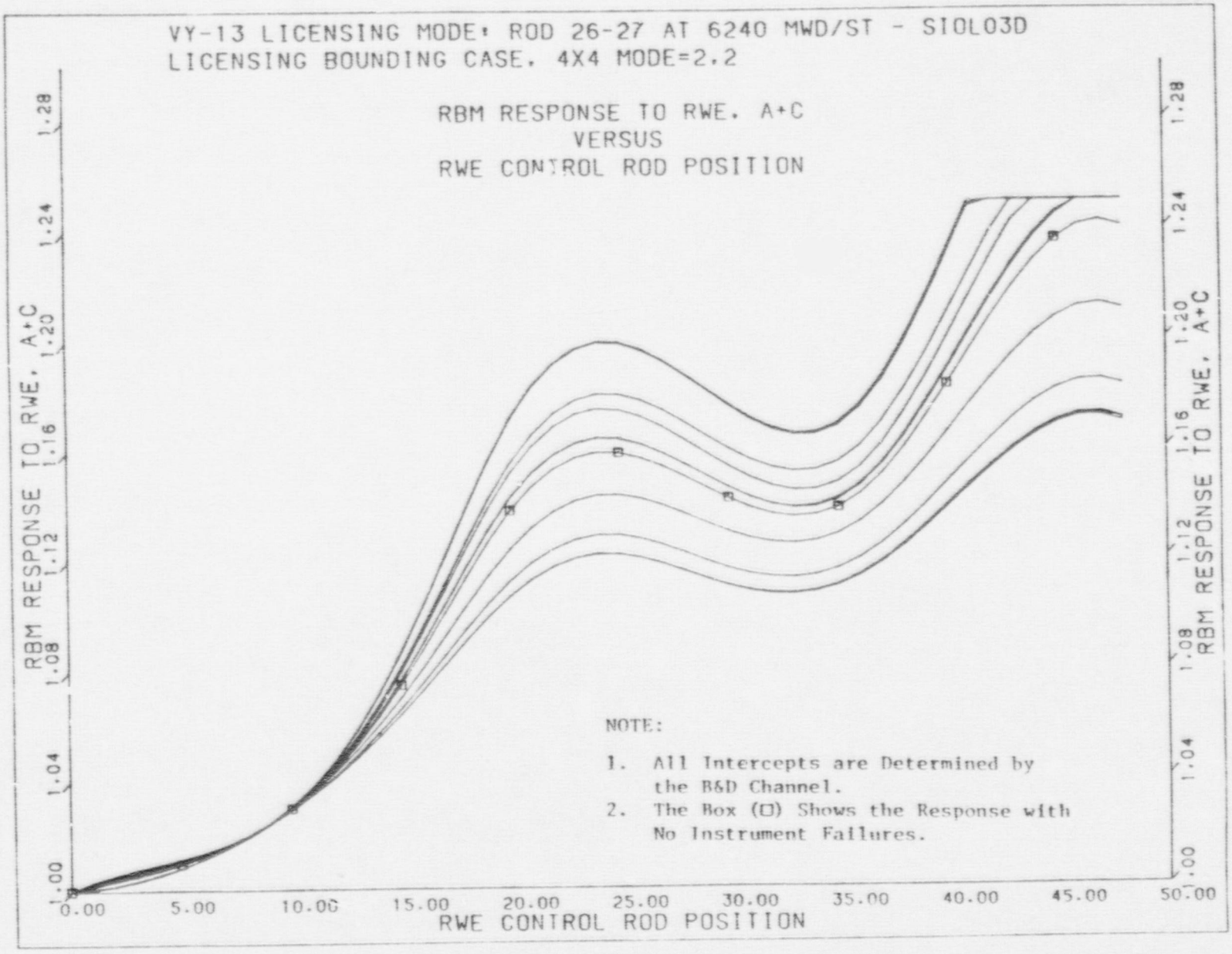

FIGURE 7.4.3

VY CYCLE 13 RWE CASE 1 - SETPOINT INTERCEPTS DETERMINED BY THE A + C CHANNEL

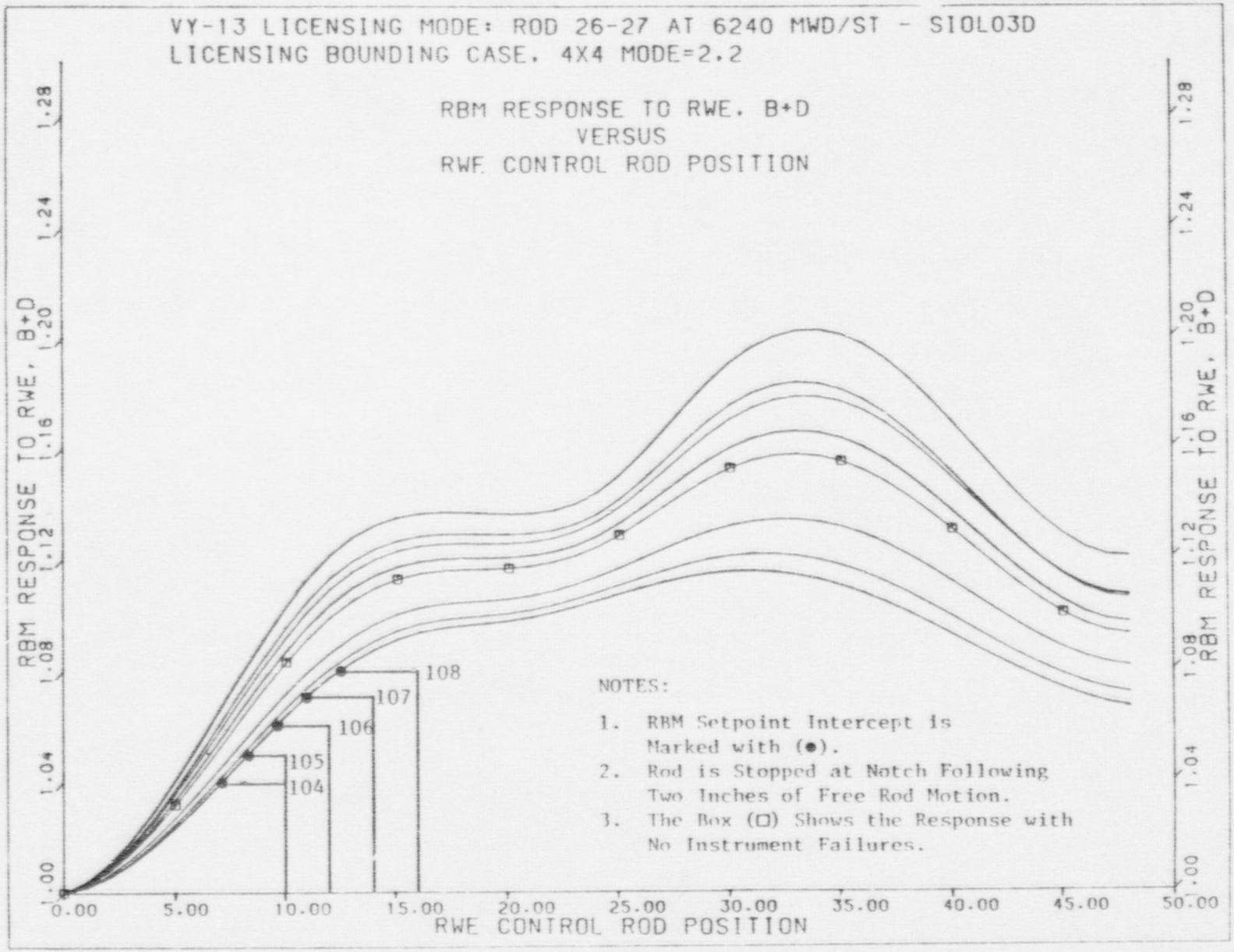

FIGURE 7.4.4

VY CYCLE 13 RWE CASE 1 - SETPOINT INTERCEPTS DETERMINED BY THE B + D CHANNEL

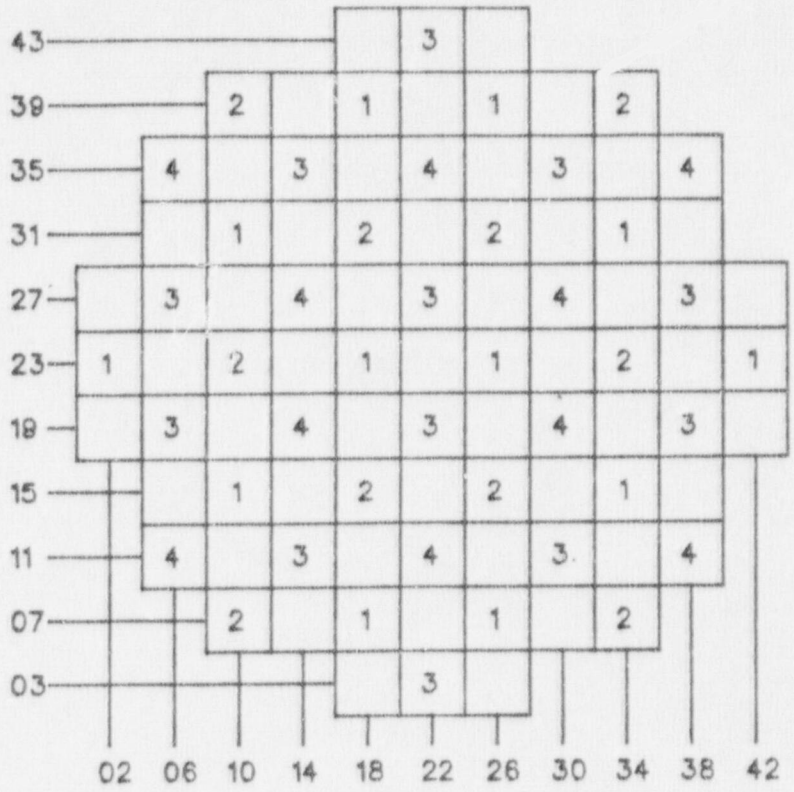

FIGURE 7.6.1 FIRST FOUR ROD ARRAYS PULLED IN THE A SEQUENCES

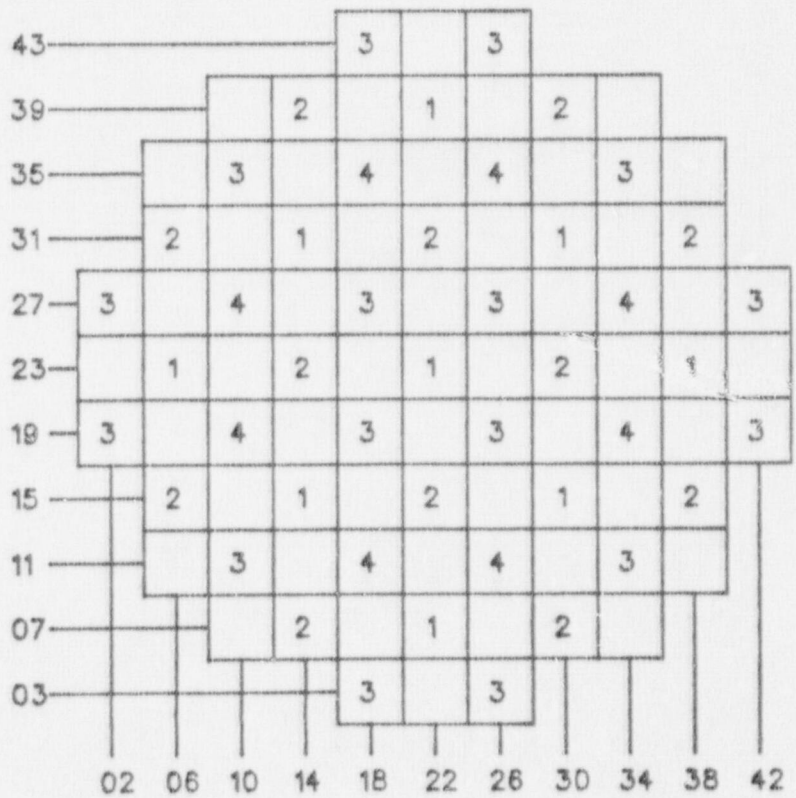

FIGURE 7.6.2 FIRST FOUR ROD ARRAYS PULLED IN THE B SEQUENCES

8.0 LOSS-OF-COOLANT ACCIDENT ANALYSIS

The results of the complete evaluation of the loss-of-coolant accident for Vermont Yankee, as documented in Reference 22, provide the required support for the operation of the Reload Cycle. The MAPLHGR limits for the new fuel type, as a function of average planar exposure, are provided in Table A.2 of Appendix A.

9.0 STARTUP PROGRAM

Following refueling and prior to vessel reassembly, fuel assembly position and orientation will be verified and videotaped by underwater television.

The Vermont Yankee Startup Program will include process computer data checks, shutdown margin demonstration, in-sequence critical measurement, rod scram tests, power distribution comparisons, TIP reproducibility, and TIP symmetry checks. The content of the Startup Test Report will be similar to that sent to the Office of Inspection and Enforcement in the past [23].

REFERENCES

1. M. A. Sironen and R. C. Potter, Vermont Yankee Cycle 10 Summary Report, YAEC-1438, September 1984.

2. R. C. Potter, Vermont Yankee Cycle 11 Summary Report, YAEC-1513, February 1986.

3. General Electric Standard Application for Reactor Fuel (GESTARII), NEDE-24011-P-A-8, GE Company Proprietary, May 1986, as amended.

4. D. M. VerPlanck, Methods for the Analysis of Boiling Water Reactors Steady State Core Physics, YAEC-1238, March 1981.

5. E. E. Pilat, Methods for the Analysis of Boiling Water Reactors Lattice Physics, YAEC-1232, December 1980.

6. S. P. Schultz and K. E. St.John, Methods for the Analysis of Oxide Fuel Rod Steady-State Thermal Effects (FROSSTEY) Code/Model Description Manual, YAEC-1249P, April 1981.

7. S. P. Schultz and K. E. St.John, Methods for the Analysis of Oxide Fuel Rod Steady-State Thermal Effects (FROSSTEY) Code Qualification and Application, YAEC-1265P, June 1981.

8. Appendix A to Operating License DPR-28 Technical Specifications and Bases for Vermont Yankee Nuclear Power Station, Docket No. 50-271.

9. A. A. F. Ansari, et al., Vermont Yankee Cycle 9 Core Performance Analysis, YAEC-1275, August 1981.

10. M. Edenius, A. Ahlin, H. Haggblom, CASMO-2: A Fuel Assembly Burnup Program, STUDSVIK/NR-81/3, Proprietary Studsvik Report.

11. A. A. F. Ansari, Methods for the Analysis of Boiling Water Reactors: Steady-State Core Flow Distribution Code (FIBWR), YAEC-1234, December 1980.

12. A. A. F. Ansari, R. R. Gay, and B. J. Gitnick, FIBWR: A Steady-State Core Flow Distribution Code for Boiling Water Reactors - Code Verification and Qualification Report, EPRI NP-1923, Project 1754-1 Final Report, July 1981.

13. General Electric Company, GEXL Correlation Application to BWR 2-6 Reactors, NEDE-25422, GE Company Proprietary, June 1981.

14. A. A. F. Ansari and J. T. Cronin, Methods for the Analysis of Boiling Water Reactors: A Systems Transient Analysis Model (RETRAN), YAEC-1233, April 1981.

15. EPRI, RETRAN - A Program for One-Dimensional Transient Thermal-Hydraulic Analysis of Complex Fluid Flow Systems, CCM-5, December 1978.

16. A. A. F. Ansari, K. J. Burns, and D. K. Beller, Methods for the Analysis of Boiling Water Reactors: Transient Critical Power Ratio Analysis (RETRAN-TCPYA01), YAEC-1299P, March 1982.

17. J. M. Holzer, Methods for the Analysis of Boiling Water Reactors Transient Core Physics, YAEC-1239P, August 1981.

18. C. J. Paone, et al., Rod Drop Accident Analysis for Large Boiling Water Reactors, NEDO-10527, March 1972.

19. R. C. Stirn, et al., Rod Drop Accident Analysis for Large Boiling Water Reactors Addendum No. 1, Multiple Enrichment Cores With Axial Gadolinium, NEDO-10527, Supplement 1, July 1972.

20. R. C. Stirn, et al., Rod Drop Accident Analysis for Large Boiling Water Reactor Addendum No. 2 Exposed Cores, NEDO-10527, Supplement 2, January 1973.

21. D. Radcliffe and R. E. Bates, "Reduced Notch Worth Procedure", SIL-316, November 1979.

22. Loss-of-Coolant Accident Analysis for Vermont Yankee Nuclear Power Station, NEDO-21697, August 1977, as amended.

23. Letter, FVY 86-92, dated October 6, 1986, R. W. Capstick to T. E. Murley, Regional Administrator, "Cycle 12 Startup Test Report".

APPENDIX A

CALCULATED OPERATING LIMITS

The MCPR limits appropriate for the Reload Cycle are calculated by adding the calculated ΔCPR to the safety limit LAMCPR of 1.07. This is done for each of the analyses in Section 7 at each of the exposure statepoints. For an exposure interval between statepoints, the highest MCPR limit at either end is assumed to apply to the whole interval.

Table A.1 provides the highest calculated MCPR limits for the Reload Cycle for each of the exposure intervals for the various scram speeds and for the various rod block lines. On Table A.1, as in the Technical Specifications, End of Cycle (EOC) is understood to mean End of Full Power Life (EOFPL).

The MAPLHGR limits, as a function of average planar exposure, for the new fuel type are provided in Table A.2.

TABLE A.1

VERMONT YANKEE NUCLEAR POWER STATION
CYCLE 13 MCPR OPERATING LIMITS

Value of "N" in RBM Equation(1)	Average Control Rod Scram Time	Cycle Exposure Range	MCPR Operating Limit(2)
42%	Equal or better than L.C.O. 3.3 C.1.1	BOC to EOC-2 GWD/T	1.28
		EOC-2 GWD/T to EOC-1 GWD/T	1.28
		EOC-1 GWD/T to EOC	1.28
	Equal or better than L.C.O. 3.3 C.1.2	BOC to EOC-2 GWD/T	1.28
		EOC-2 GWD/T to EOC-1 GWD/T	1.28
		EOC-1 GWD/T to EOC	1.32
41%	Equal or better than L.C.O. 3.3 C.1.1	BOC to EOC-2 GWD/T	1.25
		EOC-2 GWD/T to EOC-1 GWD/T	1.25
		EOC-1 GWD/T to EOC	1.27
	Equal or better than L.C.O. 3.3 C.1.2	BOC to EOC-2 GWD/T	1.25
		EOC-2 GWD/T to EOC-1 GWD/T	1.27
		EOC-1 GWD/T to EOC	1.32
≤ 40%	Equal or better than L.C.O. 3.3 C.1.1	BOC to EOC-2 GWD/T	1.25
		EOC-2 GWD/T to EOC-1 GWD/T	1.25
		EOC-1 GWD/T to EOC	1.27
	Equal or better than L.C.O. 3.3. C.1.2	BOC to EOC-2 GWD/T	1.25
		EOC-2 GWD/T to EOC-1 GWD/T	1.27
		EOC-1 GWD/T to EOC	1.32

NOTES:

(1) The Rod Block Monitor (RBM) trip setpoints are determined by the equation shown in Table 3.2.5 of the Technical Specifications.

(2) MCPR Operating Limits are increased by 0.01 for single loop operation.

2810R

TABLE A.2

VERMONT YANKEE NUCLEAR POWER STATION
MAPLHGR OPERATING LIMITS FOR BP8DRB299

Average Planar Exposure (MWd/St)	MAPLHGR for BP8DRB299 Two-Loop Operation	MAPLHGR for BP8DRB299 Single-Loop Operation	PCT °F	Oxidation Fraction
200	10.70	8.8	2030	0.019
1,000	10.80	8.9	2037	0.019
5,000	11.40	9.4	2093	0.023
10,000	12.20	10.1	2178	0.029
15,000	12.30	10.2	2198	0.031
20,000	12.20	10.1	2193	0.031
25,000	11.70	9.7	2139	0.026
35,000	10.60	8.8	1972	0.028
41,900	9.40	7.8	1800	0.012